

**The Role of the Calcium-binding of Copine-6 in synapse function  
and plasticity**

**Inauguraldissertation**

Zur

Erlangung der Würde eines Doktors der Philosophie

vorgelegt der

Philosophisch-Naturwissenschaftlichen Fakultät

der Universität Basel

von

**Diana Flores Dominguez**

Aus Mexiko

**Basel, 2019**

Genehmigt von der Philosophisch-Naturwissenschaftlichen Fakultät auf Antrag von

Prof. Dr. Markus A. Rüegg

Prof. Dr. Fiona Doetsch

**Basel, den 19.02.2019**

Prof. Dr. Martin Spiess  
Dekan

## Table of Contents

1. <b>Summary</b> .....	4
2. <b>List of abbreviations</b> .....	6
3. <b>Introduction</b> .....	8
3.1 Synaptic structure .....	8
3.2 Synaptic transmission .....	9
3.3 Synaptic development .....	10
3.4 molecular mechanism of learning and memory .....	11
3.5 cellular models of learning and memory .....	14
3.6 Copine Family .....	16
3.7 References .....	19
4. <b>Aim of the thesis</b> .....	24
5. <b>Results</b> .....	25
5.1 Manuscript: "Mutation in the second c2 domain of copine-6 cause changes in structural plasticity and strengthening and affects neuronal morphology" .....	25
Abstract .....	26
Introduction .....	27
Material and methods .....	29
Results .....	33
Discussion .....	38
References .....	45
Figures .....	50
Supplementary figures .....	58
6. <b>Appendix</b> .....	66
6.1 Publication "Inhibition of the MID1 protein complex: a novel approach targeting APP protein synthesis" .....	66
7. <b>Acknowledgment</b> .....	85
8. <b>Curriculum Vitae</b> .....	86

## 1. Summary

The molecular mechanisms involved in synaptic plasticity are thought to be the basis for the understanding of learning and memory. However, the complexity of the molecular interactions impedes a deep understanding of these mechanisms. Thus far, it has been well established that a common trigger of the synaptic plasticity mechanism is an increase in postsynaptic calcium concentration. Recently, the protein Copine-6 was found as a modulator of synaptic plasticity due to its ability to respond to calcium influx and subsequently to sequester components of the actin cytoskeleton to the postsynaptic membrane of excitatory synapses. Therefore, Copine-6 seems to be a good candidate involved in hippocampal long-term potentiation, learning and memory. Interestingly, Copine-6 has recently been related in different neurological disorders like intellectual disabilities, depression and epilepsy (Anazi et al., 2017; Han et al., 2018; Zhu et al., 2016).

In the last years, our group generated a mouse line in which a calcium-binding mutant of Copine-6 was knocked-into the *Cpne6* locus – called Cpne6<sup>D167N</sup>. Thereafter, we focused on the biochemical characterization of this mouse. We showed that the calcium-dependent enrichment of Copine-6 in membrane fractions of the mouse brain is abrogated in Cpne6<sup>D167N</sup> mice in the presence of calcium. Importantly, the calcium mutant Copine-6<sup>D167N</sup> is expressed at the same level as wild-type Copine-6. These data therefore shows that the exchange of Asp to Asn at position 167 of Copine-6 does not affect Copine-6 expression but suppresses its calcium-dependent binding to membranes.

Furthermore, we also demonstrated that calcium binding to Copine-6 is crucial for its ability to act as a synaptic plasticity modulator. We found that expression of Copine-6<sup>D167N</sup> in the CA1 region of the hippocampus affects the relative proportion of spine types *in vivo*, as neurons of the hetero- and homozygous knock-in mice express a significantly higher proportion of thin spines at expense of mature spines, a phenotype that was not observed in *Cpne6* knock-out (KO) mice. Differences in spine morphology were also observed in primary hippocampal neurons derived from homozygous Cpne6<sup>D167N</sup> mice, in which an increase in the number of "immature", filopodia-like, thin protrusions and a decrease in mushroom-like protrusions were found. These results suggest that either maturation of spines is delayed or that spines cannot be strengthened following Cpne6<sup>D167N</sup> mutation. Accordingly, we assessed synaptic strengthening of spines from wild-type, hetero- and homozygous Cpne6<sup>D167N</sup> neurons by inducing chemical long-term potentiation (cLTP). We found that while wild-type neurons responded with an increased number of mushroom spines and synapses after cLTP induction, phenotypes that have been correlated with synaptic strengthening (Papa et al., 1995; Hosokawa et al., 1995; Fortin et al., 2010) neurons from heterozygous and homozygous Cpne6<sup>D167N</sup> mice could not respond to the changes related to the cLTP induction paradigm.

This suggests that both mutant genotypes failed to undergo synaptic strengthening. Interestingly, heterozygous *Cpne6*<sup>D167N</sup> neurons showed elevated numbers of filopodia-like spines after cLTP induction, possibly as a compensatory mechanism to establish synaptic connections. Finally, we also found in *Cpne6*<sup>D167N</sup> mice morphological simplifications of CA1 hippocampal pyramidal neurons when compared to wild-type. This result suggests that the binding of calcium to Copine-6 may indirectly affect neuronal morphology as a consequence of spine immaturity.

In conclusion, the calcium-binding site point mutation of Copine-6 seems to have a more profound effect on spine structure plasticity than the complete absence of Copine-6. A similar phenomenon was observed when the phenotypes of mice deficient for CaMKII were compared with mice expressing a phosphorylation mutant of CaMKII (Giese, et al. 1998). Thus, the calcium binding site of Copine-6 seems to be a key element for its ability to act as a calcium sensor and as a further modulator of the synaptic plasticity mechanism. Finally, this work might help to deepen the molecular understanding of synaptic plasticity mechanisms and may also provide new avenues for the molecular understanding of related neurological disorders, revealing possible therapeutic targets.

## 2. Abbreviations

**ADF** actin depolymerizing factor  
**AMPA** -amino-3-hydroxy-5-methyl-4-isoxazolepropionate  
**ARP 2/3** actin related protein 2/3  
**ASN** Asparagine  
**ASD** Autism spectrum disorder  
**ASP** Aspartate  
**CREB-1** cAMP responsive element binding protein 1  
**CA 1** Cornu Ammonis field 1  
**Ca<sup>2+</sup>** Calcium  
**αCaMKII** alpha calcium/calmodulin-dependent kinase II  
**CaMKII** calcium/calmodulin-dependent kinase II  
**cAMP** cyclic adenosine monophosphate  
**CNS** central nervous system  
**Cpne6<sup>D167N</sup>** Calcium insensitive mutant mice  
**DIV** days in vitro  
**ERK** extracellular signal-regulated kinases  
**KO** Knock-out  
**KI** Knock-in  
**F/G-actin** filamentous/globular actin  
**FXS** Fragile X Syndrome  
**GAPs** GTPase- activating factors  
**GEFs** Guanine nucleotide exchange factor  
**GFP** green florescent protein  
**GluR** glutamate receptor  
**GluA1/2** Glutamate A subunit  
**GTPase** enzymes that bind and hydrolyze GTP  
**Ig** Immunoglobulin superfamily  
**kDa** kilo Dalton  
**LIMK** LIM-domain-containing protein kinase  
**LTD/LTP** long-term depression / long-term potentiation  
**MAPK** mitogen-activated protein kinase  
**Mg<sup>2+</sup>** Magnesium

**mGluR** metabotropic glutamate receptor  
**NCAM** Neural adhesion protein  
**NMDAR** N-methyl-D-aspartic acid receptor  
**Pak1** p21-activated kinase  
**PKM $\zeta$** , Protein Kinase zeta type  
**PDZ** PSD-95/Discs large/zO-1  
**PLC** Phospholipase C  
**PKA** Protein kinase A  
**PKC** Protein kinase C  
**PSD** postsynaptic density  
**Rac1** Ras-related C3 botulinum toxin substrate 1  
**Rho A** Ras homolog gene family, member A  
**RNA** ribonucleic acid  
**SynGAP** synaptic Ras GTPase activating protein  
**TARPS** Transmembrane AMPAR regulatory protein  
**vFWA** Von Willebrand factor type A  
**vGlut1** Vesicular glutamate transporter 1  
**Wt** wild-type  
 **$\beta$ -PIX**  $\beta$ -P21 activated Kinase interacting exchange factor

### 3. Introduction

The ability to perceive our surrounding, generate responses, and integrate information depends on the nervous system. The brain is considered the main hub for these interactions and thanks to its ability to remain plastic we can generate or recall information. Consequently, brain plasticity is thought to be essential for maintaining the learning and memory process. The nervous system is known as a very complex structure consisting mainly of specialized cells known as neurons and glia. Glia cells provide support to the neurons and their activity, whereas neuronal cells are the basic function unit as they are essential for the communication in the nervous system.

#### 3.1 Synaptic structure

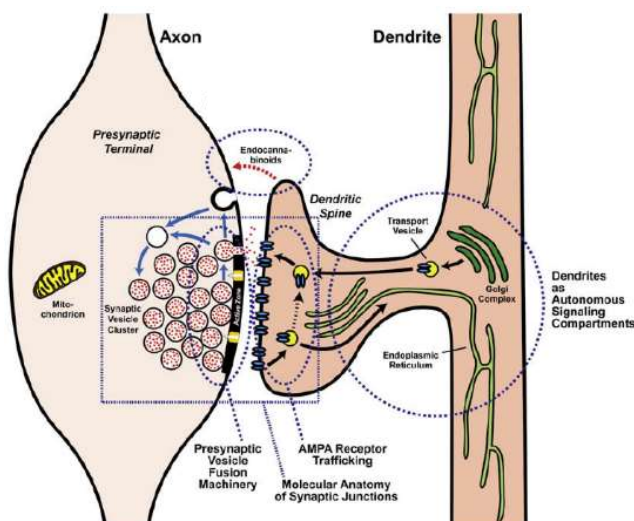


**Figure 1. Schematic view of an excitatory synapse formed by an axon and dendritic spine.** Key elements of the synapses are indicated: Presynaptic vesicle, receptors, and organelles (adapted from Südhof and Melenka, 2008).

The primary sites of communication between neurons, is the synapse. Synapses are specialized dynamic junctions, susceptible to remodeling according to the strength of the synaptic input. At the synapse, the pre-synaptic membrane of the signal passing neuron comes into close vicinity to the post-synaptic membrane of the target neuron. Both, pre- and post- synapses contain a molecular machinery that connect the two neuronal membranes and carry out the signaling process (**Figure 1**).

Synapses can be divided into chemical and electrical ones. Electrical synapses impulse transmission occurs via gap junctions between neurons, which connect their cytoplasm by channels, causing voltage change in the pre-synapses to induce changes in the post-synapse. Although a rapid and bidirectional signal transfer characterizes this type of synapse, this synapse cannot amplified the signal they transmit. In the case of the chemical synapses, the signal transmission consist on a sequence of events that initiated when an action potential invades the terminal of the presynaptic neuron. The arrival of the action potential cause a change in the membrane potential that will lead to

the opening of voltage calcium channels causing a rapid calcium influx. Consequently, a rise of the calcium concentration occurs that will allow synaptic vesicle- neurotransmitter contained to fuse with the plasma membrane of the presynaptic neuron. The neurotransmitters release occurs from pre-synaptic neuron through a small space, called synaptic cleft, to receptors on post-synaptic neuron. Thereafter, the neurotransmitter induces an ion current flow and cause that the conductance and membrane potential of the postsynaptic neuron change. Depending on the properties of the postsynaptic receptor, the signal can act as excitatory or inhibitory by increasing or decreasing the probability of generating an action potential in the postsynaptic neuron. Finally, if the sum of all the signals cause the neuron membrane to be depolarized above a specific threshold, an action potential will be fired and will lead to the postsynaptic generation of an electrical signal (amplification). In this way, information is transmitted from one neuron to another.

### 3.2 Synaptic transmission

The process that allows inter-neuronal communication at the synapse is known as synaptic transmission, which is based on a sequence of events that are initiated when an action potential invades the presynaptic terminal and is further converted into a chemical message. As previously explained, in the chemical transmission the neurotransmitters diffuse across the synaptic cleft and reach the postsynaptic membrane where they bind to specific receptors. One of these postsynaptic receptors that respond to positive potentials and presynaptic glutamate release is the N-methyl-D-aspartic acid receptor (NMDAR). Upon depolarization, NMDAR will show maximal receptor permeability as it expels  $Mg^{2+}$  from the pore relieving it from the block and allow sodium, potassium, and calcium to pass (Lüscher and Malenka, 2012). Elevation in intracellular calcium have been established as one of the trigger events at the postsynaptic neuron (Mulkey and Malenka 1992) as increase in the calcium influx through the NMDARs activates intracellular signaling cascades essential for inter-neuronal information transmission (Bliss and Collingridge, 1993). Another important signaling mechanism that occurs in the postsynaptic membrane is the increase in the number of amino-3-hydroxy-5-methyl-4-isoxazolepropionate receptors (AMPA). AMPARs are one of the principal transducers of excitatory transmission and are targets of multiple signaling pathways that regulated the strength of glutamatergic synapses. Most AMPARs consist of tetramers of four glutamate receptor subunits, GluR1-GluR4 (Hollmann and Heinemann 1994; Seeburg 1996; Dingledine et al 1999). In the case of the adult hippocampus, two forms of AMPARs are known to be predominant, Glur1/Glur2 heteromers and GluR2/GluR3 heteromers (Wenthold et al., 1996). It is suggested that the functional properties of AMPARs and their trafficking depend on their subunit composition (Collingridge et al., 2004; Malinow and Malenka, 2002). Based on

overexpression studies, the subunit-specific rules that determine the synaptic delivery of AMPARs were unraveled. It was shown that the insertion of GluR1 containing AMPARs into synapses is slow under basal conditions and is strongly stimulated by NMDAR activation, whereas insertion of GluR2/3 heteromeric receptors may occur constitutively on a much more rapid timescale (Hayashi et al., 2000; Shi et al., 2001). Overall, these events are thought to activate both pre- and postsynaptic mechanisms that will finally generate a persistent increase in synaptic strength.

### 3.3 Synapse development – Synaptogenesis

Appropriate synapse formation and its specificity is a complex mechanism, which is necessary for normal cognitive functions as it is thought to provide the substrate for perception, learning, and memory. For a synapse to form, first a contact must be made between the presynaptic and the postsynaptic site. Synapses can form, for example, from contact between axon and dendritic shaft where axonal and dendritic filopodia contact their targets in a random manner. In the case of the hippocampus it is known that during the first few weeks of postnatal life dendrites have numerous filopodia (Ziv and Smith, 1996; Fiala et al., 1998). Nevertheless, most of the contacts they establish are transitory and can result in retraction of the filopodia. However, there is evidence that a small subset of these filopodia becomes stabilized and a nascent synapse will subsequently be formed on those sites (Marrs et al., 2001).

At the molecular level, the initial formation of contacts between axons and dendrites appears to be mediated by trans-synaptic adhesion molecules, which include cadherins, integrins, Immunoglobulin superfamily (Ig), Neural cell adhesion molecule (NCAM), nectins, neuroligins, SynCAMs, and ephrins (Akins and Biederer 2006; Scheiffele 2003). It is thought that signals by these cell adhesion molecules will lead to stabilized filopodia. Filopodia stabilization seems to be a predefined event controlled either by glutamate and/or other molecule release that might attract filopodia (Lohmann et al., 2005) or by the localization of presynaptic terminal scaffolding proteins (Gerrow et al., 2006). Interestingly, *ex vivo* studies in hippocampal slices revealed a high density of highly motile filopodia-like structures in an early developmental stage. Furthermore, at later developmental times, dendritic extension and filopodia dynamics progressively decline, accompanied by a steady increase of stable spine-like structures (Dailey and Smith 1996; Ziv and Smith 1996). These observations support the earlier suggestion that dendritic filopodia may actively participate in synapse formation during synaptogenesis. The timing of synaptogenesis is usually measured by determining the time course of stable accumulation of both pre- and postsynaptic core components of the glutamatergic synapses (i.e. presynaptic vesicles, presynaptic active zone, postsynaptic glutamate receptors and scaffolding proteins). Although the initial assembly of a synapse can

be quite rapid, the development of a mature synapse is generally prolonged as evidenced by the delay in formation of its mature ultrastructure (Ahmari and Smith 2002) and decelerated maturation in electrophysiological properties (Mohrmann et al. 2003). During the time course of nascent synapses recruitment of core components occurs and afterwards, at later stages of synaptic maturation a second wave of proteins are added to the synapses, which may serve for its stabilization (e.g. AMPAR and scaffolding proteins) (Malenka 2003; Song and Huganir 2002).

One of the events related to the maturation of glutamatergic synapses in the CNS is the change of their localization. Synapses are initially formed on dendritic filopodia or dendritic shafts, but later these synapses are located on specialized small excitatory protrusion known as dendritic spines. Dendritic spines are the primary recipient of excitatory inputs in the CNS, thought as biochemical compartments that locally control the signaling mechanism at individual synapses. A general description of dendritic spines includes a continuum of shapes from short, stocky spines to long-necked spines tipped by a bulbous head (Lippman and Dunaevsky, 2005). Traditionally, and based on ultrastructural analysis of the adult cerebral cortex, spines have been divided into different types as stubby, thin, mushroom-shaped (Bourne and Harris, 2008). As it is thought that filopodia-like synapses will transform into spine synapses (Fiala et al., 1998; Ziv and Smith 1996) dendritic spines morphogenesis has been suggested as a critical event in the maturation of glutamatergic synapses (Yuste and Bonhoeffer 2004). In fact, synaptic maturation consists of synapses growing larger accompanied with a considerable increase in the amount of pre-and postsynaptic proteins.

As spines mediate most of the excitatory connections in the CNS, they have been considered as core elements in the neuronal circuitry. Neuronal circuits are established during development and modified during learning. Consequently, dendrite dynamics, synaptogenesis, and loss of superfluous synaptic connections (pruning) are key functions in the reorganization, remodeling and fine-tuning of neuronal circuits and therefore of crucial importance for nervous system function.

### 3.4 Mechanism involved in synaptic plasticity and learning and memory

Synaptic plasticity refers to a series of mechanisms that mediate the activity-dependent strengthening or weakening of neuronal circuitries at the level of the synapse (Citri and Malenka, 2008). In the adult organism, use-dependent adjustment of synaptic efficacy is thought to have a role in learning and memory, where NMDAR has been implicated in initiating the relevant structural and functional changes at synapses that will result in refinement of

synaptic connections. Consequently, learning and memory might result from changes in relative strength or efficacy of existing synapses

The molecular mechanisms leading to synaptic plasticity that underlie learning and memory are very complex and therefore not completely elucidated. *In vitro* and *in vivo* studies have shown that the opening of NMDARs increases the calcium influx and consequently activates calcium/calmodulin-dependent kinase II (CAMKII) (Silva et al., 1992; Giese et al., 1998) which upon activation translocate into the postsynaptic compartment (Lee et al., 2009). Moreover, CAMKII is involved in the stabilization of AMPARs via the phosphorylation of special sites at their C-terminal part. Another downstream target of CAMKII is the cytoskeleton molecule actin. Actin plays a key role in shaping dendritic spines and is critically important for numerous processes that contribute to the plasticity of synaptic function (Matus, 2000; Hering and Sheng, 2001; Luo, 2002; Hotulainen and Hoogenraad, 2010). Actin exists in two forms: F-actin (filamentous polymer made of globular actin) and G-actin (globular actin monomers). Actin filaments are polar structures that undergoes a continuous turnover which involves the polymerization of G-actin at the barbed end of the filament and depolymerization of F-actin at the opposite, pointed end, a process known as “actin treadmilling” (Star et al., 2002; Honkura et al., 2008).

Members of the Rho family of small GTPase are well-known regulators of the actin cytoskeleton that have profound influence on spine morphogenesis. Rho GTPases act as intracellular molecular switches that cycle between an active GTP-bound form and an inactive GDP-bound. Guanine nucleotide exchange factors (GEFs) facilitate the conversion from GDP-bound to GTP-bound form and thus are activators, whereas GTPase activating proteins (GAPs) enhance GTP hydrolysis and are thus negative regulators. GEFs and GAPs are known to postsynaptically control Rho GTPases. Two members of the Rho family, transforming protein RhoA and RAS-related C3 botulinum toxin substrate 1 (Rac1), are known to control actin cytoskeleton rearrangement in a separate and opposing manner. While RhoA inhibits, Rac1 promotes the growth and/or stability of dendritic spines. For example, Rac1 can be locally activated in dendritic spines by the GEF  $\beta$ PIX ( $\beta$ -p21-activated kinase – PAK – interacting factor). Calcium induced activation of CAMKII increases the GEF activity of PIX, which causes a further activation of Rac1 (Saneyoshi et al., 2008; Park et al., 2003). Activated Rac1 triggers the activation of p21-activated kinase 1 (PAK1), which in turn activates LIM domain kinase 1 (LIMK1). LIMK1 in turn inactivates ADF/Cofilin through phosphorylation and decreases the rate of actin polymerization (Maekawa et al., 1999). Inhibition of ADF/Cofilin maintains actin fibers and stabilizes synaptic structures. Cofilin phosphorylation and dephosphorylation will then control pools of active Cofilin in the cell and thus actin filament dynamics (Meng et al., 2002; Hayashi et al., 2004; Tashiro and Yuste, 2004) (**Figure 2**). Interestingly, Rac1 and RhoA activation have been extensively characterized as causative factors in spine formation,

enlargement, maturation and stabilization as well as in synaptic strengthening (Nakayama et al., 2000; Saneyoshi et al., 2010; Woolfrey and Srivastava, 2016).

Although most of the experimental approaches mainly show how calcium and its interaction with CAMKII activates downstream pathways that control hippocampal synapses, other signaling pathways have also shown to be critical in certain form of plasticity and/or others brain regions. One example is the synaptic plasticity dependent activation of G protein coupled receptors in the cerebellum and striatum (Ito M., 2001; Calabresi et al., 1992). Moreover, long lasting synthesis dependent forms of hippocampal plasticity cannot be exclusively explained by CaMKII pathway but by protein kinases A (PKA) activation (Abel et al., 1997; Roberson et al., 1999). Another novel protein known to have a role in the synaptic mechanism is the RAS/RAP GTPase activating protein (SynGAP1). SynGAP1 binds to the PDZ domain of PSD-95 and SAP 102. It is localized exclusively in excitatory synapses and is a major constituent of the PSD. SynGAP is thought to be a central regulator of synaptic signaling necessary for certain types of neuronal plasticity (Komiyama NH., et al., 2002; Rumbaugh G., et al., 2006). Mutations within SynGAP1 are related to intellectual disabilities, epilepsy and autism spectrum disorder (ASD) (Clement et al., 2012). In conclusion, it is likely that the synaptic plasticity mechanisms require the work of different proteins that might interact in “modules”, which will respond in accordance to the input and the neuronal plasticity type (**Figure 2**).

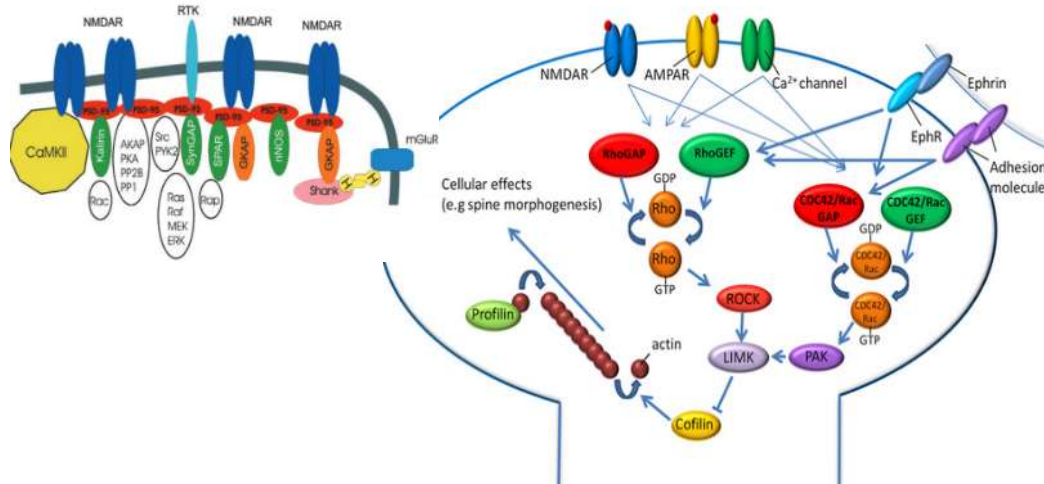


**Figure 2. Postsynaptic signaling proteins.** Proteins involved in the synaptic plasticity mechanism. Schematic representation of NMDAR and associated proteins that act accordingly to the input receive in the postsynapse (left). Activation of receptors and channels during the learning and memory lead to regulation of intracellular signaling that affect actin dynamics. Among these regulatory proteins are Rho, Rac GTPase and their effectors and actin binding proteins such as cofilin (modified from Lamprechet R., 2011; Sheng and Kim, 2002).

### 3.5 Cellular models of learning and memory

Long-term potentiation (LTP) and long-term depression (LTD) are a general class of cellular synaptic phenomenon, which can be used to demonstrate the repertoire of long-lasting modifications of individual synapses (**Figure 3A**). LTP is known as a repetitive activation of excitatory synapses in the hippocampus that causes a potentiation of synaptic strength and appears as a long lasting event. The properties of LTP make it an attractive cellular mechanism for rapid information storage as, similar to memory, LTP can be generated rapidly and is strengthened and prolonged by repetition. Important properties of LTP are 1) cooperativity, related to induced coincident activation, 2) associativity, i.e. the capacity to potentiate a weak synaptic input when it is activated in association with a strong input and 3) input specificity, i.e. LTP is elicited only at activated synapses (Nicoll et al., 1995). Consequently, the LTP mechanism is thought to provide an important key for the understanding of some of the cellular and molecular mechanism by which memories are formed (Whitlock et al., 2006; Pastalkova et al., 2006) and thus LTP is considered as a model for the molecular basis and behavioral correlates of synaptic plasticity.

The mechanism that underlie LTP start with a large NMDAR-dependent increase in dendritic spine calcium concentration, which leads to activation of intracellular signaling cascades involving a number of protein kinases, in which the most known is CAMKII (Lisman et al 2012). This leads to an increase in the conductance of synaptic AMPARs and promotes the incorporation of additional AMPARs into the PSD. Interestingly, AMPARs do not appear to be inserted directly into the PSD, but rather are exocytose at perisynaptic sites. Thus, AMPARs laterally diffuse in the plasma membrane and are trapped within the PSD due to their interaction with “trap” proteins. The candidates that bear this trap activity are the membrane associate guanylate kinase (MAGUKs) family of PSD and include PSD-95, SAP97, PSD-93, and SAP102 (Kim and Sheng 2004; Montgomery et al., 2004). The new synaptic AMPARs are stabilized through their transmembrane AMPAR regulatory proteins (TARPs) which mediated interaction with PDZ domain-containing proteins (Jackson and Nicoll, 2011). The insertion of AMPARs and associated molecules into the PSD leads to the growth of the PSD area / spine (Lisman and Harris, 1993) (**Figure 3B**). Moreover, synthesis of proteins like  $\alpha$ CAMKII or AMPAR subunits may also play a key role in structural modification during LTP. *In vitro* studies have shown that LTP induction results in a local growth of synapses, synaptic strengthening, and growth of new synapses (Matsuzaki et al., 2004; Yuste and Bonhoeffer, 2001). Similarly, neuronal activity can lead to short or long term changes in morphology, appearance or disappearance of dendritic spines. Therefore, these short and long-term changes in morphology and number of spines -known as structural plasticity- have been implicated in synaptic plasticity and are related to strengthening of existing connections between two cells.

In addition, the presynaptic active zone activity also increases, causing stable synapse enlargement. Finally, the maintenance of these changes for more than a few hours depends on the *de novo* transcription as well as local dendritic protein synthesis, presumably to provide the synapse with a supply of the critical proteins necessary for maintaining synaptic strength.

The second cellular model known as LTD is a process elicited by prolonged repetitive low-frequency stimulation (Dudek and Bear, 1992; Mulkey and Malenka 1992). LTD is input specific and, like LTP, depends upon NMDAR-dependent increase in postsynaptic calcium (Mulkey and Malenka, 1992). The predominant hypothesis is that quantitative properties of the postsynaptic calcium signal within dendritic spines dictates whether LTP or LTD is triggered, with LTD requiring a mild increase of calcium, whereas LTP requires an increase beyond a threshold value (Bliss and Cooke, 2012; Lüscher and Malenka 2012; Malenka and Bear, 2004; Cummings et al., 1996; Malenka and Nicoll, 1993). The mechanism underlying NMDAR-dependent LTD starts with a small increase in postsynaptic calcium concentration within dendritic spines due to a mild activation of NMDARs, which leads to preferential activation of protein phosphatases. This causes a dissociation of AMPARs from their molecular scaffolds in the PSD and their later movement into endocytic zones on the periphery of the PSD, where they are endocytosed and potentially degraded. The mechanism involve in LTD maintenance is not completely known. Nevertheless, there is evidence that LTD is accompanied by a shrinkage in the size of dendritic spines (Nägerl et al., 2004; Zhou et al., 2004) and that this may be due to the loss of AMPARs (Hsieh et al., 2006). As in the case of LTP, it is also thought that protein translocation may be needed for the long-term stable expression of LTD (Pfeiffer and Huber, 2006).

It is generally accepted that the activity-dependent trafficking of AMPARs into and out of synapses during LTP and LTD, respectively, is the first critical step in the morphological growth or shrinkage of synapses and that these structural modifications are the mechanism by which bidirectional changes in synaptic strength are maintained. Indeed, the size of individual synapses correlates closely with the number of AMPARs they contain (Matsuzaki et al., 2001; Takumi et al., 1999) (**Figure 3B**). Consequently, LTP and LTD appear to be essential in the stabilization and elimination of synapses during developmental fine-tuning of neuronal circuits in many areas of the brain.

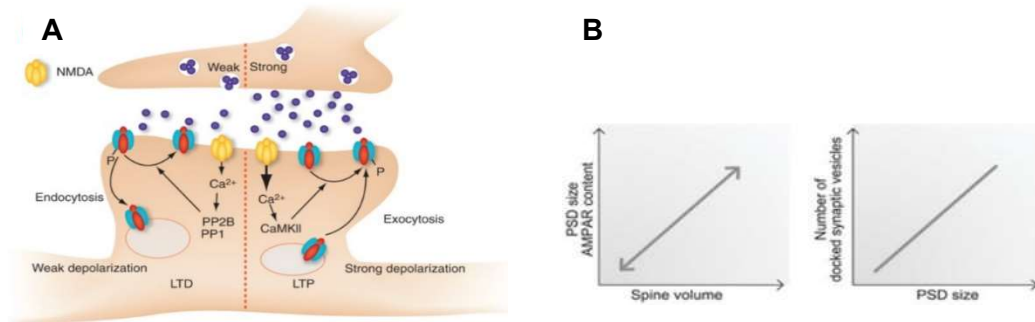


**Figure 3. (A) LTP and LTD mechanism.** Weak activity of the presynaptic neuron lead to a mild depolarization and calcium influx through the NMDAR and will lead to the activation of phosphatases that will dephosphorylate AMPARs, mechanism related with LTD. Strong activity depolarization triggers LTP in part via CAMKII, AMPAR phosphorylation. (B) PSD size and AMPAR content is directly proportional to the spine volume and the number of vesicle number correlates with PSD size, Lüscher and Malenka, (2012).

### 3.6 Copine Family

Copines are members of a ubiquitous family described as cytosolic-soluble proteins that show calcium-dependent phospholipid-binding properties. Copines share a common structure, consisting of two N-terminal C2-domains responsible for calcium binding. On the other hand, the C-terminal portion of copines show a distant relation to the “A domain” in the extracellular portion of integrins (or von Willebrand factor A (vWA)-domain) (Lee et al., 1995), which is known for binding extracellular matrix proteins. Furthermore, the C2 domain of copines have conserved aspartates that could serve as calcium ion coordination residues, whereas the A-domain is thought as a site for protein-protein interaction by which copines bind and recruit target proteins to the membrane surface (Tomsig and Creutz, 2002). Consequently, because of their domain structure, it has been suggested that copines can target proteins to the plasma membrane in response to a rise in intracellular calcium via the C2-domains acting as the calcium sensors. Interestingly, identified targets of copines are proteins involved in intracellular signal transduction pathways, which include 1) regulators of phosphorylation (MEK1, Protein phosphatase 5, CDC42 binding kinase), 2) regulators of transcription (Myc-binding protein, Sno proto-oncogene, BCL-6 corepressor), 3) calcium-binding proteins (ALG2), 4) regulators of ubiquitination/NEDDylation (UBC12, E2-230), 5) cytoskeletal regulation (Radixin, BICD2-dynamitin-binding protein) (Tomsig et al., 2003). These arrays of potential targets suggest that copines may be generally involved in providing calcium regulation of intracellular signaling pathways. Therefore, by binding to membranes and target proteins, copines may be able to specifically localize signaling pathway components to certain membranes in cells and

consequently enhance the assembly of complexes involved in signaling across the plasma membrane.

Furthermore, to exert its translocation-binding mechanisms, copines should show calcium-dependent membrane binding. Indeed, *in vitro* studies using phospholipid vesicles have found that some C2-domains of copines show phospholipid binding that is calcium dependent (Tomsig and Creutz, 2000; Damer et al., 2005). Moreover, some copines showed that replacement of the Asp to Asn in the C2B domain is sufficient to abolish calcium response. Therefore, the C2B domain has been identified as a critical component for the membrane association of copines (Perestenko et al., 2015). Besides, the highly divergent C-terminus probably confers unique characteristics to each family member. Interestingly, these C2 domains are also found in other calcium-sensing proteins like synaptotagmin, protein kinase C (PKC), phospholipase C (PLC) and rabphilin (Perestenko et al., 2010), supporting the role of Copines as calcium sensor proteins.

Homologous copine proteins are expressed in most plants, animals and protists. First described in *Paramecium tetraurelia* (Creutz et al., 1998; Tomsig and Creutz 2002) and subsequently in *Caenorhabditis elegans*, *Arabidopsis*, *Dictyostelium* and *Homo Sapiens*. The expression of copines has been found in mammalian tissues, including brain, heart, lung, liver and kidney. Screening of human tissues for human Copines 1-6 has shown that Copines 1,2 and 3 are ubiquitously expressed, whereas Copine-4 has a more restricted distribution in the brain, heart and prostate gland, and Copine-6 is brain specific (Tomsig and Creutz 2002). Nevertheless, the precise role of copines in cells remains unclear, although there is evidence that they may be involved in the regulation of plasma membrane protein or lipid content.

A key molecule from this highly conserved protein family is Copine-6, which is characterized by two C2 domains that bind phospholipids in a calcium-dependent manner and an A domain at the carboxyl terminus. Interestingly, Copine-6 expression is restricted to the brain, specifically to hippocampus and olfactory bulb. It has also been shown that Copine-6 is located in postsynaptic elements like dendrites and cell bodies (Nakayama et al., 1999; Reinhard et al., 2016; Burk et al. 2018). Furthermore, it has been shown that the levels of Copine-6 increase after the induction of kindling or long-term potentiation in the rat hippocampus (Nakayama et al. 1998); therefore suggesting that Copine-6 may be involved in synaptic potentiation. In fact, previous investigations by our group have found that *Cpne6* transcript and Copine-6 protein are expressed in the postnatal brain with peak expression in the hippocampus at time points of synapse formation. In addition, Copine-6 has been shown as a novel calcium sensor, which translates calcium signaling into changes in spine structure (Reinhard et al., 2016; Burk et al., 2018). Moreover, lack of Copine-6 prevents synapses to be strengthened and Copine-6 KO mice fail to undergo hippocampal LTP, hippocampus

dependent learning, and show memory impairment (Reinhard et al., 2016). In conclusion, these investigations reinforce the importance of Copine-6 in synaptic plasticity.

### 3.7 References

1. Abel, T., Nguyen, P. V., Barad, M., Deuel, T. A., Kandel, E. R., & Bourtchouladze, R. (1997). Genetic demonstration of a role for PKA in the late phase of LTP and in hippocampus-based long-term memory. *Cell*, 88(5), 615-626.
2. Akins, M. R., & Biederer, T. (2006). Cell-cell interactions in synaptogenesis. *Current opinion in neurobiology*, 16(1), 83-89.
3. Ahmari, S. E., & Smith, S. J. (2002). Knowing a nascent synapse when you see it. *Neuron*, 34(3), 333-336.
4. Bliss, T. V., & Cooke, S. F. (2011). Long-term potentiation and long-term depression: a clinical perspective. *Clinics*, 66, 3-17.
5. Bliss, T. V., & Collingridge, G. L. (1993). A synaptic model of memory: long-term potentiation in the hippocampus. *Nature*. 361(6407): 31.
6. Bourne, J.N., and Harris, K.M. (2008). Balancing structure and function at hippocampal dendritic spines. *Annu. Rev. Neurosci.* 31: 47-67.
7. Burk, K., Ramachandra B., Saheeb, A., Hurtado-Zavala, J., Awasthi, A., Benito, E., Faram, R., Ahmad, H., Swaminathan, A., McIlhinney J., Fischer, A., Perestenko P., Dean C. (2018). Regulation of dendritic spine morphology in hippocampal neurons by Copine-6. *Cerebral Cortex*. 28: 1087-1104.
8. Calabresi, P., Maj, R., Pisani, A., Mercuri, N. B., & Bernardi, G. (1992). Long-term synaptic depression in the striatum: physiological and pharmacological characterization. *Journal of Neuroscience*, 12(11), 4224-4233.
9. Clement, J.P., Aceti, M., Creson, T.K., Ozkan, E.D., Shi, Y., Reish N.J., et al. (2012). Pathogenic SYNGAP1 mutations impair cognitive development by disrupting maturation of dendritic spines synapses. *Cell*. 151: 709-723.
10. Citri, A., & Malenka, R. C. (2008). Synaptic plasticity: multiple forms, functions, and mechanisms. *Neuropsychopharmacology*, 33(1), 18.
11. Creutz, C. E., Tomsig, J. L., Snyder, S. L., Gautier, M. C., Skouri, F., Beisson, J., & Cohen, J. (1998). The copines, a novel class of C2 domain-containing, calciumdependent, phospholipid-binding proteins conserved from Paramecium to humans. *Journal of Biological Chemistry*, 273(3), 1393-1402.
12. Collingridge, G.L., Isaac, J. T., Wang, Y.T. (2004). Receptor trafficking and synaptic plasticity. *Nat Rev Neurosci.* 5: 952-962.
13. Cummings, J. A., Mulkey, R. M., Nicoll, R. A., & Malenka, R. C. (1996). Ca<sup>2+</sup> signaling requirements for long-term depression in the hippocampus. *Neuron*, 16(4), 825-833.
14. Dailey M.E., and Smith S.J. (1996) The dynamics of dendritic structure in developing hippocampal slices. *J. Neurosci.* 16 (9): 2983-2994.
15. Damer, C. K., Bayeva, M., Hahn, E. S., Rivera, J., & Socec, C. I. (2005). Copine A, a calcium-dependent membrane-binding protein, transiently localizes to the plasma membrane and intracellular vacuoles in Dictyostelium. *BMC cell biology*, 6(1), 46.
16. Dan, Y., and Poo, M. M. (2004). Spike timing-dependent plasticity of neural circuits. *Neuron*, 44(1), 23-30.
17. Dingledine, R., Borges, K., Bowie, D., & Traynelis, S. F. (1999). The glutamate receptor ion channels. *Pharmacological reviews*, 51(1), 7-62.
18. Dudek, S. M., & Bear, M. F. (1992). Homosynaptic long-term depression in area CA1 of hippocampus and effects of N-methyl-D-aspartate receptor blockade. *Proceedings of the National Academy of Sciences*, 89(10), 4363-4367.
19. Dunaevsky, A., Tashiro, A., Majewska, A., Mason, C., and Yuste, R. (1999). Developmental regulation of spine motility in the mammalian central nervous system. *Proc. Natl. Acad. Sci. U. S. A.* 96: 13438-13443.
20. Fiala, J. C., Feinberg, M., Popov, V., & Harris, K. M. (1998). Synaptogenesis via dendritic filopodia in developing hippocampal area CA1. *Journal of Neuroscience*, 18(21), 8900-8911.

21. Gerrow, K., & El-Husseini, A. (2006). Cell adhesion molecules at the synapse. *Front Biosci*, 11(9), 2400-2419.
22. Giese, K.P., Fedorov, N.B., Filipkowski, R.K. & Silva, A.J. (1998) Autophosphorylation at Thr286 of the alpha calcium-calmodulin kinase II in LTP and learning. *Science*. 279: 870-3.
23. Hayashi, M.L., Choi, S.Y. Rao, B.S., Jung, H.Y., Lee, H.K., Zhang D., S. Chattarji, S., Kirkwood, A.,. Tonegawa S. (2004). Altered cortical synaptic morphology and impaired memory consolidation in forebrain- specific dominant-negative PAK transgenic mice. *Neuron*. 42: 773-787.
24. Hayashi, Y., Shi, S.H., Esteban, J.A., Piccini A., Poncer, J.C., Malinow, R. (2000). Driving AMPA receptors into synapses by LTP and CaMKII: requirement for GluR1 and PDZ domain interaction. *Science*. 287: 2262-2267.
25. Hering, H. and Sheng M. (2001) Dendritic spines: structure, dynamics and regulation. *Nat. Rev. Neurosci*. 2 (12): 880-8.
26. Hollmann, M., Maron, C., & Heinemann, S. (1994). N-glycosylation site tagging suggests a three transmembrane domain topology for the glutamate receptor GluR1. *Neuron*, 13(6), 1331-1343.
27. Hotulainen, P., Hoogenraad, C.C. (2010). Actin in dendritic spines: connecting dynamics to function. *J Cell Biology*. 189 (4): 619-629.
28. Honkura, N., Matsuzaki, M., Noguchi, J., Ellis-Davies, G. C., & Kasai, H. (2008). The subspine organization of actin fibers regulates the structure and plasticity of dendritic spines. *Neuron*, 57(5), 719-729.
29. Hsieh, H., Boehm, J., Sato, C., Iwatsubo, T., Tomita, T., Sisodia, S., & Malinow, R. (2006). AMPAR removal underlies A $\beta$ -induced synaptic depression and dendritic spine loss. *Neuron*, 52(5), 831-843.
30. Ito, M. (2001). Cerebellar long-term depression: characterization, signal transduction, and functional roles. *Physiological reviews*, 81(3), 1143-1195.
31. Jackson, A. C., & Nicoll, R. A. (2011). The expanding social network of ionotropic glutamate receptors: TARPs and other transmembrane auxiliary subunits. *Neuron*, 70(2), 178-199.
32. Kim, E., & Sheng, M. (2004). PDZ domain proteins of synapses. *Nature Reviews Neuroscience*, 5(10), 771.
33. Komiyama, N. H., Watabe, A. M., Carlisle, H. J., Porter, K., Charlesworth, P., Monti, J., & O'Dell, T. J. (2002). SynGAP regulates ERK/MAPK signaling, synaptic plasticity, and learning in the complex with postsynaptic density 95 and NMDA receptor. *Journal of Neuroscience*, 22(22), 9721-9732.
34. Lamprecht, R. (2011). The roles of the actin cytoskeleton in fear memory formation. *Frontiers in behavioral neuroscience*, 5, 39.
35. Lee, J. O., Rieu, P., Arnaout, M. A., & Liddington, R. (1995). Crystal structure of the A domain from the A subunit of integrin CR3 (CD11 b/CD18). *Cell*, 80(4), 631-638.
36. Lee, S. J. R., Escobedo-Lozoya, Y., Szatmari, E. M., & Yasuda, R. (2009). Activation of CaMKII in single dendritic spines during long-term potentiation. *Nature*, 458(7236), 299.
37. Lippman, J., & Dunaevsky, A. (2005). Dendritic spine morphogenesis and plasticity. *Journal of neurobiology*, 64(1), 47-57.
38. Lisman, J. E., & Harris, K. M. (1993). Quantal analysis and synaptic anatomy—integrating two views of hippocampal plasticity. *Trends in neurosciences*, 16(4), 141-147.
39. Lisman, J., Yasuda, R., and Raghavachari, S. (2012). Mechanisms of CaMKII action in long-term potentiation. *Nat. Rev. Neurosci*. 13:169-182.
40. Lohmann, C., Finski, A., & Bonhoeffer, T. (2005). Local calcium transients regulate the spontaneous motility of dendritic filopodia. *Nature neuroscience*, 8(3), 305.
41. Luo, L. (2002). Actin cytoskeleton regulation in neuronal morphogenesis and structural plasticity. *Annual review of cell and developmental biology*, 18(1), 601-635.

42. Lüscher, C., & Malenka, R. C. (2012). NMDA receptor-dependent long-term potentiation and long-term depression (LTP/LTD). *Cold Spring Harbor perspectives in biology*, a005710.
43. Maekawa, M. et al., (1999). Signaling from Rho to the actin cytoskeleton through protein kinases ROCK and LIM-Kinase. *Science*, 285 (5429): 895-898
44. Malenka, R. C., & Bear, M. F. (2004). LTP and LTD: an embarrassment of riches. *Neuron*, 44(1): 5-21.
45. Malenka, R. C. (2003). Synaptic plasticity and AMPA receptor trafficking. *Annals of the New York Academy of Sciences*, 1003(1), 1-11.
46. Malenka, R. C., & Nicoll, R. A. (1993). NMDA-receptor-dependent synaptic plasticity: multiple forms and mechanisms. *Trends in neurosciences*, 16(12), 521-527.
47. Malenka, R., & Nicoll, R. A. (2002). AMPA receptor trafficking and synaptic plasticity. *Annu Rev Neurosci*. 25:103-126.
48. Marrs, G. S., Green, S. H., & Dailey, M. E. (2001). Rapid formation and remodeling of postsynaptic densities in developing dendrites. *Nature neuroscience*, 4(10), 1006.
49. Matsuzaki, M., Ellis-Davies, G.C.R., Nemoto, T., Miyashita, Y., Iino, M., Kasai, H. (2001). Dendritic spine geometry is critical for AMPA receptor expression in hippocampal CA1 pyramidal neurons. *Nature*. 4(11):1086-1092.
50. Matsuzaki, M., Honkura, N., Ellis-Davies, G. C., & Kasai, H. (2004). Structural basis of long-term potentiation in single dendritic spines. *Nature*, 429(6993), 761
51. Matus, A. (2000). Actin-based plasticity in dendritic spines. *Science*, 290(5492), 754-758.
52. Meng, Y., Zhang, Y., Tregoubov, V., Janus, C., Cruz, L., Jackson, M., Lu, W., MacDonald, Y. J.F., Wang, J.Y. et al (2002). Abnormal spine morphology and enhanced LTP in LIMK-1 knockout mice. *Neuron*, 35: 121-133
53. Mohrmann, R., Lessmann, V., & Gottmann, K. (2003). Developmental maturation of synaptic vesicle cycling as a distinctive feature of central glutamatergic synapses. *Neuroscience*, 117(1), 7-18.
54. Montgomery, J. M., Zamorano, P. L., & Garner, C. C. (2004). MAGUKs in synapse assembly and function: an emerging view. *Cellular and Molecular Life Sciences CMLS*, 61(7-8), 911-929.
55. Mulkey, R. M., & Malenka, R. C. (1992). Mechanisms underlying induction of homosynaptic long-term depression in area CA1 of the hippocampus. *Neuron*, 9(5), 967-975.
56. Nägerl, U. V., Eberhorn, N., Cambridge, S. B., & Bonhoeffer, T. (2004). Bidirectional activity-dependent morphological plasticity in hippocampal neurons. *Neuron*, 44(5), 759-767
57. Nakayama, T., Yaoi, T., Yasui, M., & Kuwajima, G. (1998). N-copine: a novel two C2-domain-containing protein with neuronal activity-regulated expression. *FEBS letters*, 428(1-2), 80-84.
58. Nakayama, A. Y., Harms, M. B., & Luo, L. (2000). Small GTPases Rac and Rho in the maintenance of dendritic spines and branches in hippocampal pyramidal neurons. *Journal of Neuroscience*, 20(14), 5329-5338.
59. Nakayama, T., Yaoi, T., & Kuwajima, G. (1999). Localization and subcellular distribution of N-copine in mouse brain. *Journal of neurochemistry*, 72(1), 373-379.
60. Nicoll, R. A., & Malenka, R. C. (1995). Contrasting properties of two forms of long-term potentiation in the hippocampus. *Nature*, 377(6545), 115.
61. Roberson, E. D., English, J. D., Adams, J. P., Selcher, J. C., Kondratieff, C., & Sweatt, J. D. (1999). The mitogen-activated protein kinase cascade couples PKA and PKC to cAMP response element binding protein phosphorylation in area CA1 of hippocampus. *Journal of Neuroscience*, 19(11), 4337-4348.
62. Rumbaugh, G., Adams, J. P., Kim, J. H., & Huganir, R. L. (2006). SynGAP regulates synaptic strength and mitogen-activated protein kinases in cultured neurons. *Proceedings of the National Academy of Sciences*, 103(12), 4344-4351.

63. Park, E., (2003). The Shank Family of postsynaptic density proteins interacts with and promotes synaptic accumulation of the beta PIX guanine nucleotide exchange factor for Rax1 and Cdc42. *J Biol. Chem.* 278 (21): 19220-19229.
64. Pastalkova, E., Serrano, P., Pinkhasova, D., Wallace, E., Fenton, A.A., Sacktor, T.C. (2006). Storage of spatial information by the maintenance mechanism of LTP. *Science*. 313: 1141- 1144.
65. Perestenko, P., Watanabe, M., Beusnard-Bee, T., Guna, P., & McIlhinney, J. (2015). The second C2-domain of copine-2, copine-6 and copine-7 is responsible for their calcium-dependent membrane association. *The FEBS journal*, 282(19), 3722-3736.
66. Perestenko, P. V., Pooler, A. M., Noorbakhshnia, M., Gray, A., Bauccio, C., & Jeffrey McIlhinney, R. A. (2010). Copines-1,-2,-3,-6 and-7 show different calcium-dependent intracellular membrane translocation and targeting. *The FEBS journal*, 277(24), 5174-5189.
67. Pfeiffer, B. E., & Huber, K. M. (2006). Current advances in local protein synthesis and synaptic plasticity. *Journal of Neuroscience*, 26(27), 7147-7150.
68. Reinhard, J. R., Kriz, A., Galic, M., Angliker, N., Rajalu, M., Vogt, K. E., and Ruegg, M. A. (2016). The calcium sensor Copine-6 regulates spine structural plasticity, learning, and memory. *Nat. Commun.* 7, 11613.
69. Saneyoshi, T., Wayman, G., Fortin, D., Davare, M., Hoshi, N., Nozaki, N., ... & Soderling, T. R. (2008). Activity-dependent synaptogenesis: regulation by a CaM-kinase kinase/CaM-kinase I/ $\beta$ PIX signaling complex. *Neuron*, 57(1), 94-107.
70. Saneyoshi, T., Fortin, D. A., & Soderling, T. R. (2010). Regulation of spine and synapse formation by activity-dependent intracellular signaling pathways. *Current opinion in neurobiology*, 20(1), 108-115.
71. Scheiffele, P. (2003). Cell-cell signaling during synapse formation in the CNS. *Annual review of neuroscience*, 26(1), 485-508.
72. Seeburg, P. H. (1996). The role of RNA editing in controlling glutamate receptor channel properties. *Journal of neurochemistry*, 66(1), 1-5.
73. Sheng, M., & Kim, M. J. (2002). Postsynaptic signaling and plasticity mechanisms. *Science*, 298(5594), 776-780.
74. Shi, S., Hayashi, Y., Esteban, J.A., Malinow, R. (2001). Subunit-specific rules governing AMPA receptor trafficking to synapses in hippocampal pyramidal neurons. *Cells*. 105: 331-343.
75. Silva, A.J., Paylor, R., Wehner J.M., Tonegawa S. (1992). Impaired spatial learning in  $\alpha$ -calcium-calmodulin kinase II mutant mice. *Science*. 257: 206-211.
76. Song, I., & Huganir, R. L. (2002). Regulation of AMPA receptors during synaptic plasticity. *Trends in neurosciences*, 25(11), 578-588.
77. Star, E. N., Kwiatkowski, D. J., & Murthy, V. N. (2002). Rapid turnover of actin in dendritic spines and its regulation by activity. *Nature neuroscience*, 5(3), 239.
78. Südhof, T. C., & Malenka, R. C. (2008). Understanding synapses: past, present, and future. *Neuron*, 60(3), 469-476.
79. Takumi, Y., Ramírez-León, V., Laake, P., Rinvik, E., & Ottersen, O. P. (1999). Different modes of expression of AMPA and NMDA receptors in hippocampal synapses. *Nature neuroscience*, 2(7), 618.
80. Tashiro, A., Yuste, R. (2004). Regulation of dendritic spine motility and stability by Rac1 and Rho kinase: evidence for two forms of spine motility. *Mol Cell Neurosci*, 26: 429-440.
81. Tomsig, J. L., & Creutz, C. E. (2000). Biochemical characterization of copine: a ubiquitous  $\text{Ca}^{2+}$ -dependent, phospholipid-binding protein. *Biochemistry*, 39(51), 16163-16175.
82. Tomsig, J. L., & Creutz, C. E. (2002). Copines: a ubiquitous family of  $\text{Ca}^{2+}$ -dependent phospholipid-binding proteins. *Cellular and Molecular Life Sciences CMLS*, 59(9), 1467-1477.
83. Tomsig, J. L., Snyder, S. L., & Creutz, C. E. (2003). Identification of targets for calcium signalling through the copine family of proteins. Characterization of a coiled-coil copine-binding motif. *Journal of Biological Chemistry*.

84. Wenthold R.J., Petralia, R.S., Bahos II J., Niedzielski, A.S., (1996). Evidence for multiple AMPA receptor complexes in hippocampal CA1/CA2 neurons. *J. Neurosci.* 16: 1982-1989.
85. Whitlock, J. R., Heynen, A. J., Shuler, M. G., & Bear, M. F. (2006). Learning induces long-term potentiation in the hippocampus. *Science*, 313(5790), 1093-1097.
86. Woolfrey, K. M., & Srivastava, D. P. (2016). Control of dendritic spine morphological and functional plasticity by small GTPases. *Neural plasticity*, 2016.
87. Yuste, R. and Bonhoeffer T. (2001). Morphological changes in dendritic spines associated with long-term synaptic plasticity. *Annu Rev Neurosci.* 24: 1071-89.
88. Yuste, R., & Bonhoeffer, T. (2004). Genesis of dendritic spines: insights from ultrastructural and imaging studies. *Nature Reviews Neuroscience*, 5(1), 24.
89. Ziv, N. E., & Smith, S. J. (1996). Evidence for a role of dendritic filopodia in synaptogenesis and spine formation. *Neuron*, 17(1), 91-102.
90. Zhou, Q., Homma, K. J., & Poo, M. M. (2004). Shrinkage of dendritic spines associated with long-term depression of hippocampal synapses. *Neuron*, 44(5), 749-757.

## 4 Aim of the Thesis

Synaptic plasticity is a complex mechanism that is not completely understood, however it is well known that calcium acts as an important trigger for this mechanism. An interesting candidate that seems to have a role in the synaptic plasticity is known as Copine-6. Interestingly, Copine-6 is expressed exclusively in the brain and possesses the ability to bind to phospholipids in a calcium-dependent manner. Therefore, we aim to investigate the role of the calcium binding of Copine-6 in regulating structural plasticity and synapse function in an *in vivo* model. For this end, a knock-in mouse model was generated based on the previous finding that mutation of aspartate at position 167 to asparagine renders Copine-6 (called Copine-6<sup>D167N</sup>) insensitive to calcium and thus is incapable of translocating to the postsynaptic spines upon calcium influx in hippocampal neurons. Utilizing a series of *in vitro* and *in vivo* experiments, including cultured primary hippocampal neurons, brain sections and live imaging methods we want to analyze the Copine-6<sup>D167N</sup> phenotype and establish the *in vivo* importance of the calcium binding to Copine-6 in the synaptic plasticity mechanism.

## 5. Results

**5.1 Manuscript 1:** “Mutation in the second C2 domain of Copine-6 cause changes in dendritic spines structural plasticity and strengthening and affects neuronal morphology”

**Mutation in the second C2 domain of Copine-6 cause changes in dendritic spine structural plasticity and strengthening and affects neuronal morphology**

Diana Flores Dominguez<sup>1</sup>, Judith R. Reinhard<sup>1</sup>, and Markus A. Rüegg<sup>1\*</sup>

<sup>1</sup>Biozentrum, University of Basel, Basel, Switzerland

**Key words:**    **Synaptic plasticity · calcium signaling · Copine-6 · de novo point mutation· structural Plasticity · dendritic spines · dendritic simplification**

**\*Corresponding author:**

Markus A. Rüegg  
Biozentrum  
University of Basel  
Klingelbergstrasse 70  
CH-4056 Basel  
Switzerland

Email: markus-a.ruegg@unibas.ch  
Phone: +41 61 207 22 23  
Fax: +41 61 207 22 08

## ABSTRACT

The process of learning and memory correlates with changes of synapse structure and function in response to specific patterns of neuronal activity. The initial trigger of the synaptic changes at excitatory synapses is a transient increase of calcium in the postsynaptic spine. Copine-6 is a calcium-sensitive, phospholipid-binding protein that translocates to the membrane in postsynaptic spines upon calcium influx and is required for hippocampal long-term potentiation, learning and memory in mice. Moreover, Copine-6 is also required for spine structural plasticity. Here, we mutated the calcium-binding site in Copine-6 and generated knock-in mouse mutants. Hippocampal neurons of homozygous and heterozygous Copine-6 mutant mice show changes in spine structure and dendritic maintenance in culture and *in vivo*. Time-lapse imaging shows that cultured hippocampal neurons from the calcium-insensitive mutant mice are more motile and are non-responsive to stimuli triggering spine structural plasticity. These results are strong evidence that calcium-binding of Copine-6 is important for its function. The finding that spine structures are changed in the hippocampus of the mice expressing the calcium mutant but not in those deficient for Copine-6 suggests a dominant-negative role of the calcium mutant.

## INTRODUCTION

Learning and memory are based on experience-dependent adjustments of neural circuits. There is strong evidence that the initial triggering events of learning and memory affect synaptic function. For example, long-term potentiation (LTP) and long-term depression (LTD) are both responses of synapses to particular patterns of neural activity and have both been shown to reflect the changes that occur at the synaptic level during learning and memory. One of the primary triggers for synaptic changes related to learning and memory is the transient increase of calcium in the postsynaptic spine through N-methyl-D-aspartate receptor (NMDAR) followed by activation of Calcium/calmodulin-dependent protein Kinase II (CAMKII) and enhanced  $\alpha$ -amino-3-hydroxy-5-methyl-4-isoxazolepropionic acid receptor (AMPA) subunit insertion. CAMKII is considered a major decoder of  $\text{Ca}^{2+}$  spikes and a key enzyme in activity-dependent synaptic plasticity, enabling learning and memory processes (Schulman and Greengard, 1978; Malinow et al, 1989; Silva et al., 1992; Lisman et. al, 2002, Lisman et al., 2012). However, it was shown that pharmacological inhibition of CAMKII is not sufficient to abolish the spine volume increase after long-term glutamate uncaging (Lee et al., 2009). Furthermore, research from Buard et al. (2010), found in an *in vivo* model that neither stimulated nor autonomous CAMKII activity is required for LTP maintenance or memory storage (Buard et al., 2010). Indeed, many additional molecules have been implicated in the strengthening of synapses. These include Syngap1, extracellular signal regulated kinase ERK/mitogen-activated protein kinase (MAPK), Src Kinase, protein kinase C (PKC) and PKC isozyme (PKM $\zeta$ ) (Sweatt, 2004; Thomas and Huganir, 2004; Kalia et al., 2004; Hrabetova and Sacktor 1996; Ling et al, 2002; Pastalkova et al, 2006; Serrano et al, 2005; Rumbaugh et al. 2006). It is therefore likely that many different molecules can act as “modules” that can be mixed, interconnected, and turned on and off to fine-tune the functional plasticity activity they underlie. Therefore, core components (i.e. NMDAR-Calmodulin-CAMKII) of the calcium-sensing pathway are likely linked to dozens of additional, more specialized molecular participants that fine-tune module operation in a cell-type or synapse-specific manner. Besides, information in the brain can be stored as structural alterations and / or by synapse elimination and formation (Yuste & Bonhoeffer, 2001). As such, in the adult brain, circuit changes are thought to be mediated by both structural and functional plasticity. These changes seem to be regulated by multiple plasticity mechanisms targeting multiple sites of the synaptic biochemical cascades within a larger functionally interconnected neuronal circuit.

Interestingly, *in vivo* approaches (e.g. controlled lesions, pharmacological inactivation or molecular knockouts) that specifically target the hippocampus result in either learning failure or spatial memory loss (Neves, 2008). It is thought that inappropriate loss of synaptic stability may lead to the disruption of neuronal circuits and to brain diseases. Indeed, in different

neurological diseases and pathologies that have a dysfunction in neuronal communication as a hallmark (e.g. mental retardation, schizophrenia, Parkinson's disease, autism, Alzheimer disease), loss of synaptic stability, abnormal density and morphology of dendritic spines, and aberrant synaptic signaling and plasticity occur frequently (Pfeiffer BE et. al., 2009; Stephan KE et. al., 2006; Calabresi P. et. al. 2006; Sudhof TC and Malenka R. 2008; Selkoe DJ, 2009).

Recent data strongly suggest that the novel calcium sensor, Copine-6, plays a fundamental role in synaptic plasticity. Proteomic, mass spectrometry and single cell analyses all demonstrate that Copine-6 is enriched at the postsynaptic level (Susuki et al., 2011; Zeisel et al., 2015; Heo et al., 2018). Copine-6 is a member of a highly conserved protein family composed of two C2 domains that bind phospholipids in a calcium-dependent manner and an A domain at the carboxyl terminus. Importantly, Copine-6 expression is restricted to the brain and, in hippocampal neurons, it is upregulated by experimental manipulations like brief seizure or chemical long-term potentiation (cLTP). We have previously demonstrated that *Cpne6* transcript and Copine-6 protein are expressed in the postnatal mouse brain, reaching peak expression in the hippocampus during synapse formation between postnatal day 7 and 28 (Reinhard et al., 2016). In this study, we also uncovered a novel calcium-sensing role of Copine-6, facilitating the translation of calcium signaling into changes in spine structure. Lack of Copine-6 prevented strengthening of synapses and Copine-6-depleted mice showed impaired hippocampal LTP and hippocampal-dependent learning and memory (Reinhard et al., 2016). Furthermore, mutation of aspartate167 to asparagine prevents the translocation of Copine-6 to the postsynaptic spines upon calcium influx when overexpressed in hippocampal neurons (Reinhard et al., 2016).

Based on these observations, we now aimed at understanding the significance of the calcium binding of Copine-6 for its function at synapses. To this end, we generated knock-in mice that express the Copine-6<sup>D167N</sup> mutant. We now report that unlike wild-type Copine-6, Copine-6<sup>D167N</sup> remains in the cytosol and is not enriched at postsynaptic membranes in the presence of calcium *in vivo*. Importantly, while the overall spine density in hippocampal pyramidal neurons of 6-week-old Copine-6<sup>D167N</sup> mutant mice is not changed, the relative proportion between immature and mature spines is altered. Consistent with this finding, cultured hippocampal neurons expressing Copine-6<sup>D167N</sup> have more immature and less mature protrusions than neurons lacking Copine-6. Cultured hippocampal neurons expressing Copine-6<sup>D167N</sup> fail to undergo synaptic strengthening and display less active synapses after cLTP induction. Finally, Copine-6<sup>D167N</sup> neurons show reduced dendritic complexity *in vivo* and reduced spine volumes *in vitro*. In conclusion, these findings strongly suggest that Copine-6 calcium binding is essential for its function as a modulator of structural plasticity and synaptic function.

## MATERIAL AND METHODS

### Mice

Cpne6<sup>D167N</sup> mice were generated by homologous recombination in embryonic stem cells (75% C57BL/6, 25% 129 Sv) as illustrated in Supplementary Figure S1. The targeting vector contained the genomic *Cpne6* sequence from 5kb upstream of exon 1 until exon 9 with following modifications. A loxP flanked PGK-neo cassette was introduced in the intron between exon 3 and 4. To cause an aspartate (D) to asparagine (N) substitution at amino acid position 167 of Copine-6 the corresponding GAT triplet was exchanged to a AAT. To avoid mis-splicing exon 5 and exon 6 were fused. Additionally, the targeting vector contained a MC1-HSV-TK cassette (for negative selection). Targeted embryonic stem cells were injected into C57BL/6 blastocysts to obtain chimeric mice. Founder mice were intercrossed with Hprt-cre (Cre-deleter) mice to remove the loxP-flanked neo cassette. Presence of the mutation in the founder mice was confirmed by sequencing. Regular genotyping was performed by identification of the removed intron by PCR with the following primers in exon 5 and exon 6: Cpne6D167N fw: 5'-CAG ATT GTG GCT GAG G-3' and Cpne6D167N rv: 5'-TCA CTC TGG TCT CCA TTG GT-3'. All animal experiments were performed in accordance with the Swiss regulations for animal experimentations and were approved by the veterinary commission of the canton Basel-Stadt.

### DNA constructs

The cDNAs encoding GFP and  $\beta$ -actin were cloned from reverse transcribed mRNA isolated from rat brain with following primers: GFP or including STOP codon: as BamHI 5'-CGC GGA TCC TCA TGG GCT GGG GCT GGG-3'.  $\beta$ -actin: ss EcoRI 5'-CCGGAATTCTTCGCCATGGATGAC-3' and as BamHI 5'-CGC GGA TCC GAA GCA TTT GCG GTG CAC-3'. For expression in cultured hippocampal neurons, cDNAs were subcloned into pMH4-SYN-1 (gift from T. G. Oertner, Friedrich Miescher Institute for Biomedical Research, Basel, Switzerland). tdRFP fusion constructs were generated by replacing EGFP with tdRFP sequence as previously described (Reinhard et al., 2016).

### Antibodies

For immunostainings and Western blot analysis, the following antibodies were used: Copine-6 (clone 42, Santa Cruz Cat. sc-136357); GAPDH (Cell Signaling 14C10 Cat. 2118); GluR1 (Calbiochem Cat. PC246-100UG); Na<sup>+</sup>/K<sup>+</sup>-ATPase (GeneTex Cat. GTX22872); MAP2 (Abcam Ab5392); vGLUT1 (Synaptic system Cat. 135 304),  $\beta$ -actin (Cell Signaling, Cat. 4970).

### **Quantitative real-time PCR**

Quantitative real-time PCR was performed on cDNA samples made from RNA collected from hippocampal tissue of 6-week-old mice using SYBR Green Master Mix (Applied Biosystems) on an StepOne Real time PCR detection system (Applied Biosystems). The following primers were used Copine-6s: (5'-CCC CAA GTA CCG AGA CAA GAA GA-3'); Copine-6as: (5'-GGA GGC TGT GAA GTC GAT AGC-3'); PgK1s: (5'- CTC CGC TTT CAT GTA GAG GAA G – 3'); PgK1as: (5' – GAC ATC TCC TAG TTT GGA CAG TG- 3').

### **Tissue preparation from mouse brains**

Hippocampi were dissected on ice and homogenized in lysis buffer (50 mM Tris pH 7.5, 5 mM EDTA, 150 mM NaCl, 1% NP-40, 0.5% sodium deoxycholate, including proteases and phosphatase inhibitors) by glass/Teflon homogenizer. Insoluble material was removed by centrifugation (16,000 x g, 15 min, 4°C). For Western blot analysis, the protein concentration was determined by BCA assay (Pierce) and samples were boiled in SDS-PAGE loading buffer 5 min at 95°C. Equal amounts of total protein were loaded on SDS-PAGE.

### **Primary hippocampal cultures**

Medium high density cultures (~50,000 cells per cm<sup>2</sup>) using the procedures described by Reinhard et al, 2016 with some modifications were used for expression studies. In brief, hippocampal cultures were established from 16.5-day-old fetal murine hippocampi. High density hippocampal primary neuronal cultures were prepared as follows. The hippocampi were dissected from embryonic day E16.5 mice embryos. After dissection in HBSS, hippocampi were washed in ice-cold HBSS. For dissociation, hippocampi were incubated for 12 min in trypsin at 37°C followed by suspension in plating medium (MEM with GlutaMAX, 20% glucose, fetal calf serum and pen/strep). Neurons were plated at a density of 50,000 cells per cm<sup>2</sup> on poly-L-lysine  $\mu$ -Slide 8 well (Cat.No. 80826 IBIDI GMBH). Three hours after plating, medium was exchanged by culture medium (Neurobasal medium, 0.5 mM glutamine, B27 supplement and pen/step). Hippocampal cultures were transfected at DIV7 or DIV14 with Lipofectamine 2000 (Invitrogen) following the manufacturer's instructions. Chemical LTP was induced as described previously (Fortin et al 2004), afterwards cultures were fixed with 4% paraformaldehyde (PFA) in PBS including 120 mM sucrose.

### **Histochemistry and imunohistochemistry**

Mice were transcardially perfused with 4% PFA/PBS and dissected tissue was postfixed overnight in 4% PFA/PBS and dehydrated in 30 % sucrose. Brains were embedded in O.C.T. and cut in 10  $\mu$ m-thick sections in the cryostat. Sections were stained with cresyl-violet. Slices were mounted on glass slides and imaged with Olympus microscope. Immunocytochemistry for GluA1 was performed as described previously (Fortin et al 2004), Ibidi well (Cat.No. 80826

IBIDI GMBH) were mounted with ibidi mounting medium and imaged with Leica SPE confocal microscope.

### **Analysis of spine density and morphology in CA1 neurons**

To analyze the spine density, mice were intercrossed with mice of the mouse line Thy1-mGFP, expressing a membrane-targeted GFP in a subset of CA1 neurons (line 15) De Paola, 2003. . 6-week-old male littermate pairs were transcardially perfused with 4% PFA/PBS, brains were post-fixed overnight in 4% PFA/PBS. Free-floating brain sections were cut in 50  $\mu\text{m}$  on a vibratome Sections were mounted on glass slides and imaged with confocal microscopy (Zeiss LSM700 upright). The entire imaging and analysis procedure was done blinded to genotype. In brief, low-resolution images of CA1 neurons with 1  $\mu\text{m}$  intervals along z-axis were taken. On these stacks, healthy-looking, secondary apical dendritic stretches, which were clearly traceable to the soma, were selected and imaged with high resolution (0.08  $\mu\text{m}$  z-axis intervals, 1,024 x 1,024 pixels, 2.5 x digital zoom). After deconvolution (Huygens Deconvolution software), images were analyzed with NeuronStudio software, a software designed for spine detection and analysis (Wearne et al., 2005; Rodriguez et al. 2008). Automated detection of dendrites and spines were performed and manually adjusted. For classification of spines, default NeuronStudio classification scheme was used. The morphology of neurons (dendritic ramification and Sholl analysis) was analyzed with the filament Tracing module of Imaris software (Bitplane).

### **Live imaging and image analysis**

Microscope pictures were generated with a FEI MORE System microscope and Live imagine acquisition 2.5 software. Cultured neurons were transferred into a life imaging chamber at 37°C, 95% O<sub>2</sub>, and 5% CO<sub>2</sub>. Cells were kept for 210 min under the same conditions and images were recorded every 2.5 minutes. For quantitative spine volume analysis of wild-type and Copine-6<sup>D167N</sup> spines, each frame of a series of pictures (100x, 0.120  $\mu\text{m}$  z-axis intervals) was analyzed using the surface Rendering Volume module of Imaris software (Bitplan). The region of interest was outlined base on the soma and its primary dendrite. Free rotation to a horizontal axis was done in order to get the volume of the spines without any artifact. All quantitative analyses were performed in blind fashion to genotype and treatment.

### **Dendritic spines density and synapses analysis of hippocampal cultured neurons**

Fiji software was used for the analysis of spine density and synapse analysis. Maximal intensity projection images were opened with Fiji to analyze density of the different spine morphology. Different spines morphologies were identified as thin, mushroom or filopodia structures. Afterwards, spine density was determined for each subtype in dendritic stretch of 70  $\mu\text{m}$  length. For the analysis of the synapses, different puncta were identified as vGlut1 (presynaptic),

GluA1 (postsynaptic AMPA subunit) and juxtaposition between vGlut1 and GluA1 (synapses) in a 60  $\mu\text{m}$  dendritic length. The total number of puncta (100%) is the sum of vGlut1 puncta, GluA1 puncta and puncta with an overlap of vGlut1 and GluA1. Analysis was done blinded for the genotype.

### **Spine head volume analysis**

Imaris software was used for the analysis of the spine head volume. After modeling the dendritic spine using the software, volume surface analysis was done automatically. Excel files with the volume data were obtained directly from the software. For the analysis of the delta volume changes, analysis was done as is described by Yasumatsu et al, 2008. In brief, the percentage of spine volume change ( $\Delta$  spine volume/2.5 min) was calculated from the different frames as  $(V_1 - V_0) / V_0 \times 100$ .  $V_0$  represents the starting volume and  $V_1$  is the volume after 2.5 minutes. The values from the previous formula were binned and quantified as number of events, which represents the number of times that the spine volume change fall within the bin. With this formula, spines that shrink generate values  $< 0$ , whereas those that grow result in values  $> 0$ . A total of 68 frames (time 0 to 170 min)

### **Statistical Analysis**

All data are presented as the mean  $\pm$  standard error of the mean (SEM), and are compared using paired Student's  $t$  test, Sidak-Boferroni Post hoc or Wilcoxon matched pairs  $t$  test using Prism software (GraphPad Software, San Diego, CA, USA). Statistical significance was set at  $*p < 0.05$ ,  $**p < 0.01$ ,  $***p < 0.001$ .

## RESULTS

### Mutation of Asp167 to Asn in Copine-6 does not affect protein expression but prevents calcium-mediated binding to phospholipids

Mutation of aspartate at position 167 to asparagine in Copine-6 (Copine-6<sup>D167N</sup>) prevents the calcium-mediated binding to cell membranes and the mutated protein, when overexpressed in hippocampal neurons, does not translocate to postsynaptic membranes upon NMDA receptor-mediated calcium influx (Reinhard et al., 2016). As these data suggested that calcium binding might be important for the function of Copine-6, we generated a knock-in mouse that bears the same point mutation (**Supplementary Figure S1**). These mice, referred to as Cpne6<sup>D167N</sup> mice, did not show any overt phenotype (**Figure 1A, B**). Since Copine-6 is predominately expressed in the hippocampus, we also examined the overall hippocampal structure of wild-type (Wt) and Cpne6<sup>D167N</sup> mice. The gross structure and layering of the adult brain and hippocampus was similar in both genotypes as determined by histological examination of Nissl-stained, coronal brain sections (**Figure 1C**). RT-qPCR and Western blot analysis on wild-type, hetero- and homozygous knock-in mice assured that any possible phenotype in the mutant mice was not based on changes in gene or protein expression (**Figure 1D**).

As Copine-6 translocates to membranes in a calcium-dependent manner (Nakayama et al 2001, Reinhard et al 2016), we examined whether mutation of the calcium binding site would also abolish membrane binding *in vivo*. Hippocampal tissue from wild-type, hetero- and homozygous Cpne6<sup>D167N</sup> mice were lysed with a hypotonic buffer and then submitted to differential centrifugation to isolate a cytosolic (S2) and a membrane (P2) fraction (**Figure 2A**). As previously shown (Reinhard et al., 2016), a substantial amount of Copine-6 in wild-type mice co-fractionated with the membrane fraction in the presence of 2 mM calcium, while the majority of Copine-6 appeared in the cytosolic fraction in the presence of 2 mM EDTA (**Figure 2B**). In contrast, Copine-6 immunoreactivity was mainly associated with the cytosolic fraction in Cpne6<sup>D167N</sup> mice, irrespective of the presence or absence of calcium (**Figure 2B**). Quantification of the relative amount of Copine-6 in the cytosolic and the membrane fraction confirmed this (**Figure 2C**). As expected, the amount of Copine-6 detected in the membrane fraction in the presence of calcium, was also lower in the heterozygous Cpne6<sup>D167N</sup> mice (+/Cpne6<sup>D167N</sup>) than in wild-type mice (**Supplementary Figure 2A, B**). These experiments are in line with previous *in vitro* data (Reinhard et al. 2016) and they show that mutation of one single amino acid in the second C2 domain of Copine-6 mutant is sufficient to abolish calcium-dependent phospholipid binding *in vivo*.

## **Abrogated calcium binding of Copine-6 alters spine morphology in favor of thin spines and filopodia**

As Copine-6 is involved in spine structural plasticity (Reinhard et al., 2016), we next wanted to know whether abrogation of the calcium-binding site in Copine-6 would affect spine structure. In a first step, we analyzed dendritic spine morphology of primary hippocampal neurons from wild-type and *Cpne6*<sup>D167N</sup> mice. Dendritic spine morphologies were classified as filopodia, thin or mushroom structures by co-transfecting neurons with expression constructs coding for  $\beta$ -actin-tdRFP (spine marker) and GFP (volume marker) (**Figure 3A**). Dendritic spines showing co-localization of both markers (yellow in **Figure 3A**) were analyzed at day 14 (day in vitro; DIV) and DIV 21. The morphology of the spines was classified as filopodia-like, thin or mushroom-like as described (Peter and Kaiserman-Abramof 1970; Harris et al., 1992; Fiala et al., 1998; Hering & Sheng 2001) and the number of each class of spines was determined in a segment of 70  $\mu$ m. At DIV 14, wild-type and *Cpne6*<sup>D167N</sup> expressing neurons did not show a difference in the density of filopodia and thin spines but in the mushroom-like spines (**Figure 3B; Supplementary figure S3B**). At DIV 21, the density of mushroom-like spines increased strongly in wild-type neurons compared to DIV 14, making this spine-type the most frequent one. In contrast, maturation of spines was largely delayed in *Cpne6*<sup>D167N</sup> neurons as there were still many filopodia- and thin-like spines at DIV 21 (**Figure 3B; Supplementary figure S3B**).

### **Abrogation of calcium-binding in Copine-6 affects spine motility**

Several lines of evidence show that motility differs between spines. Such intrinsic fluctuations might reflect a lack of structural stability, higher motility and immaturity (Dunaevsky et al., 1999; Bonhoeffer and Yuste, 2002; Yasumatsu et al., 2008; Bhatt et al., 2009). For example, *in vivo* and *in vitro* studies have shown that motility decreases after synaptogenesis and, conversely, spines are more motile when the input is either immature or lacking (Fischer et al., 1998; Lendvai et al., 2000; Mayewska and Sur, 2003). To understand whether abrogation of Copine-6 calcium binding correlates with immaturity of the spines, we studied next the motility of dendritic spines in wild-type and *Cpne6*<sup>D167N</sup> hippocampal neurons. Utilizing live-cell imaging techniques, we tracked the spatiotemporal dynamics of dendritic spine volume changes as an indicator of motility. Time-lapse imaging experiments were performed on DIV 14 neurons transfected to express GFP (as a volume marker) and  $\beta$ -actin-tdRFP (as marker for dendritic spines). Confocal images were collected at an interval of 2.5 min for 170 min. Subsequent analysis was restricted to spines that persisted for the entire time of recording and that appeared healthy (e.g. no blebbing). Moreover, only spines that showed a clear enrichment of  $\beta$ -actin-tdRFP were included in the analysis thus excluding any filopodia-like spines. Interestingly, we observed that dendritic spines predominantly exhibited amorphous changes in shape, known as morphing (Dunaevsky et al., 1999; Fischer et al., 1998), and also they

formed thin processes from the spine head (**Figure 4A**). Statistical analysis revealed that the mean spine head volume was significantly bigger in neurons from wild-type than from Cpne6<sup>D167N</sup> mice (**Figure 4B**). Motility of individual dendritic spines was calculated by measuring the spine volume at time zero ( $V_0$ ) and 2.5 minutes later ( $V_1$ ), which represents the next recording. The percentage of volume change ( $\Delta$  spine volume/2.5 min) was then calculated as  $(V_1 - V_0) / V_0 \times 100$ . With this formula, spines that shrink generate values  $< 0$ , whereas those that grow result in values  $> 0$ . To compare the  $\Delta$  spine volume/2.5 min between wild-type and Cpne6<sup>D167N</sup> neurons, we binned the values and generated a frequency plot (**Figure 4C**). The majority of spines of the wild-type neurons did not show big changes in  $\Delta$  spine volume/2.5 min ( $> 70\%$  are found in the -20 to +20 class). There were significantly fewer spines in the Cpne6<sup>D167N</sup> neurons that were stable in expense to an increased number of spines with higher motility (**Figure 4C**). These data clearly show that spines of hippocampal neurons isolated from Cpne6<sup>D167N</sup> mice are more motile than those from wild-type mice. These results are consistent with the result that Cpne6<sup>D167N</sup> neurons have more immature spines than wild-type neurons.

### **Primary hippocampal neurons from Cpne6<sup>D167N</sup> do not undergo structural changes after cLTP**

We next sought to determine whether Copine-6 calcium binding also affects synapse strengthening. Accordingly, we induced NMDAR-dependent structural spine plasticity in primary hippocampal cultures using a cLTP protocol that specifically stimulates NMDARs at synapses and has been shown to cause NMDAR-dependent increase in spine size (Fortin et al. 2010), similar to the changes triggered by LTP-inducing high frequency stimulations (Desmond & Levy 1990; Matsuzaki et al. 2004; Calverly & Jones 1990; Wallace et al 1991). To quantify changes in spine morphology after cLTP induction, hippocampal neurons from wild-type and Cpne6<sup>D167N</sup> mice were transfected with  $\beta$ -actin-tdRFP and GFP at DIV 14. Induction of cLTP was subsequently performed at DIV 21. Individual, transfected neurons were imaged and dendritic spine morphology was analyzed (**Figure 5A**). Quantification showed that cLTP induced a significant increase in the density of mushroom-shaped spines in Wt hippocampal neurons (**Figure 5A, right**); an effect that has been shown to be associated with mature spines (Papa et al., 1995; Hosokawa et al., 1995; Fortin et al., 2010). Conversely, cLTP induction failed to increase mushroom-like spine density in hippocampal neurons from Cpne6<sup>D167N</sup> mice (**Figure 5A, right**).

Spine morphology is intimately linked with synapse function as larger spines possess bigger PSD (post synaptic density) and hence higher amounts of plasticity-related molecules (Desmond & Levy 1986; Harris & Stevens 1989; Matsuzaki et al 2001). The structural changes along with a failure to maintain mature dendritic spines in Cpne6<sup>D167N</sup> mice suggested that

synaptic function may also be affected. Therefore, we examined the increase in surface GluA1 (AMPA receptor subunit) in juxtaposition with the vesicular glutamate transporter 1 (vGLUT1; excitatory presynaptic protein) in Wt and Cpne6<sup>D167N</sup> hippocampal cultures after cLTP induction (**Figure 5B**). GluA1 is known to translocate into spines after synaptic plasticity induction and its synaptic incorporation is necessary for the stable increase in spine size and synaptic strength in paradigms of NMDAR-dependent plasticity (Kopec et. al., 2007). Surface GluA1 content was assessed under non-permeabilizing conditions by immunofluorescence microscopy using an antibody directed against the N-terminal, extracellular proportion of the receptor (Fortin et al, 2010). Induction of cLTP resulted in an increase in the number of excitatory synapses, defined by the juxtaposition of vGLUT1 and surface GluA1, in wild-type but not in Cpne6<sup>D167N</sup> neurons (**Figure 5B, right**). In fact, in neurons derived from Cpne6<sup>D167N</sup> mice, the number of excitatory synapses slightly decreased after cLTP induction compared to ACSF condition. Together, these data reveal an association between synapse number and spine expansion, determined by the increase in mushroom-like spine number. This suggests that Copine-6 calcium binding is important for the maintenance of strong synapses and consequently the stability of mature spines.

#### **Filopodia-like protrusions are increased in primary hippocampal neurons from heterozygous Cpne6<sup>D167N</sup> mice after cLTP**

Using the same approach as described above, we also tested whether synapse strengthening was affected in heterozygous Cpne6<sup>D167N</sup> neurons (+/Cpne6<sup>D167N</sup>) (**Supplementary Figure S4A**). We found that the number of mushroom spines was not increased, whereas the number of filopodia-like structures was significantly increased in +/Cpne6<sup>D167N</sup> after cLTP induction compared to wild-type neurons (**Supplementary Figure S4A, right**). It has been established that filopodia like protrusions are important during spine development as they help to find possible connections to further mature and stabilize. To address whether there is a correlation between the number of synapses and the increased number of filopodia-like protrusions after cLTP induction we next analyzed the juxtaposition of the presynaptic marker vGLUT1 and the GluA1, AMPA subunit (**Supplementary Figure S4B**). Our result showed that the number of synapses was significantly lower in +/Cpne6<sup>D167N</sup> compared to wild-type neurons at both treatment conditions (cLTP and ACSF). Second, the cLTP-triggered increase in the number of synapses that could be detected in wild-type mice was completely blocked in +/Cpne6<sup>D167N</sup> neurons (**Supplementary Figure S4B, right**), indicating that although there is half of the Copine-6 wild-type the half Cpne6<sup>D167N</sup> mutation already cause a change in the synaptic activity.

## Pyramidal neurons in Cpne<sup>6D167N</sup> mice show aberrant dendritic spine structure and stunted growth

To assess whether the changes observed *in vitro* also translate into changes in spine structure *in vivo*, we crossed Cpne<sup>6D167N</sup> mice with a Thy-mGFP line (De Paola et al., 2003) in which GFP is expressed in a subset of pyramidal neurons in the CA1 area of the hippocampus (**Figure 6A**). Secondary apical dendrites were imaged at high magnification and the density and morphology of spines in young adult (6 weeks old) were analyzed in wild-type, hetero- and homozygous Cpne<sup>6D167N</sup> mice (**Figure 6B; Supplementary Figure S5A**). As cultured hippocampal neurons from Cpne<sup>6D167N</sup> mice differ in their spine structure, we classified the spines into thin, mushroom and stubby morphological categories according to the program NeuroVision (**Figure 6B, right**). While there was no difference in the overall spine density between wild-type and Cpne<sup>6D167N</sup> mutant mice (**Figure 6C**), morphometric analysis of dendritic spines from Thy-mGFP-Cpne<sup>6D167N</sup> mice showed that CA1 pyramidal neurons contained a higher density of thin spines and a lower density of mushroom spines with no difference in the density of stubby spines compared to wild-type mice (**Figure 6D**). In the case of heterozygous Thy-mGFP-Cpne<sup>6D167N</sup> mutant mice (+/Cpne<sup>6D167N</sup>), we found an increased spine density in +/Cpne<sup>6D167N</sup> mutant mice when compared to wild-type mice (**Supplementary Figure S5B**). The morphometric analysis showed high density of thin spines, and decrease density of stubby spines compared to wild-type (**Supplementary Figure S5C**).

Finally, we also assessed whether the loss of calcium binding in Copine-6 affected the overall morphology of pyramidal neurons. Firstly, dendritic ramifications of pyramidal neurons from the CA1 of Wt and Cpne<sup>6D167N</sup> mice were analyzed using the IMARIS filament tracer (**Figure 7A, B**). We found that both basal and apical dendritic branch points were reduced in Cpne<sup>6D167N</sup> mice compared to wild-type mice (**Figure 7C**). A further analysis of the complexity of the basal and apical dendrites of pyramidal neurons of the CA1 area was conducted by Sholl analysis (see **Supplementary Figure S6** for details). This Sholl curve analysis showed that both the basal and apical dendritic trees from Cpne<sup>6D167N</sup> mice were markedly less complex than those from the wild-type mice (**Figure 7D**). Specifically, at radii at the distance between 40 and 60  $\mu\text{m}$  away from the soma, the number of intersections was significantly lower in basal dendrites of the Cpne<sup>6D167N</sup> mice than in controls (**Figure 7D, left**). A lowering of the number of intersections in Cpne<sup>6D167N</sup> mice was also observed on the apical dendrites at a distance of 80 to 100  $\mu\text{m}$  (**Figure 7D, right**). The significant reduction in branching and intersections of pyramidal neurons from the CA1 area of Cpne<sup>6D167N</sup> mice demonstrates reduced dendritic complexity, strongly suggesting that abrogation of calcium binding in Copine-6 may indirectly restrict dendritic complexity.

## DISCUSSION

Copine-6 has been identified as a calcium-sensor regulating mechanisms involved in synaptic plasticity (Reinhard et al 2016; Burk et al 2018). Due to the similarity of Copine-6 to other calcium sensors (e.g. synaptotagmin, PKC, and Doc2) and the finding that it translocate to dendritic spines in a calcium-dependent manner after NMDAR activation (Reinhard et al., 2016), we here asked whether Copine-6 calcium binding is a key functional component required for its role in synaptic plasticity. Utilizing a series of *in vitro* and *in vivo* experiments, we demonstrate that in the knock-in Cpne6<sup>D167N</sup> mouse model, Copine-6 cannot localize to the postsynaptic area of hippocampal synapses in a calcium-dependent manner, we show that the density of mature spines is reduced while that of immature spines increases. Finally, cultured hippocampal neurons from the mutant mice do not undergo synaptic strengthening after potentiation and pyramidal CA1 neuronal complexity is decreased.

We found that a single amino acid change of Asp167 to Asn in the C2 domain was sufficient to prevent calcium/phospholipid-dependent translocation of Copine-6 in the knock-in mice (**Figure 2**). Although done in neurons, our results are consistent with an early report overexpressing a Copine-6 calcium insensitive mutant, which shows that Ca<sup>2+</sup>-dependent translocation of Copine-6 to the membrane was abolished (Reinhard et al., 2016). Therefore, our work demonstrate for the first time that a point mutation blocks Copine-6 calcium-dependent translocation *in vivo*.

### **Calcium binding to Copine-6 is critical for its modulator function in spine structure plasticity**

Calcium compartmentalization and translocation of Copine-6 in a calcium dependent manner to the dendritic spines suggest a role of Copine-6 in the regulation of spine structural plasticity. We found that Cpne6<sup>D167N</sup> point mutation induces a shift of the dendritic spine morphology from mushroom spines to thin spines (**Figure 3 and 6**). Interestingly, Burk and colleagues also found a reduction in the number of mushroom spines using a Copine-6 mutant (called cpne6CaM), which cannot bind to membranes in a calcium-dependent manner. Although they did not analyze the number of thin spines, they also found an increase in filopodia-like spines in their preparation (Burk et al., 2018). Thin spines have been identified as “learning” spines, and are thought to represent an immature state of dendritic spines (Kasai et al., 2003; Holtmaat et al., 2005; Zuo et al., 2006). Current investigations suggests that when compared to bigger mushroom spines, thin spines are structurally more motile, transient, and have weaker synapses (Kasai et al., 2003; Holtmaat et al., 2005). In addition, spine motility is considered a marker of synaptic maturation as it decreases over time (Dailey & Smith, 1996; Ziv & Smith, 1996). Our results confirm that the immature spines that we observed *in vitro* and *in vivo*, are

also highly motile and possess a small head volume (**Figure 4**), suggesting that mice expressing the Cpne6<sup>D167N</sup> mutant are delayed in neuronal maturation, which may also affect spine maintenance and stability. Besides, increased calcium influx via NMDAR cause Copine-6 to be enriched in dendritic spines, thus Copine-6 calcium binding may be important to strengthen and stabilized potentiated synapses. Using an LTP-inducing paradigm, we show that Cpne6<sup>D167N</sup> neurons fail to undergo strengthening by showing a decreased number of mature spines and excitatory synapses (**Figure 5**). NMDAR-dependent calcium influx can induce LTP and LTD (Lüscher and Malenka, 2012), therefore it seems likely that Cpne6<sup>D167N</sup> immature neurons fail to potentiated after LTP induction and removal or endocytosis of synaptic AMPAR may occur as an LTD response. Interestingly, Burk et al., found in Copine-6 knockdown slices that the initial phase of LTD was increased compared to control (Burk et al., 2018). Therefore, these results suggest that because of abrogated Copine-6 calcium binding there is a decrease in intracellular calcium levels that may cause activation of other pathways (e.g. Phosphatases). Besides, the lack of maturation of Cpne6<sup>D167N</sup> spines may affect spike-timing dependent plasticity (Dan and Poo 2004; Caporale and Dan 2008), consequently the direction of synaptic plasticity between pre- and post-synapses may not coincide with the appropriate timing. These results corroborate that the calcium binding to Copine-6 is crucial for its function as a modulator of synaptic plasticity and consequently important for the stability of spines.

### **Non- synaptic filopodia-like structures are predominant in the heterozygous Cpne6<sup>D167N</sup> mutant mice**

The effect of the heterozygous mice expressing Cpne6<sup>D167N</sup> and one wild-type copy of Copine-6 was also analyze. We found that a proportion of Copine-6 translocate to the membrane fraction in a calcium dependent manner (**Supplementary Figure S2**). This result suggest that a dose effect might occur in the heterozygous Cpne6<sup>D167N</sup>, as 50% of the wild-type Copine-6 still harbor the ability to translocate. However, the remaining 50% from the Cpne6<sup>D167N</sup> mutation seems to be sufficient to cause spine structure changes as in heterozygous Cpne6<sup>D167N</sup> mice there is an increase in spines density, in which thin spines increases seems to occur at expenses of stubby spines (**Supplementary Figure S5**). Although the presence of filopodia-like spines is a distinguishable phenotype of the +/CPNE6<sup>D167</sup> neurons, we did not find any significant morphological differences in our *in vitro* data (**Supplementary Figure S3**). A possible explanation might be that the number of experiments needs to be increase to get a significant result. Nevertheless, these results suggest a dominant-negative effect by the 50% of the calcium insensitive mutation, which seems to be enough to affect Copine-6 function as a modulator of synaptic plasticity. Interestingly, cLTP-inducing paradigms caused an increase in non-synaptic filopodia-like spines in the +/Cpne6<sup>D167N</sup> neurons (**Supplementary Figure S4**).

Although, we could not detect a decrease in mushroom spines, our results are similar to the increase of filopodia-like structures in Copine-6 knockdown neurons (Burk et al., 2018). Based on this, the effect observed in the heterozygous Cpne6<sup>D167N</sup> mice may be based on the expression of only 50% of the wild-type Copine-6. However, a dominant-negative effect of the mutant Copine-6 is more likely, as overexpression of the calcium mutant in the wild-type background also affect spine size adjustments after cLTP (Reinhard et al., 2016) and that heterozygous Copine-6 knockout mice do not show a similar phenotype as the heterozygous Cpne6<sup>D167N</sup> mice (unpublished data). In addition, the increase in filopodia-like spines suggest a compensatory mechanism that may be related with a recapitulation of a developmental stage, which is use to revert the 50% of the Cpne6<sup>D167N</sup> mutation by trying to establish new connections. Therefore, the heterozygous Cpne6<sup>D167N</sup> seems to undergo a process of sampling, resampling, rewiring and refining, which is necessary to generate a well-tuned mature network. However, spines in the heterozygous Cpne6<sup>D167N</sup> mice might become destabilized, as there is less calcium influx and translocated Copine-6. In addition, the calcium mutant could scavenge Rac1 and thus keep this GTPase away from the postsynaptic spines. This in turn, could revert spines to filopodia-like structures that consequently cannot be potentiated and are further eliminated. All together, these results support the previous finding in the homozygous Cpne6<sup>D167N</sup>, demonstrating that Copine-6 calcium binding is crucial for the maintenance and stabilization of synapses.

### **Abrogation of calcium binding to Copine-6 cause changes in neuronal complexity, implying that learning and behavioral abilities might be affected**

It is known that subtle changes in dendritic or synaptic structure can lead to changes in information processing, causing a remodeling of the neuronal circuitry (Holmaat & Svoboda, 2009; Penzes et al, 2011). Therefore, spine morphology and dendritic arborisation are key determinants of neuronal connectivity and play critical roles in learning, memory and behavioral function. Here, we found a decrease in dendritic branching and intersections of Cpne6<sup>D167N</sup> pyramidal neurons *in vivo* (**Figure 7**). In addition, Cpne6<sup>D167N</sup> neurons showed significantly less apical dendritic complexity at 100 µm from the soma into the stratum radiatum region, which is a functionally distinct compartment receiving strong inputs from the CA3 region via Schaffer Collaterals. Consequently, it seems that when Cpne6<sup>D167</sup> fails to stablish mature contacts there is a profound effect that may led to formation of immature structures that will indirectly fail to keep a well-tuned mature network (**Supplementary Figure S7**). Suggesting that Copine-6 calcium binding indirectly promotes dendritic complexity, by maintaining mature synapses that are able to integrate synaptic inputs.

Besides, we found that the point mutation of Copine-6 does not cause any differences in body and brain mass, along with gross morphology of the brain and hippocampus (**Figure 1**). Although differences in structural morphology are observed in various mouse models of neurological disorders (e.g. Alzheimer Disease, Fragile X syndrome, and Autism), other parameters such as changes in dendrites, spine morphology and potentiation (Kaufmann & Moser 2000; Fiala et al., 2002) also correlate with impaired synaptic plasticity and learning and memory. For example, studies of Fragile-X syndrome (FXS) mouse models have shown a correlation between spine morphology, neuron functionality and behavior, supporting the importance of proper dendritic spine morphology and density for normal synaptic plasticity and behavior (Nosyreva and Huber, 2006; Comery et al., 1997; Pilpel et al., 2009). Furthermore, reduction in the size and complexity of dendritic arbors are common in disorders associated with intellectual disability (Kaufmann and Mosser, 2000). The structural-morphological changes observed in *Cpne6*<sup>D167N</sup> mice suggest that Copine-6 calcium binding is essential for its basal function at synapses. Interestingly, *CPNE6* (encoding Copine-6) has been mapped as a possible candidate gene involved in intellectual disability resulting from a missense mutations in a specific locus of the Von Willebrand A domain (vWFA) (Anazi et al, 2017). Moreover, Copine-6 has also been related with other neurological disorders, such as depression and refractory epilepsy, as both syndromes are correlated with decreased levels Copine-6 and a loss of strength or plasticity and increased levels of Copine-6 with hyperactivity of synapses, respectively (Han et al., 2018; Zhu et al., 2016; Lai et al., 2016). These investigations support a role of Copine-6 as an important regulator of hippocampal synaptic plasticity, with a possible role in hippocampal learning and memory.

**The calcium-binding site is key for the function of Copine-6 as its mutation has a more profound effect in synaptic plasticity than the complete abolishment of Copine-6.**

Increase of calcium after the NMDA activation, and the further activation of CAMKII is the best characterized molecular mechanism related to the strengthening of excitatory synapses. Moreover, the T286 autophosphorylation site of CAMKII is thought to act as a molecular switch, which translated the increase postsynaptic calcium level into kinases signaling (De Koninck and Schulman 1998; Giese et al., 1998). Interestingly, Copine-6 bears some functional similarity to CAMKII, like its activation via the NMDAR calcium influx and its recruitment ability into active spines (Shen and Meyer, 1999; Lee et al., 2009). Here we identified the Copine-6 calcium-binding site as a possible molecular switch acting as a sensor of calcium levels and further initiating signaling cascades important for synaptic function. The phenomenon observed in the different phenotype in mice expressing a phosphorylation mutant of CaMKII compared to mice deficient of CaMKII (Giese et al., 1998) is similar to our finding of a more

profound effect by the calcium site abrogation than the complete elimination of Copine-6. This base on that the knockout Copine-6 model shows no difference in basal synaptic function compare to the knock-in calcium insensitive mutant. One possible explanation that complete loss of Copine-6 does not affect spine structure could be a partial compensation by other copines. For example, Copine-4 and -7 are known to be expressed in the brain (Tomsig and Creutz, 2002) and to respond to calcium/phospholipid binding (Perestenko et al., 2010, Perestenko et al., 2015). Copines have different affinities for calcium; therefore, their translocation to membranes might occur at different rates, causing them to respond to different patterns of neuronal activity. It might be that Copine-7 cannot cope with the increase amount of calcium and consequently fail to keep synapses strengthened. Further, the proper localization of proteins is critical for their correct functioning (Hung and Link, 2011). We show that a single amino acid change affects the subcellular localization of Copine-6 and proteins interactions, situation that can either reduce - loss of function- or induce -gain of function- a specific protein localization. Copine-6 seems to rely on its ability to translocate to the dendritic spines in a calcium-dependent manner, where it acts as a calcium sensor and is engaged with signaling molecules that have an important role in synaptic plasticity - e.g. BDNF/TrkB/ERK, Rac1/Cofilin/Actin - (Burk et al., 2018; Reinhard et al., 2016). Therefore, the inability of Copine-6 to translocate to spines might affect the signaling efficiency of those proteins involved in the synaptic structural plasticity. On the other hand, it is also possible that mislocalization of these proteins may trigger other interactions that cause an impairment of the synaptic mechanism.

In addition, Copine-6 has been mainly found in post-synapses (Burk et al., 2018; Reinhard et al., 2016; Bayes et al., 2011; Schrimpf et al., 2005; Nakayama et al., 1999), therefore its role as a modulator of synaptic plasticity seems to be correlated with its localization and translocation via its calcium sensor ability (Burk et al., 2018; Reinhard et al., 2016). Recently, a publication by Liu et al. found Copine-6 in the pre-synapses where it acted as a calcium sensor regulator of spontaneous neurotransmitter release by its interaction with syb2 (Liu et al., 2018). They claim that Copine-6 can act as a SNARE protein in pre- and post-synapses, a phenome observe in other calcium sensors (i.e. syb2) (Jurado et al., 2013). Interestingly, a proteomic analysis from LOT axons (primary axons projected from the olfactory bulb to the lateral surface of the telencephalon) shows that Copine-6 levels are upregulated during early stage (from E14.5-E18.5) of maturation of axonal projections. However, in a further analysis done in primary hippocampal culture neurons they shows that Copine-6 did not reach a significant difference in its expression levels at different developmental stages (E15.5, E. 15.5 and P0) (Yamatani et al., 2010). Important to note is that the analysis was done from cells of different areas, therefore the expression of Copine-6, as well as it function could differ according to that. In this work, we focus on the hippocampus as Copine-6 has been shown to be predominately express in that brain area. Copine-6 is a novel protein and therefore its role

in the CNS need to be further investigating. Regardless of its localization, all these investigations clearly showed that Copine-6 has an important role as a calcium sensor that interacts with other molecules amplifying the signaling cascade.

In conclusion, understanding the molecular mechanism may shed light into the functional and structural changes that occur during synaptic plasticity. Transgenic, knock-in and knockout animal models are becoming increasingly useful for disentangling the roles of pre and post-synaptic structures, as the use of these models allow us to investigate the effect that the mutant gene had, therefore give us insight to understand key functions. Copine-6 has been show to rely on its calcium sensor ability, therefore our knock-in Cpne6<sup>D167N</sup> mouse model allowed us to specifically investigate the effect of the abrogation of the calcium binding of Copine-6. Thanks to the generation of our knock-in mouse model, we can conclude that expression of the calcium mutant in the Cpne6<sup>D167N</sup> mice causes a severe disruption of the maturation, maintenance and potentiation of excitatory synapses and has deleterious consequences on dendritic complexity. Thus, our results suggest that calcium binding to the C2B domain is a key functional component for Copine-6 to act as a sensor switch that regulates synaptic plasticity mechanism.

Here, we demonstrate that this calcium binding of Copine-6 is critical component for its function as a regulator in the synaptic plasticity mechanism and consequently for the spine structure of pyramidal neurons *in vivo*. While Copine-6 has been shown to interact with several signaling pathways that have also been implicated in synaptic function (Reinhard et al., 2016; Burk et al., 2018; Han et al., 2018), it still remains largely upon as to how the calcium mutant affects spine structure *in vivo*. It might be that the presence of multiply pathways enables the cell to selectively regulate individual pathways in response to physiological stimuli and thereby to regulate specific aspect of synaptic function, causing it to be robust. Therefore, it seems that different pathway are needed in order to keep the synaptic mechanism suggesting that one of this pathway may be regulated by Copine-6. One possibility is that the calcium mutant act as a scavenger of those interacting proteins and hence prevents their calcium-dependent transport to synapses.

Finally, the number of immature spines and its relation with ID and neurological disorders identified Copine-6 as a regulator of the synaptic plasticity mechanism, which also imply a role in learning and memory mechanism. Therefore, further investigation should be done to access whether Copine-6 calcium- binding mutation also affects murine learning and memory. Nevertheless, our results opened a new avenue for continuing the investigation of Copine-6 and its role in the synaptic plasticity, learning and memory. The mouse model presented here will allow to further investigate the mechanisms that are involved in this process and may also allow to get more insights into the mechanisms involved in intellectual disability (Anazi et al, 2017) and other neurological diseases in which spine structure and the process

of learning and memory is affected. Such studies might provide new avenues for the molecular understanding of these disorders and may reveal possible therapeutic targets.

## REFERENCE AND NOTES

1. Anazi, S., Maddirevula, S., Faeih E., Alsedairy, H., Alzahrani, F., Shamseldin, H.E., Patel, N., et al. (2017) Clinical genomics expands the morbid genome of intellectual disability and offers a high diagnostic yield. *Mol. Psychiatry*. 22: 615-624.
2. Bayés, À., Van De Lagemaat, L. N., Collins, M. O., Croning, M. D., Whittle, I. R., Choudhary, J. S., & Grant, S. G. (2011). Characterization of the proteome, diseases and evolution of the human postsynaptic density. *Nature neuroscience*, 14(1), 19.
3. Bhatt, D. H., Zhang, S., & Gan, W. B. (2009). Dendritic spine dynamics. *Annual review of physiology*, 71: 261-282.
4. Bonhoeffer, T., & Yuste, R. (2002). Spine motility: phenomenology, mechanisms, and function. *Neuron*, 35(6): 1019-1027.
5. Bourne, J.N., and Harris, K.M. (2008). Balancing structure and function at hippocampal dendritic spines. *Annu. Rev. Neurosci.* 31: 47-67
6. Buard, I., Coultrap, S. J., Freund, R. K., Lee, Y. S., Dell'Acqua, M. L., Silva, A. J., & Bayer, K. U. (2010). CaMKII "autonomy" is required for initiating but not for maintaining neuronal long-term information storage. *Journal of Neuroscience*, 30(24): 8214-8220.
7. Burk, K., Ramachandra B., Saheeb, A., Hurtado-Zavala, J., Awasthi, A., Benito, E., Faram, R., Ahmad, H., Swaminathan, A., McIlhinney J., Fischer, A., Perestenko P., Dean C. (2018). Regulation of dendritic spine morphology in hippocampal neurons by Copine-6. *Cerebral Cortex*. 28: 1087-1104.
8. Calabresi, P., Picconi, B., Parnetti, L., & Di Filippo, M. (2006). A convergent model for cognitive dysfunctions in Parkinson's disease: the critical dopamine–acetylcholine synaptic balance. *The Lancet Neurology*, 5(11), 974-983.
9. Calverley R.K.S., and Jones, D.G. (1990) Contributions of dendritic spines and perforated synapses to synaptic plasticity. *Brain Research Reviews*. 15 (3): 215-249.
10. Caporale, N., & Dan, Y. (2008). Spike timing–dependent plasticity: a Hebbian learning rule. *Annu. Rev. Neurosci.*, 31, 25-46.
11. Comery, T. A., Harris, J. B., Willems, P.J., Oostra, B.A., Irwin, S. A., Weiler, I. J., et al., (1997). Abnormal dendritic spines in the fragile X knock out mice: maturation and pruning deficits. *Proc. Natl. Acad. Sci. U.S.A.* 94: 5401-5404.
12. Dailey M.E., and Smith S.J. (1996) The dynamics of dendritic structure in developing hippocampal slices. *J. Neurosci.* 16 (9): 2983-2994
13. Dan, Y., and Poo, M. M. (2004). Spike timing-dependent plasticity of neural circuits. *Neuron*, 44(1), 23-30.
14. De Paola, V., Arber, S., & Caroni, P. (2003). AMPA receptors regulate dynamic equilibrium of presynaptic terminals in mature hippocampal networks. *Nature neuroscience*, 6(5), 491.
15. De Koninck, P., & Schulman, H. (1998). Sensitivity of CaM kinase II to the frequency of Ca<sup>2+</sup> oscillations. *Science*, 279(5348), 227-230.
16. Desmond, N. L, Levy, W.B. (1990). Morphological correlates of long-term potentiation imply modifications of existing synapses, not synaptogenesis, in the hippocampal dentate gyrus. *Synapse*. 5 (2): 139-143.
17. Dunaevsky, A., Tashiro, A., Majewska, A., Mason, C., and Yuste, R. (1999). Developmental regulation of spine motility in the mammalian central nervous system. *Proc. Natl. Acad. Sci. U. S. A.* 96: 13438-13443.
18. Fiala, J.C., Feinberg, M., Popov, V., and Harris, K.M. (1998). Synaptogenesis via dendritic filopodia in developing hippocampal area CA1. *J. Neurosci.* 18: 8900-8911.
19. Fiala, J.C., Spacek, J., Harris, K.M. (2002) Dendritic spine pathology: cause or consequence of neurological disorders. *Brain Research Reviews*. 39: 29-54.
20. Fischer, M., Kaech, S., Knutti, D., and Matus, A. (1998). Rapid actin-based plasticity in dendritic spines. *Neuron*. 20: 847-854.

21. Fortin, D.A., Davare, M.A., Srivastava, R., Brady, J.D., Nygaard, S., Derkach, V.A., Soderling, T.R. (2010). Long-term potentiation-dependent spine enlargement requires synaptic  $\text{Ca}^{2+}$ - permeable AMPA receptor recruited by CaM-Kinase I. *J. Neurosci.* 30(35): 11565-11575.
22. Giese, K.P., Fedorov N.B., Filipkowski R.K. Silva A.J. (1998). Autophosphorylation at Thr<sup>286</sup> of the  $\alpha$ -calcium-calmodulin kinase II in LTP and Learning. *Science*. 279 (5352): 870-873.
23. Han, Y. X., Tao, C., Gao, X. R., Wang, L. L., Jiang, F. H., Wang, C., ... & Ge, J. (2018). BDNF-related imbalance of Copine 6 and synaptic plasticity markers couples with the depression-like behavior and immune activation in CUMS rats. *Frontiers in neuroscience*, 12, 731.
24. Harris, K.M., and Stevens, J.K. (1989). Dendritic spines of CA1 Pyramidal cells in the rat hippocampus: serial electron microscopy with reference to their biophysical characteristic. *J. Neurosci.* 9(8): 2982-2997.
25. Harris, K. M., Jensen, F. E., & Tsao, B. (1992). Three-dimensional structure of dendritic spines and synapses in rat hippocampus (CA1) at postnatal day 15 and adult ages: implications for the maturation of synaptic physiology and long-term potentiation [published erratum appears in J Neurosci 1992 Aug; 12 (8): following table of contents]. *Journal of Neuroscience*, 12(7): 2685-2705.
26. Heo, S., Diering, G. H., Na, C. H., Nirujogi, R. S., Bachman, J. L., Pandey, A., & Haganir, R. L. (2018). Identification of long-lived synaptic proteins by proteomic analysis of synaptosome protein turnover. *Proceedings of the National Academy of Sciences*, 115(16), E3827-E3836.
27. Hering, H. and Sheng M. (2001) Dendritic spines: structure, dynamics and regulation. *Nat. Rev. Neurosc.* 2 (12): 880-8.
28. Holmaat, A., and Svoboda, K. (2009). Experience-dependent structural synaptic plasticity in the mammalian brain. *Nat. Rev. Neurosci.* 10: 647- 658.
29. Hosokawa, T., Rusakov, D. A., Bliss, T. V., & Fine, A. (1995). Repeated confocal imaging of individual dendritic spines in the living hippocampal slice: evidence for changes in length and orientation associated with chemically induced LTP. *Journal of Neuroscience*, 15(8), 5560-5573.
30. Hrabetova, S., and Sacktor, T.C. (1996). Bidirectional regulation of protein Kinase M $\zeta$  in the maintenance of long-term potentiation and long term depression. *J. Neurosci.* 16(17) :5324-5333.
31. Hung, M. C., & Link, W. (2011). Protein localization in disease and therapy. *J Cell Sci*, 124(20), 3381-3392.
32. Jurado, S., Goswami, D., Zhang, Y., Molina, A. J. M., Südhof, T. C., & Malenka, R. C. (2013). LTP requires a unique postsynaptic SNARE fusion machinery. *Neuron*, 77(3), 542-558.
33. Kalia, L.V., Gingrich, J.R., Salter, M.W. (2004). Src in synaptic transmission and plasticity. *Oncogene*. 23: 8007-8016.
34. Kasai, H., Matsuzaki, M., Noguchi, J., Yasumatsu, N., and Nakahara, H. (2003). Structure-stability-function relationships of dendritic spines. *Trends Neurosci.* 26: 360-368.
35. Kaufmann, W.E., and Moser, H.W. (2000). Dendritic anomalies in disorders associated with mental retardation. *Cerebral Cortex*. 10:981-991.
36. Kopec, C.D., Real, E., Kessels, H.W., Malinow, R. (2007). GluR1 links structural and functional plasticity at excitatory synapses. *J. Neurosci.* 27(50): 13706-13718.
37. Lai, Y., Hu, X., Chen, G., Wang, X., & Zhu, B. (2016). Down-regulation of adenylylate kinase 5 in temporal lobe epilepsy patients and rat model. *Journal of the neurological sciences*, 366, 20-26.
38. Lee, S. J. R., Escobedo-Lozoya, Y., Szatmari, E. M., & Yasuda, R. (2009). Activation of CaMKII in single dendritic spines during long-term potentiation. *Nature*, 458(7236), 299

39. Lendvai, B., Stern, E.A., Chen, B., Svoboda, K. (2000). Experience-dependent plasticity of dendritic spines in the developing rat barrel cortex *in vivo*. *Nature*. 404: 876-881.
40. Ling, D.S.F., Benardo, L.S., Serrano, P.A., Blace, N., Kelly, M.T., Cray, J.F., and Sacktor, T.C. (2002). Protein Kinase M $\zeta$  is necessary and sufficient for LTP maintenance. *Nat Neurosci*. 5: 295-296.
41. Lisman, J., Schulman, H., Cline, H. (2002). The molecular basis of CaMKII function in synaptic and behavioral memory. *Nat. Rev.* 3: 175-190.
42. Lisman, J., Yasuda, R., and Raghavachari, S. (2012). Mechanisms of CaMKII action in long-term potentiation. *Nat. Rev. Neurosci*. 13:169-182.
43. Liu, P., Khvotchev, M., Li, Y. C., Chanaday, N. L., & Kavalali, E. T. (2018). Copine-6 binds to SNAREs and selectively suppresses spontaneous neurotransmission. *Journal of Neuroscience*, 38(26), 5888-5899.
44. Lüscher, C., & Malenka, R. C. (2012). NMDA receptor-dependent long-term potentiation and long-term depression (LTP/LTD). *Cold Spring Harbor perspectives in biology*, a005710.
45. Matsuzaki, M., Ellis-Davies, G.C.R., Nemoto, T., Miyashita, Y., Iino, M., and Kasai H. (2001). Dendritic spine geometry is critical for AMPA receptor expression in hippocampal CA1 pyramidal neurons. *Nat. Neurosci*. 4: 1086-1092.
46. Matsuzaki, M., Honkura, N., Ellis-Davies, G.C., and Kasai, H. (2004). Structural basis of long-term potentiation in single dendritic spines. *Nature*. 429: 761-766.
47. Majewska, A., & Sur, M. (2003). Motility of dendritic spines in visual cortex *in vivo*: changes during the critical period and effects of visual deprivation. *Proceedings of the National Academy of Sciences*, 100(26), 16024-16029.
48. Majewska, A. K., Newton, J. R., & Sur, M. (2006). Remodeling of synaptic structure in sensory cortical areas *in vivo*. *Journal of Neuroscience*, 26(11): 3021-3029.
49. Malinow, R., Schulman, H., Tsien, R.W. (1989). Inhibition of postsynaptic PKC or CaMKII blocks induction but not expression of LTP. *Science*. 245: 862- 865.
50. Matsuzaki, M., Ellis-Davies, G.C.R., Nemoto, T., Miyashita, Y., Iino, M., Kasai, H. (2001). Dendritic spine geometry is critical for AMPA receptor expression in hippocampal CA1 pyramidal neurons. *Nature*. 4(11):1086-1092.
51. Nakayama, T., Yaoi, T., & Kuwajima, G. (1999). Localization and subcellular distribution of N-copine in mouse brain. *Journal of neurochemistry*, 72(1), 373-379.
52. Neves, G., Cooke, S.F., and Bliss T.V.P. (2008). Synaptic plasticity, memory and the hippocampus: a neural network approach to causality. *Nat. Rev. Neurosci*. 9: 65-75.
53. Nosyreva, E.D., and Huber, K.M. (2006). Metabotropic receptor-dependent long-term depression persists in the absence of protein synthesis in the mouse model of fragile X syndrome. *J. Neurophysiol*. 95: 3291-3295.
54. Papa, M., Bundman, M. C., Greenberger, V., & Segal, M. (1995). Morphological analysis of dendritic spine development in primary cultures of hippocampal neurons. *Journal of Neuroscience*, 15(1), 1-11.
55. Pastalkova, E., Serrano, P., Pinkhasova, D., Wallace, E., Fenton, A.A., Sacktor, T.C. (2006). Storage of spatial information by the maintenance mechanism of LTP. *Science*. 313: 1141- 1144.
56. Peters, A., & Kaiserman-Abramof, I. R. (1970). The small pyramidal neuron of the rat cerebral cortex. The perikaryon, dendrites and spines. *American Journal of Anatomy*, 127(4): 321-355.
57. Penzes, P., Cahill, M.E., Jones, K.A., Vanleeuwen, J.E., and Woolfrey, K.M. (2011). Dendritic spine pathology in neuropsychiatric disorder. *Nat. Neurosci*. 14: 285-293
58. Perestenko, P.V., Pooler, A.M., Noorbakhshnia, M., Gray, A. Bauccio, C., and Jeffrey McIlhinney, R.A. (2010). Copines-1,-2,-3,-6 and -7-show different intracellular membrane translocation and targeting. *Febs J*. 277: 5174-5189.
59. Perestenko, P., Watanabe, M., Beusnard-Bee, T., Guna P., and McIlHinney (2015). The second C2-domain of copine-2 copine-6 and copine-7 is responsible for their calcium-dependent membrane association. *Febs J*. 282: 3722-3736.

60. Pilpel, Y., Kolleker, A., Berberich, S., Ginger, M., Frick, A., Mientjes, E., Seeburg, P. H. (2009). Synaptic ionotropic glutamate receptors and plasticity are developmentally altered in the CA1 field of Fmr1 knockout mice. *The Journal of physiology*, 587(4), 787-804.
61. Pfeiffer, B.E., and Huber, K.M. (2009). The state of synapses in Fragile X syndrome. *The Neuroscientist*. 15(5): 549-567.
62. Reinhard, J. R., Kriz, A., Galic, M., Angliker, N., Rajalu, M., Vogt, K. E., and Ruegg, M. A. (2016). The calcium sensor Copine-6 regulates spine structural plasticity, learning, and memory. *Nat. Commun.* 7, 11613.
63. Rumbaugh, G., Adams, J. P., Kim, J. H., and Huganir, R. L. (2006). SynGAP regulates synaptic strength and mitogen-activated protein kinases in cultured neurons. *Proc.Natl. Acad. Sci. U.S.A.* 103 (12): 4344-4351.
64. Schrimpf, S. P., Meskenaite, V., Brunner, E., Rutishauser, D., Walther, P., Eng, J., ... & Sonderegger, P. (2005). Proteomic analysis of synaptosomes using isotope-coded affinity tags and mass spectrometry. *Proteomics*, 5(10), 2531-2541.
65. Schulman, H., and Greengard, P. (1978). Ca<sup>2+</sup> dependent protein phosphorylation system in membranes from various tissues and its activation by "calcium-dependent regulator". *Proc.Natl. Acad. Sci. U.S.A.* 75(11): 5432-5436.
66. Selkoe, D. J., & Hardy, J. (2016/2009). The amyloid hypothesis of Alzheimer's disease at 25 years. *EMBO molecular medicine*. 8(6), 595-608.
67. Serrano, P., Yao, Y., Sacktor, T.C. (2005). Persistent phosphorylation by protein kinase Mζ Maintains late-phase long-term potentiation. *J. Neurosci.* 25(8): 1979-1984.
68. Shen, K., & Meyer, T. (1999). Dynamic control of CaMKII translocation and localization in hippocampal neurons by NMDA receptor stimulation. *Science*, 284(5411), 162-167.
69. Silva, A.J., Paylor, R., Wehner J.M., Tonegawa S. (1992). Impaired spatial learning in α- calcium-calmodulin kinase II mutant mice. *Science*. 257: 206-211.
70. Stephan, K.E., Baldeweg, T., Friston, K.J. (2006). Synaptic plasticity and dysconnection in Schizophrenia. *Biological Psychiatry*. 59(10): 929-939.
71. Sudhof, T.C., and Malenka, R. (2008). Understanding synapses: Past, present, and future. *Neuron*. 60(3):469-476.
72. Suzuki, T., Zhang, J., Miyazawa, S., Liu, Q., Farzan, M. R., & Yao, W. D. (2011). Association of membrane rafts and postsynaptic density: proteomics, biochemical, and ultrastructural analyses. *Journal of neurochemistry*, 119(1), 64-77.
73. Sweatt, J.D. (2004). Mitogen-activated protein kinase in synaptic plasticity and memory. *Curr. Op. in Neurobiology*. 14(3): 311-317.
74. Tomsig, J. L., & Creutz, C. E. (2002). Copines: a ubiquitous family of Ca<sup>2+</sup>-dependent phospholipid-binding proteins. *Cellular and Molecular Life Sciences CMLS*, 59(9), 1467-1477.
75. Thomas, G.M., and Huganir, R.L. (2004). MAPK cascade signalling and synaptic plasticity. *Nat. Rev.* 5: 173-183.
76. Wearne, S.L., Rodriguez, A., Ehlenberger, D. B., Rocher, A. B., Henderson, S.C., and Hof, P. R. (2005). New Techniques for imaging, digitalization and analysis of three-dimensional neuronal morphology on multiple scales. *Neuroscience*. 136: 661-680.
77. Yamatani H., Kawasaki T, Mita S., Inagaki N., Hirata T (2010). Proteomics analysis of the temporal changes in axonal proteins during maturation. *Dev Neurobiol.* 70: 523-537.
78. Yasumatsu, N., Matsuzaki, M., Miyazaki, T., Noguchi, J., and Kasai, H. (2008). Principles of Long-Term Dynamics of Dendritic spines. *J. Neurosci.* 28 (50): 13592-608.
79. Yuste, R. and Bonhoeffer T. (2001). Morphological changes in dendritic spines associated with long-term synaptic plasticity. *Annu Rev Neurosci.* 24: 1071-89.
80. Zeisel, A., Muñoz-Manchado, A. B., Codeluppi, S., Lönnerberg, P., La Manno, G., Juréus, A., ... & Rolny, C. (2015). Cell types in the mouse cortex and hippocampus revealed by single-cell RNA-seq. *Science*, 347(6226), 1138-1142.
81. Ziv, N.E., and Smith, S.J. (1996). Evidence for a role of dendritic filopodia in synaptogenesis and spine formation. *Neuron*.17: 91-102.

82. Zuo, Y., Lin, A., Chang, P., & Gan, W. B. (2005). Development of long-term dendritic spine stability in diverse regions of cerebral cortex. *Neuron*, 46(2), 181-189.
83. Zhu, B., Zha, J., Long, Y., Hu, X., Chen, G., & Wang, X. (2016). Increased expression of copine VI in patients with refractory epilepsy and a rat model. *Journal of the neurological sciences*, 360, 30-36.

**ACKNOWLEDGMENT:** We thank Dr. Daniel J. Ham for his remarks on the manuscript and the Image Core Facility-Biozentrum for technical assistance. **FUNDING:** This work was supported by the Cantons of Basel-Stadt and Basel-Land, grants from the Swiss National Foundation and the Consejo Nacional de Ciencia y Tecnologia Mexico (CONACyT). **AUTHOR CONTRIBUTIONS:** D.F.D. designed and performed most of the experiments, analyzed the data and wrote the paper; J.R.R. collaborated on the experimental design of the knock-in mouse and performed the Western blot of Copine-6. M.A.R. designed the experiments, supervised the entire project and wrote the paper. All authors contributed and commented on the manuscript. **COMPETING INTEREST:** The authors declare that they have no competing interests.

## FIGURES

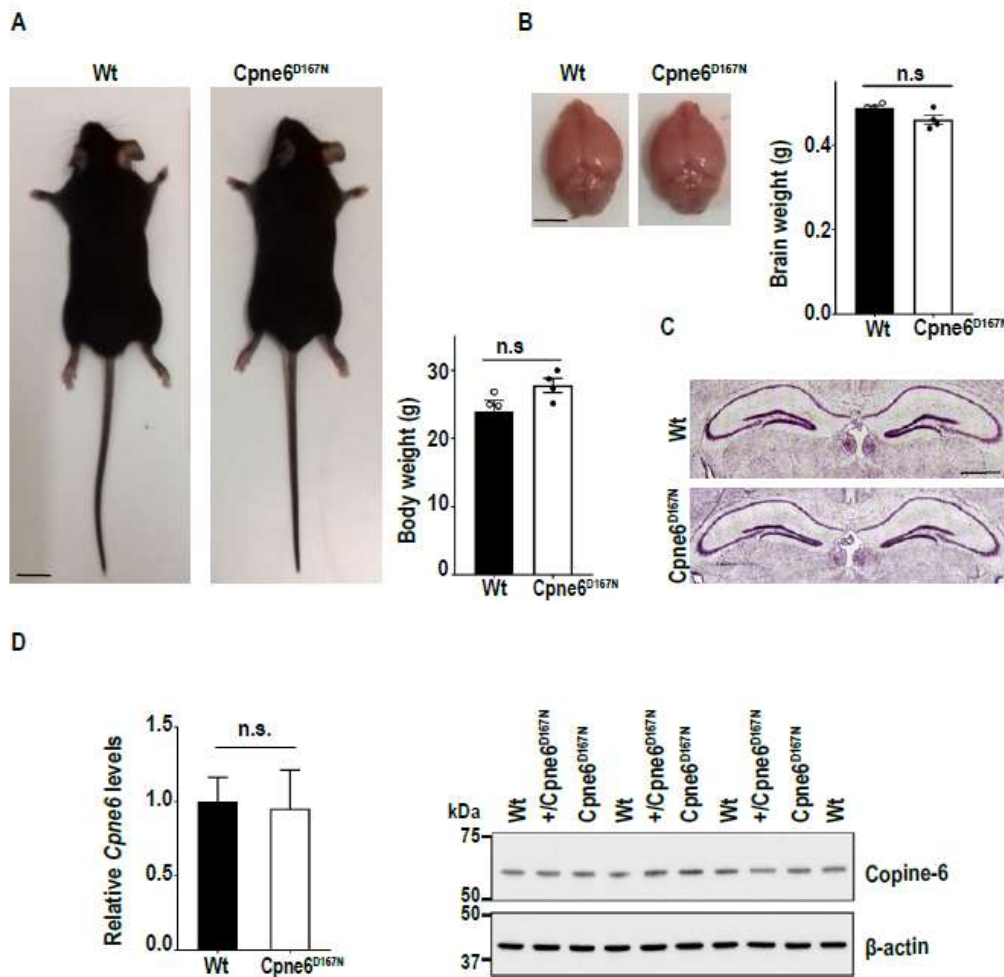


**Figure 1. Characterization of the mice expressing the Copine-6<sup>D167N</sup> calcium mutant. (A)** Representative pictures of wild-type (Wt) and mice expressing the calcium-insensitive Copine-6 mutant (Cpne6<sup>D167N</sup>) and body weight quantification (right). **(B)** Picture of dissected adult brains from Wt and Cpne6<sup>D167N</sup> mice and brain weight quantification (right). Data are mean  $\pm$ SEM from  $n = 4$  male mice (13 weeks old) per genotype. n.s.  $P > 0.05$  by Student's t-test. Scale bar, 5 mm. **(C)**. Cresyl violet-stained coronal brain sections of 13-week-old wild-type (Wt) and Cpne6<sup>D167N</sup> mutant mice at the hippocampus level. The overall organization of mutant and wild type mice is the same. **(D)** Cpne6 mRNA levels were measured in hippocampal lysates from wild-type (Wt) and Cpne6<sup>D167N</sup> mutant mice by real-time PCR. Data are mean  $\pm$ SEM from  $n = 3$  male mice (6 weeks old) per genotype. n.s.  $P > 0.05$  by Student's t-test. Right: Western blot analysis of hippocampal lysates from mice of the indicated genotype. Note that there is no change in the transcript and the protein levels between the different mice.

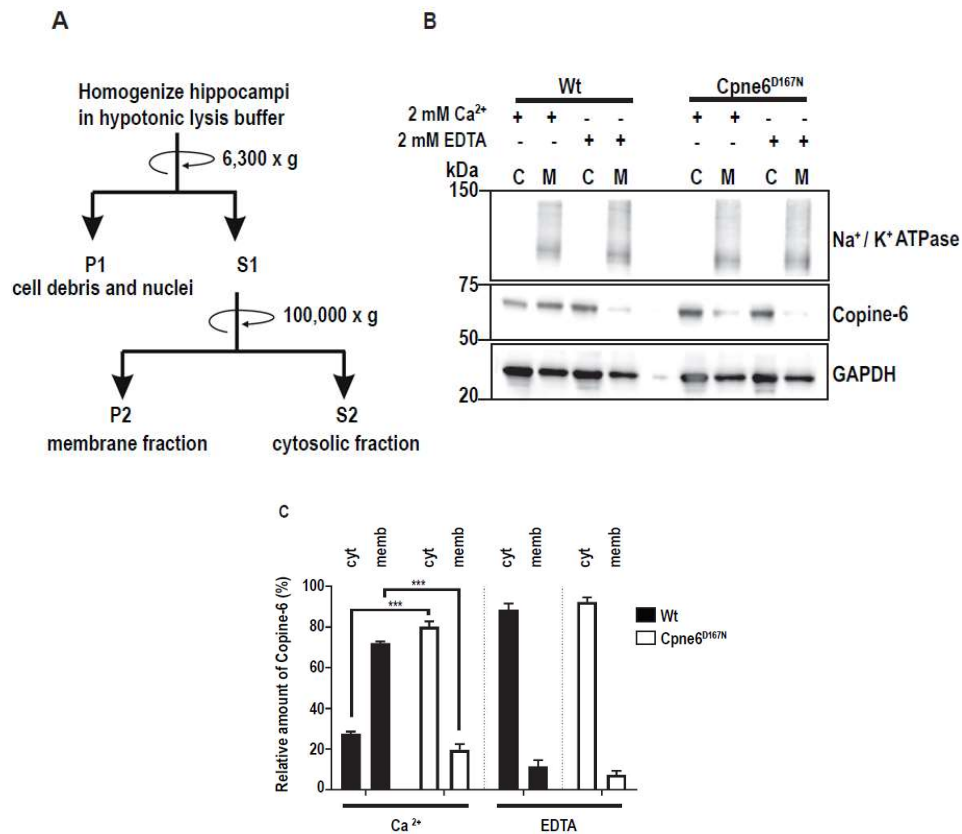


**Figure 2. Calcium-mediated membranal translocation is abrogated by Cpne6<sup>D167N</sup> mutation *in vivo*.** (A) Hippocampal lysates were separated into cytoplasm and membrane fractions by high-speed centrifugation. Abbreviations are as follow: S1 – S2, supernatants; P1 – P2, pellets (B) Representative Western blot analysis from subcellular fractionation of adult mice hippocampus in the presence of calcium or EDTA added after first centrifugation. (C) Quantification of the levels of Copine-6 immunoreactivity in the cytosolic (cyt) fraction S2 and the membrane (memb) fraction P2 in the presence of calcium or EDTA. GAPDH was used as loading control to compare the different genotypes. Copine-6 from wild-type mice partitions in the membrane fraction in the presence of calcium. In contrast, the distribution of the mutated Copine-6<sup>D167N</sup> mice is not affected by Ca<sup>2+</sup> as it largely partitions with the cytoplasmic fraction. Data are represented as mean ± SEM from n = male 4 mice per genotype. \**p* < 0.05, \*\**p* < 0.01, \*\*\**p* < 0.001, Student's t-test and Sidak-Bonferroni Post hoc analysis.

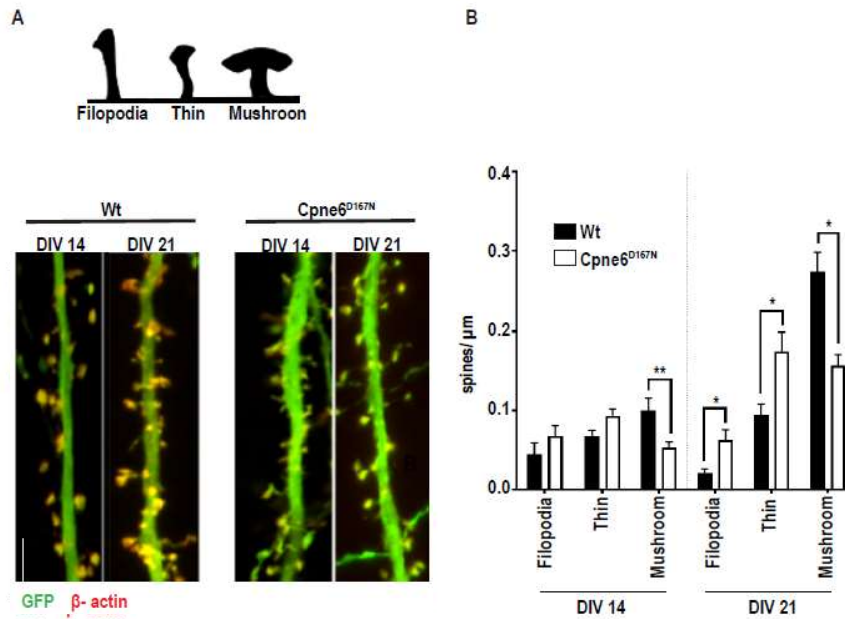


**Figure 3. The Copine-6<sup>D167N</sup> calcium mutant affects spine structure in cultured hippocampal neurons. (A)** Upper row: Scheme of the different spine morphologies analyzed. Lower row: Maximal intensity projection of representative dendrites hippocampal neurons at DIV 14 and DIV 21 from wild-type (Wt) and Cpne6<sup>D167N</sup> mice. Neurons were transfected with cDNAs encoding β-actin-tdRFP (spine marker) and GFP (volume marker) at DIV07 or DIV 14, respectively. Scale bar 10 μm. **(B)** Quantification of filopodia-like, thin and mushroom spines at the indicated time points. Mushroom-like spines density is higher in wild-type mice compared to Cpne6<sup>D167N</sup> mice at DIV 14 and 21. Density of spines was quantified from 70 μm dendritic length. Data are mean ± SEM from n = 15-20 neurons; Wt: n = 877 spines, Cpne6<sup>D167N</sup>: n= 1112 spines; \*p < 0.05, \*\*p < 0.01, \*\*\*p < 0.001, Student's t-test and Sidak-Bonferroni Post hoc analysis.

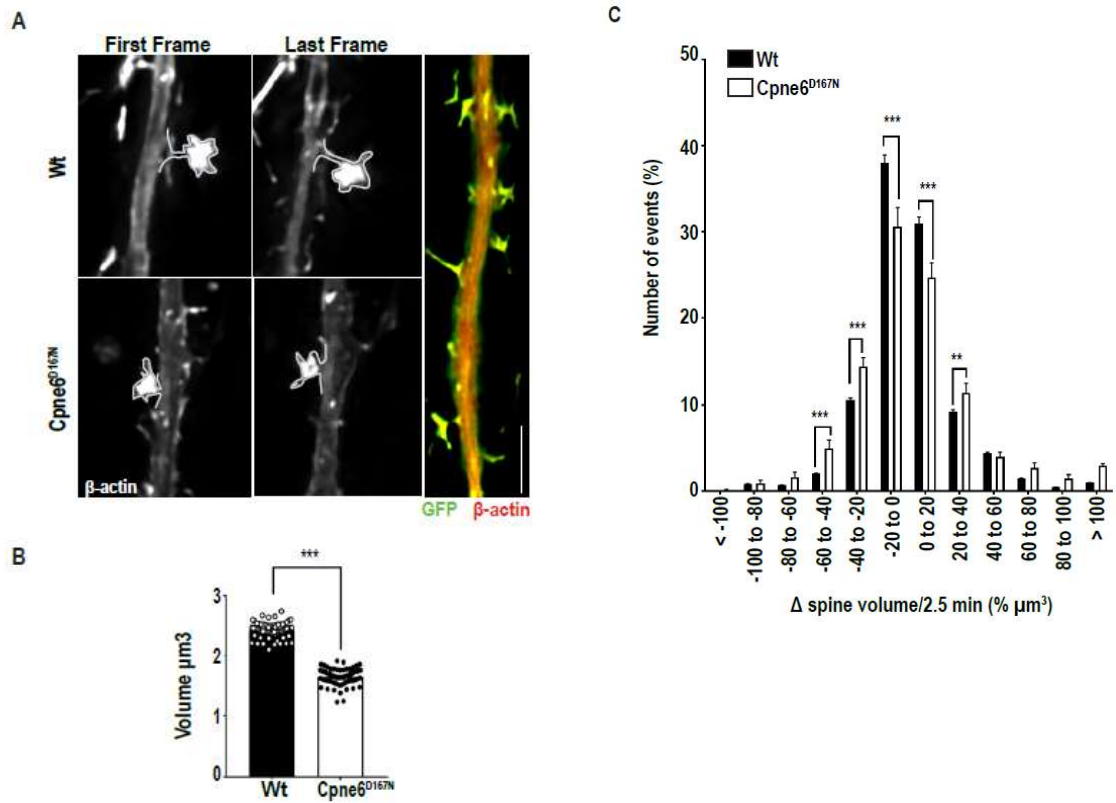


**Figure 4. Dendritic spines of hippocampal neurons from Cpne6<sup>D167N</sup> mice are more motile.** (A) Deconvolved images of a representative dendrite of wild-type (Wt) and Cpne6<sup>D167N</sup> mutant hippocampal neurons expressing  $\beta$ -actin-tdRFP (spine marker) and GFP (volume marker) at DIV 14. Representative image of a dendrite from wild-type hippocampal cultured neuron (right). Scale bar 10  $\mu\text{m}$ . (B) Mean spine volume in Wt and Cpne6<sup>D167N</sup> neurons over the entire recording. (C) Distribution of relative spine volume changes within 2.5 minutes of Wt and Cpne6<sup>D167N</sup> neurons. Data are mean  $\pm$ SEM from  $n = 73$  dendritic spines from 5 independent experiments. \* $p < 0.05$ , \*\* $p < 0.01$ , \*\*\* $p < 0.001$ ; unpaired  $t$  test;  $t$  test.

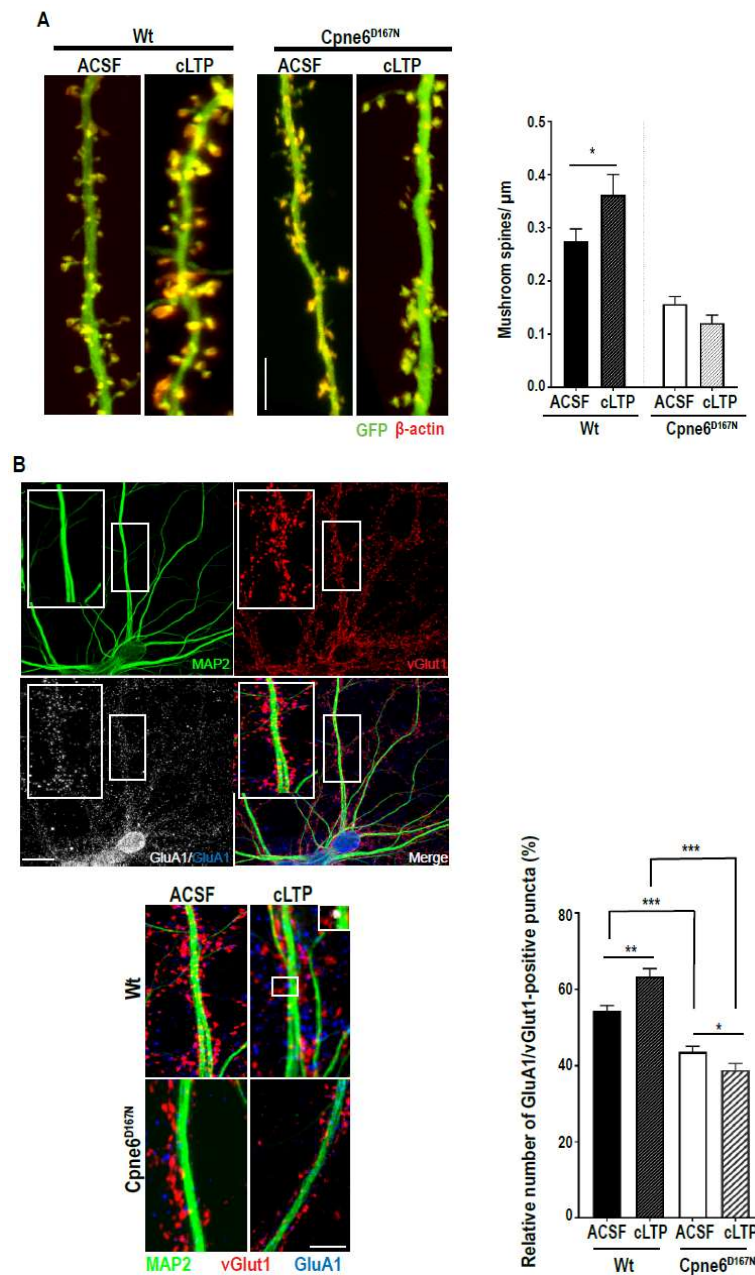


**Figure 5. Copine-6<sup>D167N</sup>-expressing neurons do not show spine structural plasticity. (A)** Representative confocal pictures of DIV 21 neurons isolated from wild-type (Wt) or Cpne6<sup>D167N</sup> mice, which were transfected at DIV14 with constructs coding for  $\beta$ -actin-tdRFP (red; spine marker) and GFP (green; volume marker). Cultures were incubated with ACSF or cLTP-inducing ACSF (cLTP) for 10 min. Spine morphology analysis 60 mins after ACSF/cLTP treatment. Scale bar 10  $\mu$ m. Right column: Quantification of mushroom-like spines from neurons isolated from Wt and Cpne6<sup>D167N</sup> mice. Density of the spine morphology was determined by the number of spines in 70  $\mu$ m dendritic length. Density of mushroom-like spines is increased after cLTP induction in Wt but not in Cpne6<sup>D167N</sup> neurons. Data are mean  $\pm$  SEM

from  $n = 15-20$  neurons from four independent cultures. Wt:  $n = 600$  spines,  $n = 540$  spines from ACSF and cLTP condition, respectively. Cpne6<sup>D167N</sup>:  $n = 512$  spines,  $n = 542$  spines from ACSF and cLTP condition, respectively. Scale bar,  $10\ \mu\text{m}$ .  $*p < 0.05$ ,  $**p < 0.01$ ,  $***p < 0.001$ , Student's t-test with Sidak-Bonferroni post hoc test. **(B)** Representative immunofluorescence image of dissociated hippocampal neurons (DIV 21) stained for MAP2 (green) vGlut1 (red) and surface GluA1 (blue/grey). Scale bar  $10\ \mu\text{m}$ . Bottom: Cultures after 10 min incubation with ACSF or cLTP-inducing (cLTP) medium for 10 minutes, stained for MAP2 (green), vGlut1 (red) and GluA1 (blue). Example of surface GluA1 juxtaposed to vGlut1 is indicated by a white rectangle. Right: Quantification of the number of synapses, as defined by the juxtaposition of GluA1 and vGlut1. Data represent the percentage of Glutv1/GluA1-positive synapses normalized to the sum of vGlut1, GluA1 and Glutv1/GluA1puncta.  $N = 18-19$  neurons per genotype from 4 independent cultures. Wt:  $n = 943$  puncta,  $n = 1052$  puncta from ACSF and cLTP condition, respectively. Cpne6<sup>D167N</sup>:  $n = 836$  puncta,  $n = 943$  puncta from ACSF and cLTP condition, respectively.  $*p < 0.05$ ,  $**p < 0.01$ ,  $***p < 0.001$ , Student's t-test with Sidak-Bonferroni post hoc test.

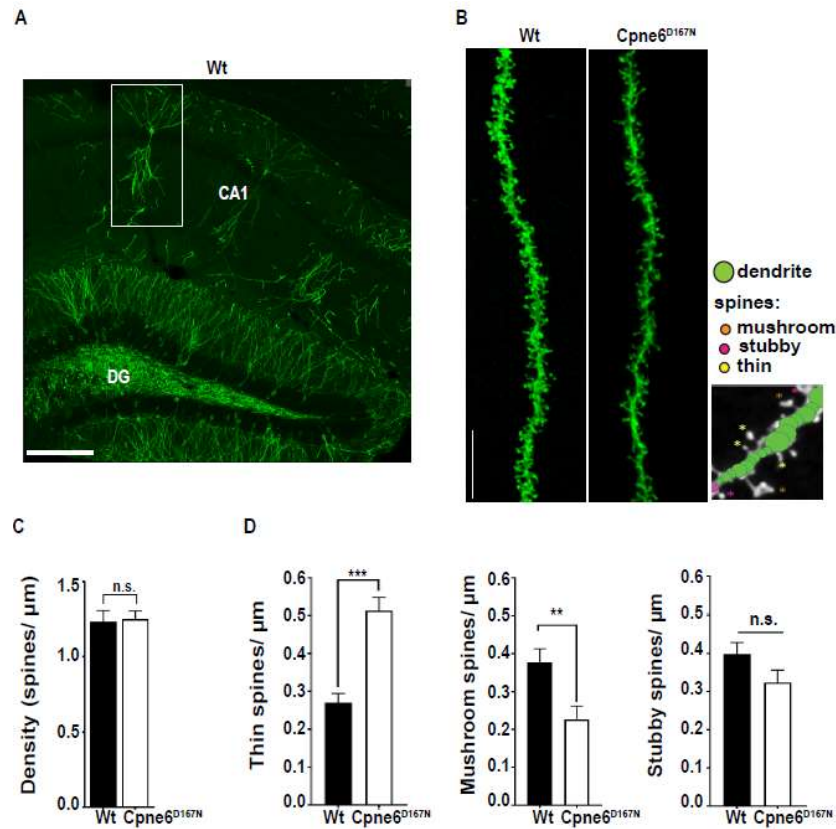


**Figure 6. Spine morphology is altered in mice expressing the Copine-6<sup>D167N</sup> mutant.** (A) Representative low-power view of the hippocampus of a 6-week-old wild-type (Wt) mouse expressing sparsely membrane-associated GFP (Thy-mGFP mice). Abbreviations are: DG (Dentate Gyrus), CA1 (Cornu Ammonis 1). Scale bar= 50  $\mu\text{m}$ . (B) Representative high magnification of secondary apical dendrites of CA1 neurons in Thy-mGFP mice on wild-type (Wt) and Cpne6<sup>D167N</sup> background. Scale bar = 10  $\mu\text{m}$ . Representative image of the classification of the spines by NeuroVision (right corner). (C) Quantification of the spine density in Wt and Cpne6D167N mice. (D) Quantification of the density of thin, mushroom and stubby spines in the different mice. The density of thin spines is increased in Cpne6D167N compared to Wt mice while the density of mushroom spines decreases. Data are mean  $\pm$  SEM from n = 21-26 dendrites from three 6-week-old mice per genotype. Wt: n = 1734 spines; Cpne6<sup>D167N</sup>: n = 1444 spines. n.s. \* $p < 0.05$ , \*\* $p < 0.01$ , \*\*\* $p < 0.001$ , Student's t-test with Sidak-Bonferroni post hoc test.

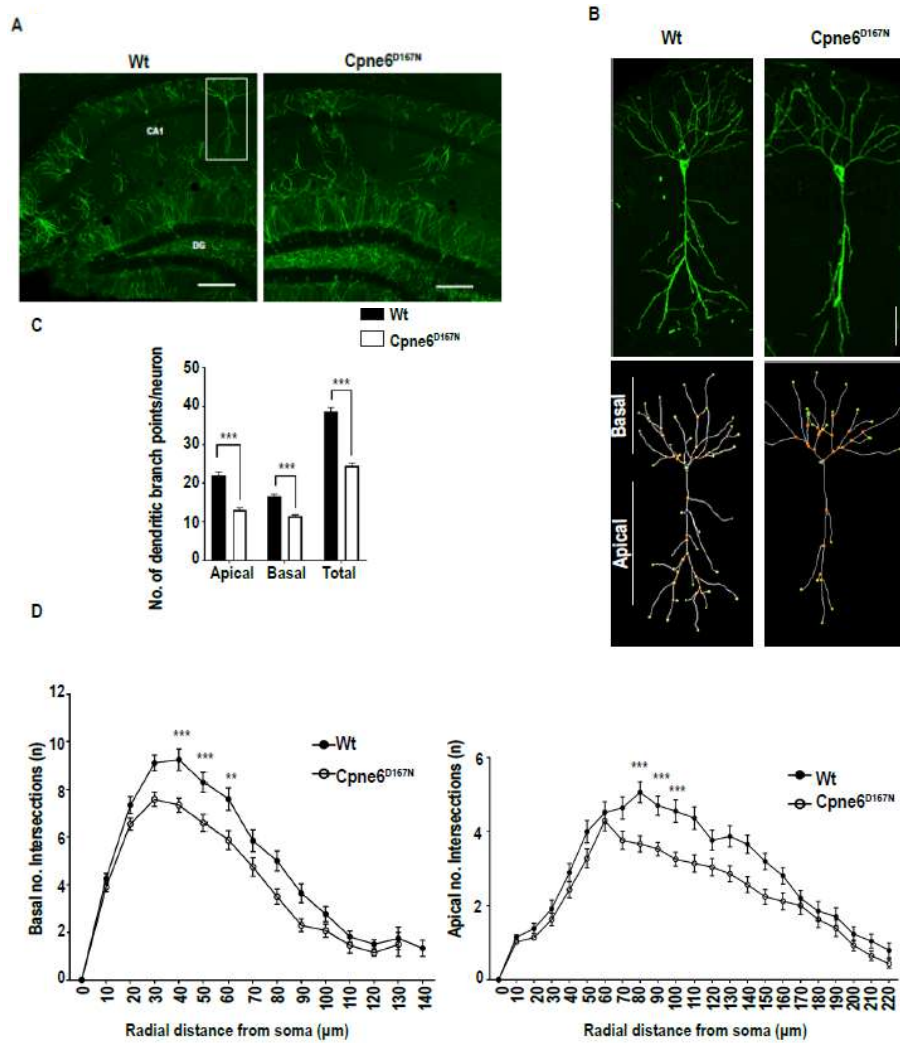
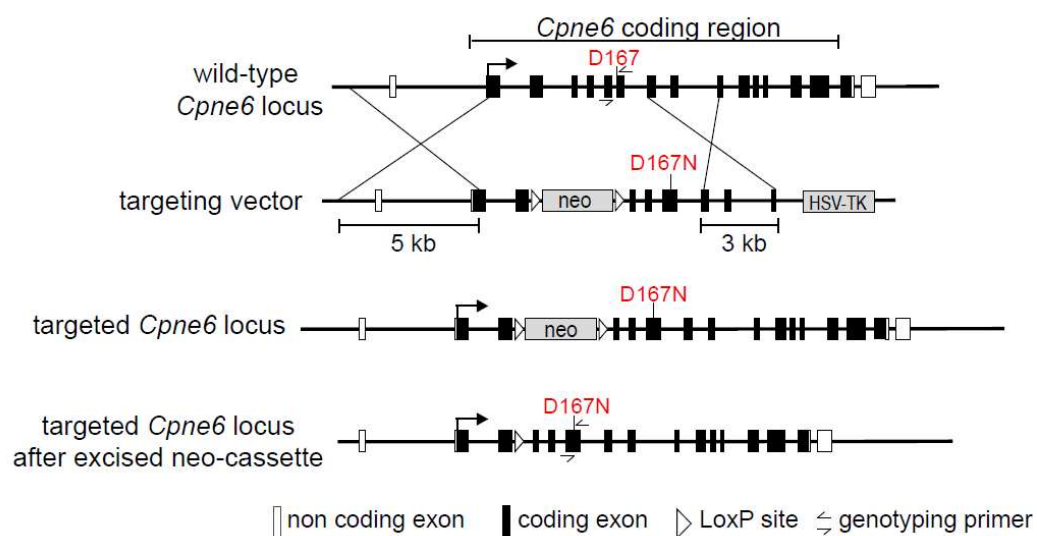
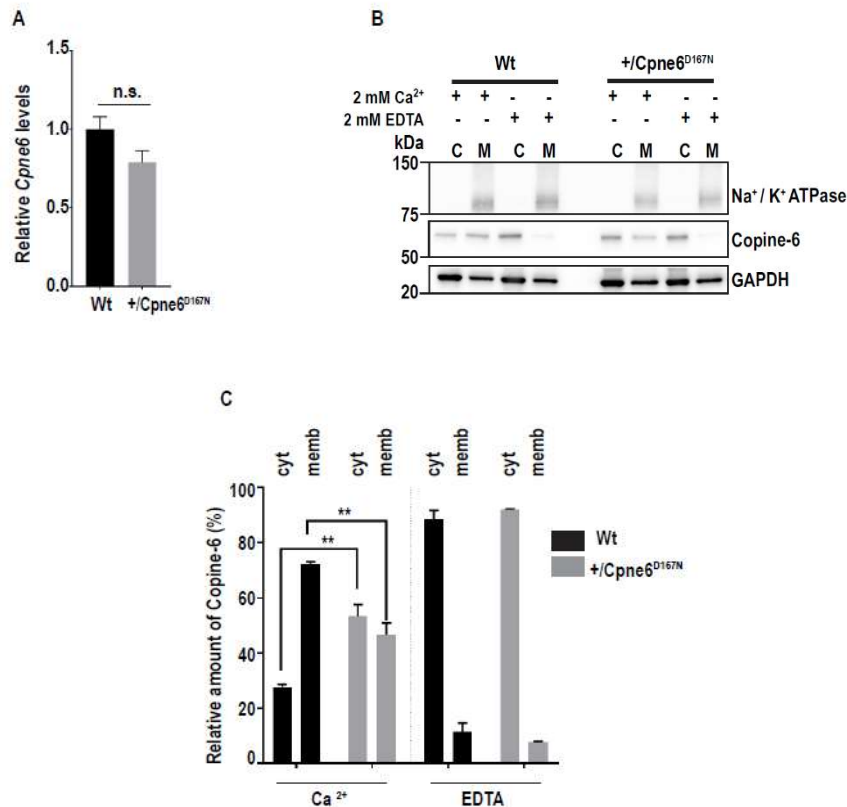


**Figure 7. Dendritic ramification of neurons of the CA1 hippocampal area are simplified in *Copine-6*<sup>D167N</sup> mice.** (A) Representative images of coronal brain sections showing the Cornu Ammonis (CA1) and Dentate Gyrus (DG) areas of the hippocampus in wild-type (Wt) and *Cpne6*<sup>D167N</sup> mice expressing Thy-mGFP. Scale bar = 50 μm (B) Maximum intensity projections of pyramidal neurons of the CA1 area and their respective filament analysis by IMARIS. Scale bar = 50 μm (C) Quantification of the number of apical, basal and total dendritic branch points per neuron. (D) Sholl analysis of the apical and basal arbors of pyramidal neurons in Wt and *Cpne6*<sup>D167N</sup> mice. Data are mean ± SEM from six-week-old mice genotype (n = 6 per genotype); Wt: n = 53 neurons, *Cpne6*<sup>D167N</sup>: n = 56 neurons. \**p* < 0.05, \*\**p* < 0.01, \*\*\**p* < 0.001, Student's t-test with Sidak-Bonferroni post hoc test.

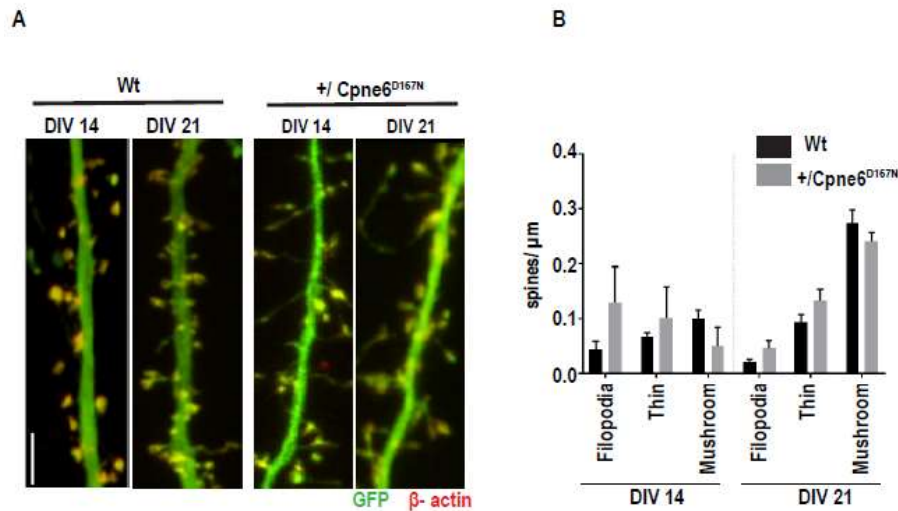
## SUPPLEMENTARY FIGURES



**Supplementary Figure S1. Design of the Copine-6<sup>D167N</sup> calcium mutant mice.** The GAT triplet coding for Asp at position 167 (which is required for calcium binding) was mutated to AAT (encoding Asn). Note: because of the proximity of the GAT codon to the splice junction between exon 5 and 6, the two exons were fused in the targeting vector.

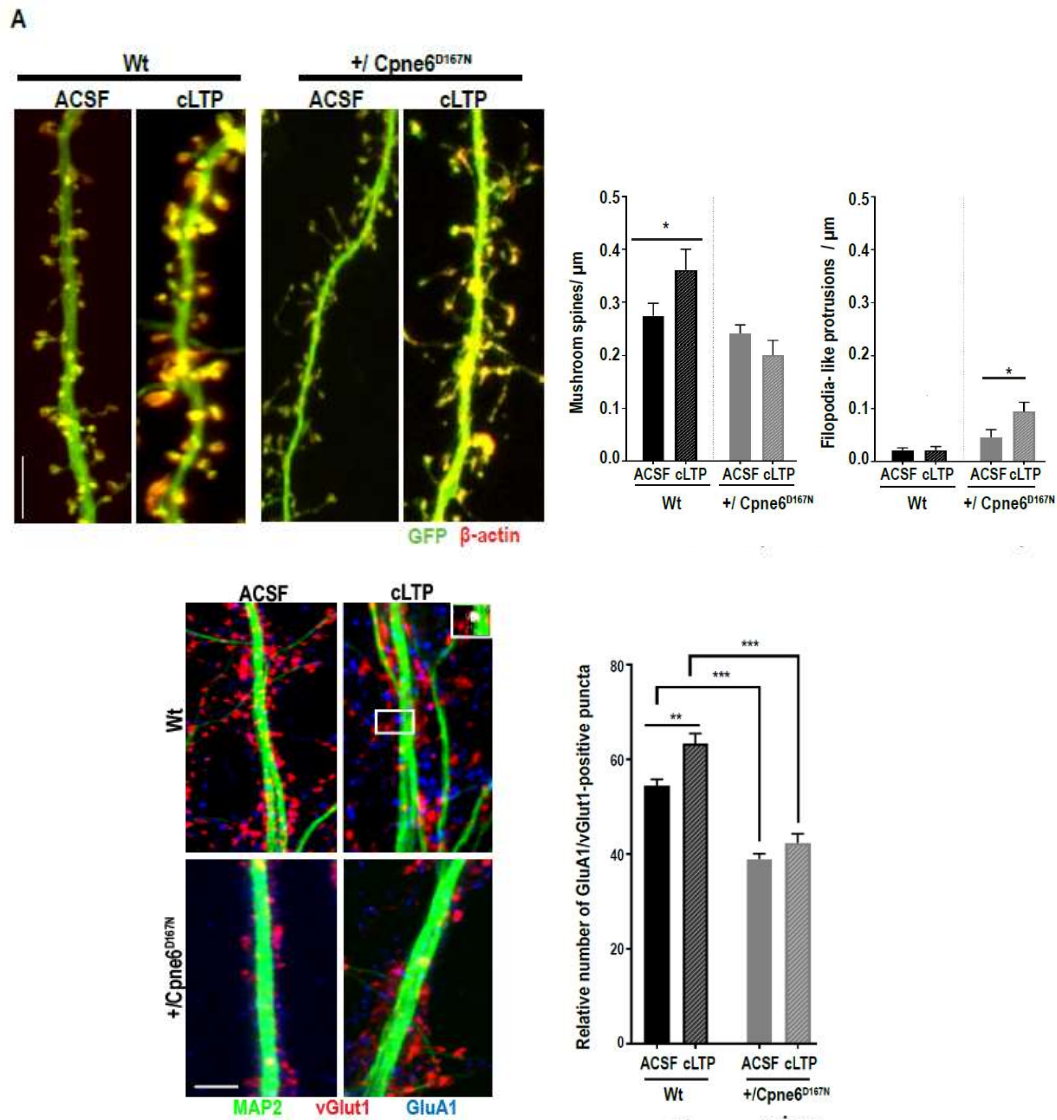


**Supplementary Figure S2. Calcium-mediated membranal translocation of the heterozygous Copine-6<sup>D167N</sup> mutant mice.** Transcript and protein levels of Copine-6. **(A)** *Cpne6* mRNA levels were measured by real-time PCR from hippocampal RNA extracts of six-week-old male wild-type (Wt) and *Cpne6*<sup>D167N</sup> mice (n = 3) (left). Levels of the mutated transcript do not differ between Wt and +/*Cpne6*<sup>D167N</sup>. **(B)** Representative Western blot from subcellular fractionations of adult mice hippocampus in the presence of calcium or EDTA. **(C)** Quantification of the levels of Copine-6 immunoreactivity in the cytosolic (cyt) fraction S2 and the membrane (memb) fraction P2 in the presence of calcium or EDTA from wild-type (Wt) and +/*Cpne6*<sup>D167N</sup> mutant mice. GAPDH was used as loading control to compare the different genotypes. Copine-6 from wild-type and heterozygous *Cpne6*<sup>D167N</sup> mice partitions in the membrane fraction in the presence of calcium. Data are represented as mean ± SEM from n = male 4 mice per genotype. \**p* < 0.05, \*\**p* < 0.01, \*\*\**p* < 0.001, Student's t-test and Sidak-Bonferroni Post hoc analysis.



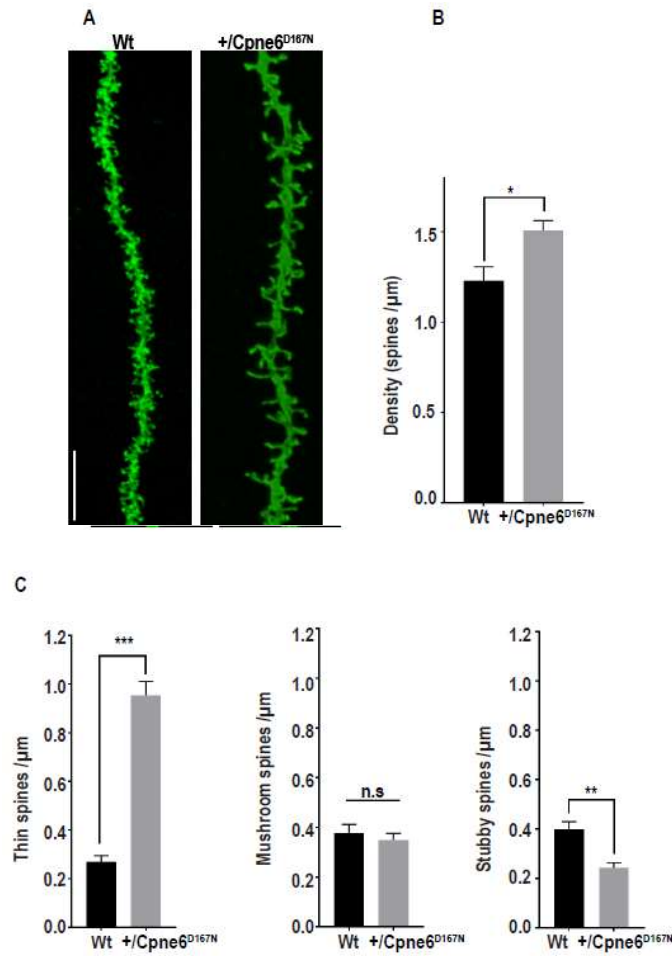
**Supplementary Figure S3. The heterozygous Copine-6<sup>D167N</sup> hippocampal neurons does not show to have changes in the spines structure plasticity.**

**(A)** Representative scheme of the different spine morphologies analyzed (upper row). Maximal intensity projection of representative dendrites of wild type (Wt) and +/Cpne6<sup>D167N</sup> hippocampal neurons at DIV 14 and DIV 21 transfected at DIV07 or DIV 14 with β-actin-tdRFP (spine marker) and GFP (volume marker), respectively (lower row). Scale bar, 10 μm. **(B)** Quantification of filopodia, thin, and mushroom spines from neurons isolated from wild type (Wt) and +/Cpne6<sup>D167N</sup>. Density of spines was quantified from 70 μm dendritic length. Data are density mean ± SEM from n = 15-20 neurons; Wt: n = 877 spines, +/Cpne6<sup>D167N</sup>: n = 976 spines; \**p* < 0.05, \*\**p* < 0.01, \*\*\**p* < 0.001, Student's t-test and Sidak-Boferroni Post hoc analysis.

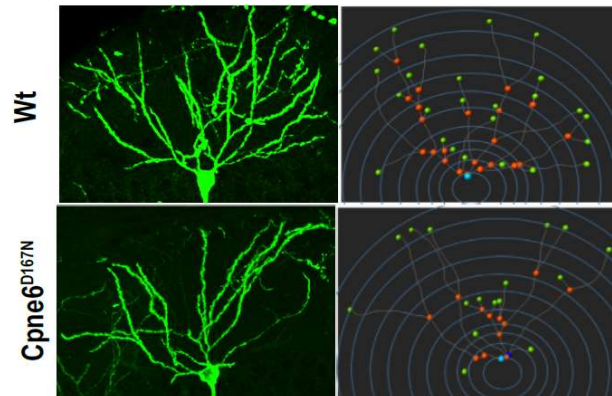


**Supplementary Figure S4. Heterozygous Copine-6<sup>D167N</sup>-expressing neurons show impairments in structural spine plasticity and synaptic strengthening.** (A) Representative confocal pictures of DIV21 primary neurons isolated from wild-type (Wt) or +/Cpne6<sup>D167N</sup> mice, which were transfected at DIV14 with constructs coding for β-actin-tdRFP (red; spine marker) and GFP (green; volume marker). Cultures were incubated with ACSF or induced cLTP (cLTP) for 10 min. Spine morphology analysis 60 mins after ACSF/cLTP treatment. Scale bar 10 μm. Right column: Quantification of mushroom-like spines from neurons isolated from Wt and Cpne6<sup>D167N</sup> mice. Density of the spine morphology was determined by the number of spines in 70 μm dendritic length. Density of mushroom-like spines is increased after cLTP induction in Wt but not in +/Cpne6<sup>D167N</sup> neurons, while density of filopodia-like spines is increased in

+/*Cpne6*<sup>D167N</sup> neurons but not in Wt. Data are density mean  $\pm$ SEM from n = 15-20 neurons per genotype from four independent cultures. Wt: n = 600 spines, n = 540 spines from ACSF and cLTP condition, respectively. +/*Cpne6*<sup>D167N</sup>: n = 666, n = 789 spines from ACSF and cLTP condition, respectively. Scale bar, 10  $\mu$ m. \**p* < 0.05, \*\**p* < 0.01, \*\*\**p* < 0.001, Student's t-test with Sidak-Bonferroni post hoc test. **(B)** Cultures after 10 min incubation with ACSF or cLTP-inducing (cLTP) medium for 10 minutes, stained for MAP2 (green), vGlut1 (red) and GluA1 (blue). Example of surface GluA1 juxtaposed to vGlut1 is indicated by a white rectangle. Right: Quantification of the number of synapses, as defined by the juxtaposition of GluA1 and vGlut1. Data represent the percentage of Glutv1/GluA1-positive synapses normalized to the sum of vGlut1, GluA1 and Glutv1/GluA1 puncta. Scale bar, 10  $\mu$ m. N = 18-19 neurons per genotype from 4 independent cultures. Wt: n = 943 puncta, n = 1052 puncta from ACSF and cLTP condition, respectively. +/*Cpne6*<sup>D167N</sup>: n = 838 puncta, n = 767 puncta from ACSF and cLTP condition, respectively. \**p* < 0.05, \*\**p* < 0.01, \*\*\**p* < 0.001, Student's t-test with Sidak-Bonferroni post hoc test.



**Supplementary Figure S5. Structural spine plasticity in heterozygous Copine-6<sup>D167N</sup> mutant mice is altered.** (A) Representative high magnification of secondary apical dendrites of CA1 neurons in Thy-mGFP mice on wild-type (Wt) and heterozygous Cpne6<sup>D167N</sup> (+/Cpne6<sup>D167N</sup>) background. Scale bar = 10  $\mu$ m. (B) Quantification of the overall density of spines in +/Cpne6<sup>D167N</sup> and wild-type mice (C) Quantification of the density of thin, mushroom and stubby spines in wild type (Wt) and +/Cpne6<sup>D167N</sup> mice. The density spines is increased in +/Cpne6<sup>D167N</sup> compared to Wt mice. Thin spines density is increased while the density of stubby spines decreases. Data are mean  $\pm$ SEM from n = 21-26 dendrites from three 6-week-old mice (n = 3 per genotype). Wt: n = 1734 spines; +/Cpne6<sup>D167N</sup>: n = 1673 spines. n.s p > 0.05, \*p < 0.05, \*\*p < 0.01, \*\*\*p < 0.001, Student's t-test with Sidak-Bonferroni post hoc test.



**Supplementary Figure S6. Representative Sholl analysis from CA1 basal dendrites of six-week-old Thy-mGFP Wt and Cpne6<sup>D167N</sup> mice.** Images were processed and analyzed by IMARIS software (for more details see methods).



## 6. Appendix

### 6.1 Publication1: “Inhibition of the MID1 protein complex: a novel approach targeting APP protein synthesis”

Matthes et al. *Cell Death Discovery* (2018)4:4  
DOI 10.1038/s41420-017-0003-8

Cell Death Discovery

ARTICLE

Open Access

## Inhibition of the MID1 protein complex: a novel approach targeting APP protein synthesis

Frank Matthes<sup>1</sup>, Moritz M. Hettich<sup>1</sup>, Judith Schilling<sup>1</sup>, Diana Flores-Dominguez<sup>1</sup>, Nelli Blank<sup>1</sup>, Thomas Wiggenda<sup>2</sup>, Alexander Buntru<sup>2</sup>, Hanna Wolf<sup>1</sup>, Stephanie Weber<sup>1</sup>, Ina Vorberg<sup>1</sup>, Alina Dagane<sup>2</sup>, Gunnar Dittmar<sup>2,3</sup>, Erich Wanker<sup>2</sup>, Dan Ehringer<sup>1</sup> and Sybille Krauss<sup>1</sup>

### Abstract

Alzheimer's disease (AD) is characterized by two neuropathological hallmarks: senile plaques, which are composed of amyloid- $\beta$  (A $\beta$ ) peptides, and neurofibrillary tangles, which are composed of hyperphosphorylated tau protein. A $\beta$  peptides are derived from sequential proteolytic cleavage of the amyloid precursor protein (APP). In this study, we identified a so far unknown mode of regulation of APP protein synthesis involving the MID1 protein complex: MID1 binds to and regulates the translation of APP mRNA. The underlying mode of action of MID1 involves the mTOR pathway. Thus, inhibition of the MID1 complex reduces the APP protein level in cultures of primary neurons. Based on this, we used one compound that we discovered previously to interfere with the MID1 complex, metformin, for in vivo experiments. Indeed, long-term treatment with metformin decreased APP protein expression levels and consequently A $\beta$  in an AD mouse model. Importantly, we have initiated the metformin treatment late in life, at a time-point where mice were in an already progressed state of the disease, and could observe an improved behavioral phenotype. These findings together with our previous observation, showing that inhibition of the MID1 complex by metformin also decreases tau phosphorylation, make the MID1 complex a particularly interesting drug target for treating AD.

### Introduction

Alzheimer's disease (AD), the most common form of dementia in the elderly, is characterized by two neuropathological hallmarks: senile plaques, which are composed of A $\beta$  peptides, and neurofibrillary tangles, which are composed of hyperphosphorylated tau protein. The disease was first described in 1907 by Alois Alzheimer<sup>1</sup>, who observed these two pathological hallmarks in patients' brains. A $\beta$  peptides are derived from sequential proteolytic cleavage of the amyloid precursor protein

(APP). While the non-amyloidogenic pathway involves sequential cleavage of full-length APP by the  $\alpha$ -secretases and  $\gamma$ -secretase, the amyloidogenic pathway causing the production of A $\beta$  peptides requires the cleavage of full-length APP by the  $\beta$ -secretase BACE1 and the  $\gamma$ -secretase<sup>2</sup>. Multiple lines of evidence suggest that overproduction of A $\beta$  results in neuronal dysfunction and, finally, in neuronal loss<sup>3</sup>. The second pathological hallmark of AD, neurofibrillary tangles, are mainly composed of hyperphosphorylated tau protein<sup>4,5</sup>. Tau is a microtubule-associated protein that stimulates and stabilizes microtubule assembly. Upon hyperphosphorylation, tau dissociates from microtubules, resulting in microtubule destabilization and neuronal death. The main tau phosphatase is protein phosphatase 2A (PP2A),

Correspondence: Dan Ehringer (danehringer@dzne.de) or Sybille Krauss (sybille.krauss@dzne.de)

<sup>1</sup>Deutsches Zentrum für Neurodegenerative Erkrankungen e.V., Bonn, Germany

<sup>2</sup>Max Delbrück Center for Molecular Medicine (MDQ) Berlin-Buch, Berlin, Germany

Full list of author information is available at the end of the article

Frank Matthes, Moritz M. Hettich, and Judith Schilling contributed equally to this work

Edited by A. Rufin

© The Author(s) 2018



**Open Access** This article is licensed under a Creative Commons Attribution 4.0 International License, which permits use, sharing, adaptation, distribution and reproduction in any medium or format, as long as you give appropriate credit to the original author(s) and the source, provide a link to the Creative Commons license, and indicate if changes were made. The images or other third party material in this article are included in the article's Creative Commons license, unless indicated otherwise in a credit line to the material. If material is not included in the article's Creative Commons license and your intended use is not permitted by statutory regulation or exceeds the permitted use, you will need to obtain permission directly from the copyright holder. To view a copy of this license, visit <http://creativecommons.org/licenses/by/4.0/>.

Official journal of the Cell Death Differentiation Association

**SPRINGER NATURE**  
CDDpress

which is capable of dephosphorylating tau at AD-relevant phospho-sites<sup>6</sup>.

As we have shown previously, the MID1-PP2A protein complex regulates the phosphorylation of tau<sup>7</sup>. MID1 acts as an E3 ubiquitin ligase and promotes the ubiquitin-dependent degradation of PP2A<sup>8</sup>. Therefore, MID1 is a negative regulator of PP2A activity and thus inhibition of the MID1-PP2A complex is a promising approach to activate PP2A, and thereby induce its activity towards its target protein tau. In line with this, we have shown previously that the anti-diabetic drug metformin is capable of dephosphorylating tau at AD-relevant phospho-sites by interfering with the assembly of the MID1-PP2A-complex<sup>7</sup>. Upon metformin treatment, the MID1-dependent degradation of PP2Ac is inhibited, resulting in increased PP2A activity and dephosphorylation of tau at AD specific sites<sup>7</sup>. Besides regulating PP2A activity, MID1 also regulates the activity of the PP2A opposing kinase mTOR<sup>9</sup>. Both enzymes, PP2A and mTOR, play a crucial role in the regulation of translation initiation by the eukaryotic initiation factor (eIF) complex. In detail, in absence of mTOR, a negative regulatory protein complex containing 4E-BP1 in association with eIF4E binds to the 5' end of the mRNA and inhibits translation. To activate translation mTOR phosphorylates 4E-BP1, thereby releasing its inhibitory action and allowing a heterotrimeric complex containing eIF4E, eIF4A, and eIF4G to assemble at the 5' end of the mRNA. At the same time, mTOR also phosphorylates and thereby activates p70 S6 kinase (S6K). S6K in turn phosphorylates and thereby activates its downstream targets eIF4B and S6. S6 is part of the small ribosomal subunit (40S). eIF3 is a multi-subunit protein that recruits 40S to the mRNA. Once associated with the mRNA, 40S starts scanning towards the ATG start codon. Upon start codon recognition, the large ribosomal subunit (60S) binds and, together with

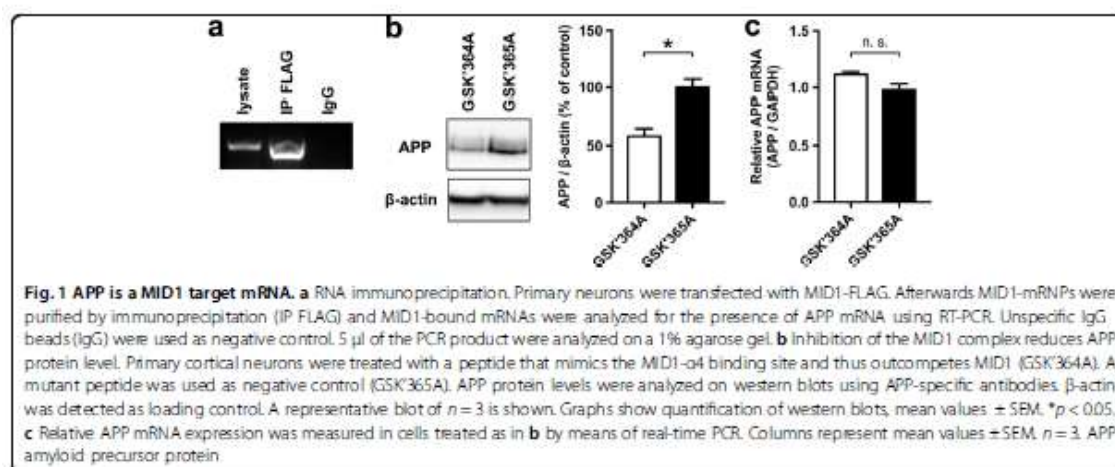
40S, forms the translationally competent ribosome. The eIF complex is released from the mRNA and translation starts<sup>10</sup>. PP2A and mTOR control translation by regulating the phosphorylation of 4E-BP1 and S6K. MID1 binds to GC-rich mRNAs and recruits its interacting proteins, including S6K and S6<sup>11,12</sup>. By regulating the activity of both PP2A and mTOR, MID1 controls the translation of mRNAs bound to the MID1 complex<sup>11–14</sup>.

In this study we asked if MID1, besides its regulatory action on phospho-tau, could also affect APP. We show here a so far unknown connection between MID1 and APP: MID1 binds to the APP mRNA and regulates its translation. The underlying mode of action of MID1 involves the mTOR-dependent translation initiation pathway. Furthermore, we used metformin, a compound that we had shown previously to interfere with the MID1 complex and inactivate translation of MID1-target mRNAs<sup>7,14,15</sup>, for a chronic treatment of an AD mouse model at a progressed state of disease. Our data show that metformin treatment decreases the protein levels of APP and consequently A $\beta$ . This together with our previous observation that disassembly of the MID1 protein complex by metformin also decreases tau-phosphorylation<sup>7</sup>, makes the MID1 protein complex a particularly interesting drug target for treating AD.

## Results

### Translation of APP is regulated by MID1

To investigate if the APP mRNA is regulated by the MID1-PP2A complex, we first tested if MID1 is able to bind to APP mRNA. For this we performed RNA-immunoprecipitations. Primary cortical neurons of wild-type mice were transfected with FLAG-MID1. After UV-crosslinking FLAG-MID1 was purified and MID1-bound mRNAs were isolated from the immunoprecipitates. As negative control an immunoprecipitation using unspecific



IgGs was performed. RT-PCRs clearly showed the presence of APP mRNA in the MID1-immunoprecipitates (Fig. 1a).

In previous studies we showed that binding of the MID1-complex to its target mRNAs induces protein translation from the respective mRNA<sup>1,2,15,16</sup>. Therefore, we asked if the observed binding between APP mRNA and MID1 leads to an induction of APP translation. To test this we performed an experiment in primary cortical neurons with a peptide that mimics the binding sequence between MID1 and the  $\alpha$ 4-PP2A complex and therefore specifically outcompetes MID1. Depletion of MID1 led to a significant reduction of APP protein as shown on a western blot (Fig. 1b). Of note, the mRNA level of APP did not change significantly (Fig. 1c), which is in line with an inhibition at the protein synthesis level.

#### MID1 regulates APP translation by interacting with the mTOR-dependent translation initiation pathway

As we have shown previously, the MID1-complex regulates translation in concert with mTOR. To identify at which exact step of the mTOR-dependent translation initiation MID1 functions, we analyzed proteins that bind to MID1. For this we performed an immunoprecipitation of FLAG-MID1 and analyzed all MID1-bound proteins by mass spectrometry. As expected, we detected several members of the mTOR-translation initiation cascade (Fig. 2a and Table 1), several of which we validated on a western blot of FLAG-MID1-immunoprecipitates using specific antibodies (Fig. 2b). Interestingly, all MID1-bound proteins identified here were proteins of the mTOR-dependent translation pathway that act downstream of mTOR as well as S6K and 4E-BP, suggesting that MID1 regulates the mTOR-dependent translation by acting on either the eIFs or the ribosome. Thus, in a second set of experiments we added EDTA during the co-immunoprecipitation. EDTA dissociates ribosomal particles<sup>17</sup>. While binding of most of the identified proteins to MID1 was abolished by the treatment, RPLP0, a member of the large subunit of the ribosome remained attached to MID1 (Fig. 2c). Since all of the proteins identified by mass spectrometry bind RNA in general, their presence in the MID1-immunoprecipitate may be explained by RNA-mediated indirect binding rather than by direct protein-protein interaction. To test which of the identified proteins bind to MID1 independent of RNA, we performed co-immunoprecipitation experiments in the presence or absence of RNase. Binding of the identified eIF proteins to MID1 was abolished by RNase treatment, while RPLP0, RPL5, and RPS3 remained attached to MID1 (Fig. 2d). These data suggest that MID1 directly binds to the ribosome to stimulate mTOR-dependent translation. In line with a MID1-mTOR dependent translation of APP, application of an mTOR inhibitor reduced APP

translation both in an in vitro translation assay (Fig. 2e) as well as in primary neurons (Fig. 2f).

#### Metformin reduces APP protein and APP cleavage products

To target MID1 we decided to use metformin, a compound that we had shown previously to interfere with the MID1 complex and inactivate translation of MID1-target mRNAs<sup>7,14,15</sup>. In line with what we have observed for other MID1-target mRNAs, metformin treatment of primary cortical neurons also led to a reduction of APP protein in a dose-dependent manner (Fig. 3a).

Finally, to investigate this effect in vivo, we chronically treated transgenic APP/PS1 mice with 5 g/l metformin in the drinking water for 8 months. In line with our data from primary neurons, full-length APP protein was significantly reduced in metformin treated mice (Fig. 4a), while APP mRNA levels were not significantly changed after metformin treatment (Fig. 4b). Together, these data suggest that the APP protein level was decreased in vivo on the translational level, which can be explained by inhibition of the MID1 complex. In line with an mTOR-MID1-PP2A-dependent down-regulation of APP in these mice, the phosphorylation of S6 was significantly reduced in brain lysates of these mice, as determined by western blots (Fig. 4c).

A reduction of APP should lead to a reduced A $\beta$  plaque burden in the treated animals. To quantify this we first measured levels of A $\beta$  on dot blots, showing that A $\beta$  levels were significantly decreased in metformin treated animals (Fig. 5a). Second, in an ELISA measuring the levels of A $\beta$ 40 and A $\beta$ 42, a significant decrease of A $\beta$  peptides was observed in both female and male mice (Fig. 5b). Of note, there was also a significant difference in A $\beta$  levels between female and male mice. To investigate the A $\beta$  plaque burden in the hippocampus, we performed Thioflavin-S stainings. In line with dot blot and ELISA experiments, thioflavin staining showed less aggregates in metformin treated animals (Fig. 5c). To test if metformin affects learning and memory, APP/PS1 mice that were treated with metformin were examined in behavioral tests. A significantly improved performance in the Morris water maze was observed in animals that were treated with metformin (Fig. 5d).

Besides regulating translation, mTOR is also a known regulator of autophagy. Therefore, in our in vivo set-up we cannot rule out that the observed reduction of A $\beta$  could be at least partially due to increased clearance via autophagy. To address this, we analyzed the degradation of A $\beta$  in SH-EP cells containing TAMRA-A $\beta$ 42 aggregates. Clearly, no increased degradation of A $\beta$  was detectable in these cells, suggesting that metformin treatment does not induce autophagocytic degradation of A $\beta$  (Fig. 6).

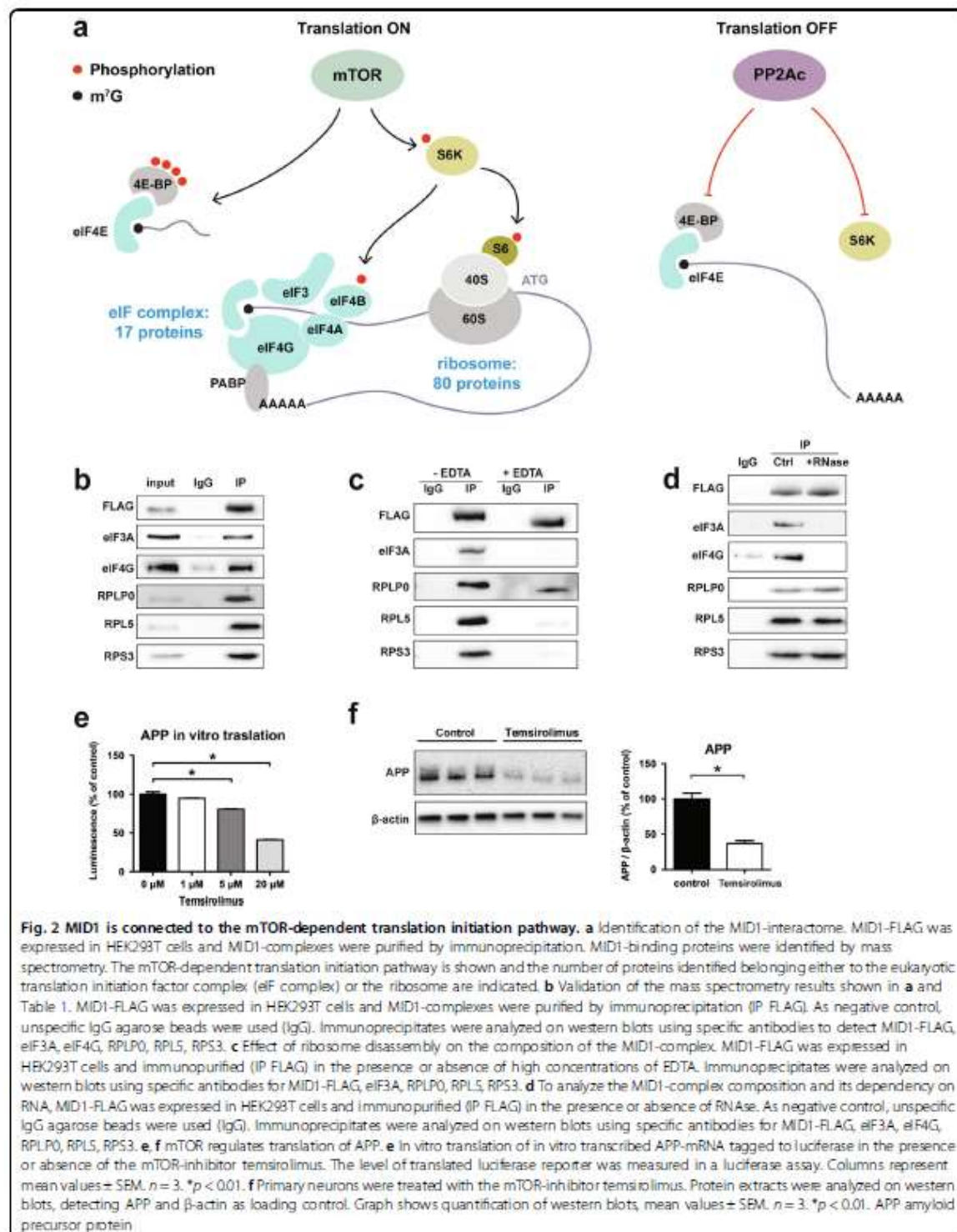


**Fig. 2** MID1 is connected to the mTOR-dependent translation initiation pathway. **a** Identification of the MID1-interactome. MID1-FLAG was expressed in HEK293T cells and MID1-complexes were purified by immunoprecipitation. MID1-binding proteins were identified by mass spectrometry. The mTOR-dependent translation initiation pathway is shown and the number of proteins identified belonging either to the eukaryotic translation initiation factor complex (eIF complex) or the ribosome are indicated. **b** Validation of the mass spectrometry results shown in **a** and Table 1. MID1-FLAG was expressed in HEK293T cells and MID1-complexes were purified by immunoprecipitation (IP FLAG). As negative control, unspecific IgG agarose beads were used (IgG). Immunoprecipitates were analyzed on western blots using specific antibodies to detect MID1-FLAG, eIF3A, eIF4G, RPLP0, RPL5, RPS3. **c** Effect of ribosome disassembly on the composition of the MID1-complex. MID1-FLAG was expressed in HEK293T cells and immunoprecipitated (IP FLAG) in the presence or absence of high concentrations of EDTA. Immunoprecipitates were analyzed on western blots using specific antibodies for MID1-FLAG, eIF3A, RPLP0, RPL5, RPS3. **d** To analyze the MID1-complex composition and its dependency on RNA, MID1-FLAG was expressed in HEK293T cells and immunoprecipitated (IP FLAG) in the presence or absence of RNase. As negative control, unspecific IgG agarose beads were used (IgG). Immunoprecipitates were analyzed on western blots using specific antibodies for MID1-FLAG, eIF3A, eIF4G, RPLP0, RPL5, RPS3. **e** **f** mTOR regulates translation of APP. **e** In vitro translation of in vitro transcribed APP-mRNA tagged to luciferase in the presence or absence of the mTOR-inhibitor temsirolimus. The level of translated luciferase reporter was measured in a luciferase assay. Columns represent mean values  $\pm$  SEM,  $n = 3$ . \* $p < 0.01$ . **f** Primary neurons were treated with the mTOR-inhibitor temsirolimus. Protein extracts were analyzed on western blots, detecting APP and  $\beta$ -actin as loading control. Graph shows quantification of western blots, mean values  $\pm$  SEM,  $n = 3$ . \* $p < 0.01$ . APP amyloid precursor protein

**Table 1** Statistical analysis of proteins identified mass spectrometry analysis of MID1 immunoprecipitates

Protein name	Gene ID	Log2 ratio	P-value
ATP-binding cassette sub-family D member 3	ABCD3	2.75E+01	2.04E-03
ATP-binding cassette sub-family F member 2	ABCF2	2.88E+01	5.96E-04
Apoptotic chromatin condensation inducer in the nucleus	ACN1	2.72E+01	1.39E-02
Aldehyde dehydrogenase X, mitochondrial	ALDH181	2.62E+01	3.61E-04
Mitochondrial 10-formyltetrahydrofolate dehydrogenase	ALDH1L2	2.66E+01	1.97E-02
THO complex subunit 4	ALYREF	2.99E+01	7.55E-04
Serine/threonine-protein phosphatase 6 reg. ankyrin repeat subunit A	ANKRD28	2.63E+01	1.85E-02
Coatamer subunit delta	ARCN1	2.65E+01	2.36E-02
Activating signal cointegrator 1 complex subunit 3	ASCC3	2.59E+01	7.96E-03
ATPase family AAA domain-containing protein 3A	ATAD3A	1.77E+00	3.98E-02
Sodium/potassium-transporting ATPase subunit alpha-1	ATP1A1	2.72E+01	4.39E-04
Ribosome biogenesis protein BMS1 homolog	BMS1	2.90E+01	8.92E-03
Ribosome biogenesis protein BRX1 homolog	BRX1	2.68E+01	1.41E-02
Caprin-1	CAPRIN1	2.80E+01	5.88E-03
Coiled-coil domain-containing protein 124	CCDC124	2.94E+01	1.91E-04
T-complex protein 1 subunit gamma	CCT3	2.63E+01	4.86E-02
T-complex protein 1 subunit epsilon	CCT5	2.64E+01	1.42E-03
Cell division cycle 54-like protein	CDCSL	3.04E+01	3.51E-03
Centrosomal protein of 170 kDa	CEP170	2.71E+01	2.53E-03
Chromatin target of PRMT1 protein	CHTOP	2.81E+01	3.45E-02
CLIP-associating protein 2	CLASP2	2.74E+01	4.83E-03
Methylome subunit pCln	CLNS1A	2.97E+01	2.16E-03
Coatamer subunit gamma-2	COPG2	2.59E+01	2.98E-04
Coronin-1C	CORO1C	3.03E+01	2.00E-02
Cleavage and polyadenylation specificity factor subunit 6	CPSF6	2.93E+01	4.13E-03
Cleavage and polyadenylation specificity factor subunit 7	CPSF7	2.73E+01	2.20E-03
Probable ATP-dependent RNA helicase DDX17	DDX17	3.22E+01	1.28E-02
Probable ATP-dependent RNA helicase DDX20	DDX20	2.73E+01	2.81E-02
Nucleolar RNA helicase 2	DDX21	3.01E+01	8.42E-03
Probable ATP-dependent RNA helicase DDX23	DDX23	2.93E+01	4.58E-03
ATP-dependent RNA helicase DDX3X	DDX3X	2.66E+01	5.42E-04
Probable ATP-dependent RNA helicase DDX41	DDX41	2.73E+01	4.88E-03
Probable ATP-dependent RNA helicase DDX5	DDX5	2.97E+01	1.38E-02
ATP-dependent RNA helicase DDX50	DDX50	2.65E+01	5.75E-03
Putative pre-mRNA-splicing factor ATP-dependent RNA helicase DHX15	DHX15	2.76E+01	6.67E-03
Putative ATP-dependent RNA helicase DHX30	DHX30	2.99E+01	1.03E-02
ATP-dependent RNA helicase A	DHX9	7.63E+00	4.50E-03
Elongation factor 2	EEF2	4.68E+00	8.14E-03
116 kDa U5 small nuclear ribonucleoprotein component	EFTUD2	3.04E+01	6.54E-03

**Table 1** continued

Protein name	Gene ID	Log2 ratio	P-value
Eukaryotic translation initiation factor 3 subunit A	EIF3A	3.34E+01	2.89E-04
Eukaryotic translation initiation factor 3 subunit B	EIF3B	3.19E+01	6.22E-03
Eukaryotic translation initiation factor 3 subunit C	EIF3C	3.23E+01	1.43E-03
Eukaryotic translation initiation factor 3 subunit D	EIF3D	3.01E+01	1.72E-03
Eukaryotic translation initiation factor 3 subunit E	EIF3E	3.15E+01	2.60E-03
Eukaryotic translation initiation factor 3 subunit F	EIF3F	3.08E+01	9.00E-03
Eukaryotic translation initiation factor 3 subunit G	EIF3G	2.99E+01	1.64E-04
Eukaryotic translation initiation factor 3 subunit I	EIF3I	3.07E+01	4.95E-03
Eukaryotic translation initiation factor 3 subunit J	EIF3J	2.75E+01	2.97E-04
Eukaryotic translation initiation factor 3 subunit K	EIF3K	2.75E+01	4.35E-02
Eukaryotic translation initiation factor 3 subunit L	EIF3L	3.20E+01	1.62E-03
Eukaryotic translation initiation factor 3 subunit M	EIF3M	3.06E+01	2.52E-02
Eukaryotic translation initiation factor 3 subunit H	EIF3S3	2.98E+01	4.34E-03
Eukaryotic initiation factor 4A-I	EIF4A1	2.82E+01	1.28E-02
Eukaryotic initiation factor 4A-III	EIF4A3	2.66E+01	2.37E-02
Eukaryotic translation initiation factor 4B	EIF4B	3.07E+01	1.05E-02
Eukaryotic translation initiation factor 6	EIF6	2.71E+01	1.74E-02
Emerin	EMD	2.73E+01	1.99E-02
Erlin-2	ERLIN2	2.81E+01	7.54E-03
Exosome component 10	EXOSC10	2.76E+01	3.45E-03
Exosome complex component RRP45	EXOSC9	2.59E+01	2.53E-02
Constitutive coactivator of PPAR-gamma-like protein 1	FAM120A	2.74E+01	1.36E-02
Phenylalanine--tRNA ligase alpha subunit	FARSA	2.78E+01	7.54E-03
Phenylalanine--tRNA ligase beta subunit	FARSB	2.78E+01	1.17E-02
40S ribosomal protein S30	FAU	2.86E+01	2.31E-03
Protein flurry homolog-like	FRYL	3.02E+01	2.54E-02
Gem-associated protein 4	GEMIN4	2.71E+01	2.53E-03
Guanine nucleotide-binding protein subunit beta-2-like 1	GNB2L1	3.25E+01	3.47E-04
Nucleolar GTP-binding protein 2	GNL2	2.75E+01	7.11E-03
Guanine nucleotide-binding protein-like 3	GNL3	2.69E+01	4.03E-04
Golgin subfamily A member 3	GOLGA3	2.98E+01	3.96E-03
General transcription factor 3C polypeptide 2	GTF3C2	2.75E+01	3.97E-03
General transcription factor 3C polypeptide 3	GTF3C3	2.57E+01	3.56E-02
General transcription factor 3C polypeptide 4	GTF3C4	2.70E+01	2.46E-03
Nucleolar GTP-binding protein 1	GTPBP4	2.87E+01	1.26E-02
Histone H2B	HIST1H2BN	2.99E+01	1.62E-02
Heterogeneous nuclear ribonucleoproteins C1/C2	HNRNPC	3.08E+01	3.22E-04
Heterogeneous nuclear ribonucleoprotein D0	HNRNPD	2.60E+01	2.60E-02
Heterogeneous nuclear ribonucleoprotein F	HNRNPF	2.74E+01	4.67E-03
Heterogeneous nuclear ribonucleoprotein K	HNRNPK	2.96E+01	9.43E-04

**Table 1** continued

Protein name	Gene ID	Log2 ratio	P-value
Heterogeneous nuclear ribonucleoprotein M	HNRNPM	6.56E+00	1.98E-02
Heterogeneous nuclear ribonucleoprotein R	HNRNPR	2.99E+01	4.29E-03
Heterogeneous nuclear ribonucleoprotein U	HNRNPU	3.23E+01	2.34E-03
Isoleucine-tRNA ligase, cytoplasmic	IARS	2.72E+01	3.12E-03
Insulin-like growth factor 2 mRNA-binding protein 1	IGF2BP1	3.18E+01	1.09E-03
Insulin-like growth factor 2 mRNA-binding protein 3	IGF2BP3	2.81E+01	1.22E-02
Interleukin enhancer-binding factor 2	ILF2	3.10E+01	1.08E-02
Interleukin enhancer-binding factor 3	ILF3	3.27E+01	2.99E-03
Importin-8	IPO8	2.74E+01	1.30E-02
Insulin receptor substrate 4	IRS4	1.33E+00	3.38E-03
Influenza virus NS1A-binding protein	IVNS1ABP	3.33E+01	3.05E-03
Tyrosine-protein kinase JAK1	JAK1	2.88E+01	4.64E-03
BTB/POZ domain-containing protein KCTD17	KCTD17	2.96E+01	1.23E-02
BTB/POZ domain-containing protein KCTD5	KCTD5	2.96E+01	3.67E-04
Kinesin-like protein KIF11	KIF11	1.48E+00	1.25E-03
La-related protein 1	LARP1	3.17E+01	9.37E-04
La-related protein 4	LARP4	2.86E+01	7.22E-03
La-related protein 4B	LARP4B	2.65E+01	8.21E-03
IIM domain and actin-binding protein 1	IIMA1	2.98E+01	7.34E-03
Leucine-rich PPR motif-containing protein, mitochondrial	LRPPRC	2.63E+01	8.82E-03
Putative RNA-binding protein Luc7-like 2	LUCL7L2	3.00E+01	3.39E-03
Luc7-like protein 3	LUCL7L3	2.81E+01	5.20E-03
Microtubule-associated protein 1B	MAP1B	3.01E+01	3.76E-03
Serine/threonine-protein kinase MARK2	MARK2	2.60E+01	3.76E-03
Methionine-tRNA ligase, cytoplasmic	MARS	2.62E+01	1.62E-03
Matrin-3	MATR3	2.87E+01	1.32E-03
DNA replication licensing factor MCM7	MCM7	2.83E+01	8.19E-03
E3 ubiquitin-protein ligase Midline-1	MID1	3.76E+01	3.26E-04
Putative helicase MOV10	MOV10	2.77E+01	2.49E-02
28S ribosomal protein S17, mitochondrial	MRPS17	2.91E+01	6.96E-03
28S ribosomal protein S22, mitochondrial	MRPS22	2.74E+01	4.69E-03
28S ribosomal protein S25, mitochondrial	MRPS25	2.71E+01	1.14E-02
28S ribosomal protein S27, mitochondrial	MRPS27	2.64E+01	3.48E-02
Protein LYRIC	MTDH	2.72E+01	1.03E-02
Myb-binding protein 1A	MYBBP1A	2.90E+01	1.44E-04
Myosin-10	MYH10	1.13E+00	2.28E-02
Myosin-9	MYH9	2.92E+01	4.78E-03
Unconventional myosin-Ib	MYO1B	2.71E+01	2.88E-02
Nicotinamide phosphoribosyltransferase	NAMPT	2.75E+01	8.55E-03
Nucleosome assembly protein 1-like 1	NAP1L1	2.57E+01	7.18E-03

**Table 1** continued

Protein name	Gene ID	Log2 ratio	P-value
Nuclear cap-binding protein subunit 1	NCBP1	2.81E+01	4.89E-04
Nucleolin	NCL	2.86E+01	6.74E-03
Nucleolar complex protein 4 homolog	NOC4L	2.80E+01	8.27E-03
Probable 28S rRNA (cytosine(4447)-C(5))-methyltransferase	NOP2	2.62E+01	5.08E-03
Cleavage and polyadenylation specificity factor subunit 5	NUDT21	2.96E+01	6.21E-04
OTU domain-containing protein 4	OTUD4	2.74E+01	1.45E-03
Prolyl 4-hydroxylase subunit alpha-1	P4HA1	2.79E+01	4.44E-03
Proliferation-associated protein 2G4	PA2G4	3.08E+01	7.55E-03
Polyadenylate-binding protein 1	PABPC1	3.23E+01	2.17E-03
Polyadenylate-binding protein 4	PABPC4	3.22E+01	2.78E-03
Programmed cell death protein 4	PDCD4	2.94E+01	8.37E-03
Proline-, glutamic acid- and leucine-rich protein 1	PELP1	2.66E+01	9.09E-03
Serine/threonine-protein phosphatase PGAM5, mitochondrial	PGAM5	2.86E+01	3.52E-03
Protein arginine N-methyltransferase 5	PRMT5	3.54E+01	6.16E-04
Pre-mRNA-processing factor 19	PRPF19	3.02E+01	3.67E-03
U4/U6 small nuclear ribonucleoprotein Prp3	PRPF3	2.70E+01	1.69E-02
U4/U6 small nuclear ribonucleoprotein Prp31	PRPF31	2.97E+01	8.19E-04
U4/U6 small nuclear ribonucleoprotein Prp4	PRPF4	2.64E+01	3.83E-03
Pre-mRNA-processing factor 6	PRPF6	2.98E+01	6.12E-03
Pre-mRNA-processing-splicing factor 8	PRPF8	3.11E+01	3.06E-03
Ribose-phosphate pyrophosphokinase 1	PRPS1	5.58E+00	3.60E-03
Ribose-phosphate pyrophosphokinase 2	PRPS2	2.93E+01	1.56E-02
Phosphoribosyl pyrophosphate synthase-associated protein 1	PRPSAP1	3.05E+01	8.50E-03
Phosphoribosyl pyrophosphate synthase-associated protein 2	PRPSAP2	3.25E+01	2.15E-04
Protein PRRC2A	PRRC2A	2.85E+01	8.43E-03
Protein PRRC2C	PRRC2C	2.97E+01	2.05E-02
26S protease regulatory subunit 4	PSMC1	2.97E+01	5.78E-03
26S protease regulatory subunit 7	PSMC2	3.07E+01	8.06E-04
26S protease regulatory subunit 6A	PSMC3	2.89E+01	5.50E-03
26S protease regulatory subunit 6B	PSMC4	1.19E+00	1.54E-02
26S protease regulatory subunit 8	PSMC5	4.55E+00	3.71E-04
26S protease regulatory subunit 10B	PSMC6	2.84E+01	1.52E-03
26S proteasome non-ATPase regulatory subunit 1	PSMD1	2.97E+01	2.12E-03
26S proteasome non-ATPase regulatory subunit 10	PSMD10	2.85E+01	2.02E-02
26S proteasome non-ATPase regulatory subunit 11	PSMD11	3.02E+01	1.94E-02
26S proteasome non-ATPase regulatory subunit 12	PSMD12	2.90E+01	4.18E-03
26S proteasome non-ATPase regulatory subunit 13	PSMD13	2.95E+01	3.11E-03
26S proteasome non-ATPase regulatory subunit 14	PSMD14	2.80E+01	1.85E-03
26S proteasome non-ATPase regulatory subunit 2	PSMD2	2.15E+00	4.38E-03
26S proteasome non-ATPase regulatory subunit 3	PSMD3	3.04E+01	1.48E-04

**Table 1** continued

Protein name	Gene ID	Log2 ratio	P-value
26S proteasome non-ATPase regulatory subunit 4	PSMD4	2.79E+01	1.70E-04
26S proteasome non-ATPase regulatory subunit 6	PSMD6	2.96E+01	9.65E-03
26S proteasome non-ATPase regulatory subunit 7	PSMD7	3.75E+00	1.13E-02
26S proteasome non-ATPase regulatory subunit 8	PSMD8	2.75E+01	1.56E-03
Poly(U)-binding-splicing factor PUF60	PUF60	2.75E+01	9.95E-04
Pyrroline-5-carboxylate reductase	PYCR1	2.55E+01	3.49E-03
RNA-binding protein 10	RBM10	3.30E+01	4.88E-04
RNA-binding protein 14	RBM14	2.94E+01	6.57E-03
RNA-binding protein 25	RBM25	2.75E+01	7.71E-03
RNA-binding protein 26	RBM26	2.63E+01	3.79E-02
RNA-binding protein 27	RBM27	2.70E+01	1.20E-02
RNA-binding protein 28	RBM28	2.63E+01	5.02E-03
RNA-binding motif protein, X chromosome	RBMX	3.01E+01	8.90E-03
RNA 3-terminal phosphate cyclase-like protein	RCL1	2.65E+01	1.64E-03
Reticulocalbin-2	RCN2	2.73E+01	2.67E-03
Replication factor C subunit 3	RFC3	2.62E+01	2.34E-02
Telomere-associated protein RIF1	RIF1	3.04E+01	9.16E-03
Serine/threonine-protein kinase RIO1	RIOK1	3.02E+01	3.05E-03
RING finger protein 219	RNF219	2.94E+01	2.50E-03
RNA-binding protein 39	RNPC2	2.86E+01	8.92E-03
60S ribosomal protein L10	RPL10	3.26E+01	7.84E-03
60S ribosomal protein L10a	RPL10A	3.22E+01	2.24E-02
60S ribosomal protein L11	RPL11	3.19E+01	1.04E-03
60S ribosomal protein L12	RPL12	3.18E+01	6.43E-03
60S ribosomal protein L13	RPL13	3.30E+01	4.30E-04
60S ribosomal protein L13a	RPL13A	3.17E+01	2.25E-03
60S ribosomal protein L14	RPL14	3.07E+01	7.88E-04
60S ribosomal protein L15	RPL15	5.67E+00	8.90E-03
60S ribosomal protein L17	RPL17	3.16E+01	4.69E-04
60S ribosomal protein L18	RPL18	3.28E+01	1.68E-03
60S ribosomal protein L18a	RPL18A	3.24E+01	2.10E-03
Ribosomal protein L19	RPL19	3.26E+01	4.36E-03
60S ribosomal protein L21	RPL21	3.11E+01	1.99E-03
60S ribosomal protein L22	RPL22	3.05E+01	1.47E-03
60S ribosomal protein L22-like 1	RPL22L1	2.70E+01	6.60E-03
60S ribosomal protein L23	RPL23	3.09E+01	4.70E-03
60S ribosomal protein L23a	RPL23A	3.24E+01	1.26E-03
60S ribosomal protein L24	RPL24	3.03E+01	1.24E-03
60S ribosomal protein L26	RPL26	3.24E+01	1.20E-03
60S ribosomal protein L27	RPL27	3.18E+01	3.06E-03

**Table 1** continued

Protein name	Gene ID	Log2 ratio	P-value
60S ribosomal protein L27a	RPL27A	3.06E+01	5.33E-04
60S ribosomal protein L28	RPL28	3.22E+01	6.23E-04
60S ribosomal protein L29	RPL29	3.19E+01	3.76E-04
60S ribosomal protein L3	RPL3	7.15E+00	6.72E-03
60S ribosomal protein L30	RPL30	3.04E+01	2.06E-03
60S ribosomal protein L31	RPL31	3.15E+01	3.12E-04
60S ribosomal protein L32	RPL32	3.18E+01	3.51E-04
60S ribosomal protein L34	RPL34	2.90E+01	4.73E-03
60S ribosomal protein L35	RPL35	3.13E+01	1.43E-02
60S ribosomal protein L35a	RPL35A	3.14E+01	2.01E-02
60S ribosomal protein L36	RPL36	3.02E+01	1.49E-02
60S ribosomal protein L36a	RPL36A	2.97E+01	5.51E-04
60S ribosomal protein L37a	RPL37A	3.07E+01	1.05E-04
60S ribosomal protein L38	RPL38	2.90E+01	3.49E-02
60S ribosomal protein L4	RPL4	3.36E+01	1.82E-03
60S ribosomal protein L5	RPL5	3.26E+01	6.62E-03
60S ribosomal protein L6	RPL6	6.39E+00	9.35E-03
60S ribosomal protein L7	RPL7	3.33E+01	2.21E-03
60S ribosomal protein L7a	RPL7A	8.22E+00	1.74E-03
60S ribosomal protein L8	RPL8	3.33E+01	9.73E-04
60S ribosomal protein L9	RPL9	3.06E+01	1.10E-04
60S acidic ribosomal protein P0	RPLP0	3.23E+01	2.18E-03
60S acidic ribosomal protein P2	RPLP2	2.87E+01	4.32E-03
40S ribosomal protein S10	RPS10	3.21E+01	1.86E-03
40S ribosomal protein S11	RPS11	3.24E+01	1.88E-03
40S ribosomal protein S12	RPS12	3.14E+01	4.05E-04
40S ribosomal protein S13	RPS13	3.22E+01	1.60E-03
40S ribosomal protein S14	RPS14	3.15E+01	4.92E-04
40S ribosomal protein S15	RPS15	3.15E+01	3.33E-02
40S ribosomal protein S15a	RPS15A	3.19E+01	1.70E-03
40S ribosomal protein S16	RPS16	3.24E+01	1.08E-03
40S ribosomal protein S17	RPS17	3.19E+01	1.78E-03
40S ribosomal protein S18	RPS18	8.03E+00	7.90E-09
40S ribosomal protein S19	RPS19	3.22E+01	1.65E-03
40S ribosomal protein S2	RPS2	3.28E+01	1.71E-03
40S ribosomal protein S20	RPS20	3.21E+01	4.89E-04
40S ribosomal protein S21	RPS21	2.88E+01	2.47E-03
40S ribosomal protein S23	RPS23	3.25E+01	1.31E-03
40S ribosomal protein S24	RPS24	3.00E+01	1.10E-04
40S ribosomal protein S25	RPS25	3.14E+01	5.19E-03

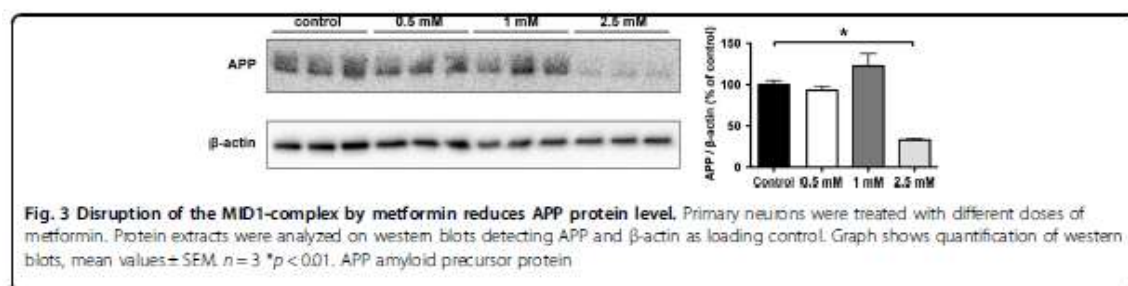
**Table 1** continued

Protein name	Gene ID	Log2 ratio	P-value
40S ribosomal protein S26	RPS26	3.08E+01	2.54E-02
40S ribosomal protein S27	RPS27	3.00E+01	3.65E-03
40S ribosomal protein S3	RPS3	3.28E+01	3.26E-03
40S ribosomal protein S3a	RPS3A	3.30E+01	4.75E-04
40S ribosomal protein S4, X isoform	RPS4X	6.65E+00	2.28E-03
40S ribosomal protein S6	RPS6	3.18E+01	2.28E-03
40S ribosomal protein S7	RPS7	3.28E+01	1.99E-02
40S ribosomal protein S8	RPS8	3.24E+01	3.63E-03
40S ribosomal protein S9	RPS9	3.31E+01	3.94E-03
40S ribosomal protein S4	RPS4	3.32E+01	1.29E-03
Ribosome-binding protein 1	RRBP1	2.84E+01	3.20E-02
RRP12-like protein	RRP12	2.58E+01	1.13E-02
Ribosomal L1 domain-containing protein 1	RSL1D1	2.69E+01	1.56E-02
U4/U6.U5 tri-snRNP-associated protein 1	SART1	2.91E+01	1.18E-04
Splicing factor, arginine/serine-rich 15	SCAF4	2.74E+01	1.68E-02
Protein SDA1 homolog	SDAD1	2.64E+01	1.69E-02
Plasminogen activator inhibitor 1 RNA-binding protein	SERBP1	3.28E+01	2.19E-02
Splicing factor 3B subunit 1	SF3B1	2.81E+01	8.87E-03
Splicing factor 3B subunit 3	SF3B3	2.72E+01	1.14E-02
Superkiller viralicidic activity 2-like 2	SKIV2L2	2.75E+01	8.05E-03
U5 small nuclear ribonucleoprotein 200 kDa helicase	SNRNP200	3.06E+01	5.98E-03
U5 small nuclear ribonucleoprotein 40 kDa protein	SNRNP40	2.72E+01	1.41E-02
Small nuclear ribonucleoprotein Sm D1	SNRPD1	3.02E+01	1.48E-03
Small nuclear ribonucleoprotein Sm D2	SNRPD2	2.92E+01	2.94E-04
Small nuclear ribonucleoprotein Sm D3	SNRPD3	2.95E+01	1.93E-02
Small nuclear ribonucleoprotein-associated proteins B and B	SNRPN	3.06E+01	4.62E-04
Spectrin alpha chain, non-erythrocytic 1	SPTAN1	3.41E+01	9.63E-04
Spectrin beta chain, non-erythrocytic 1	SPTBN1	3.41E+01	9.41E-05
SRSF protein kinase 1	SRPK1	2.94E+01	5.81E-03
SRSF protein kinase 2	SRPK2	2.60E+01	2.88E-02
Serine/arginine repetitive matrix protein 1	SRRM1	2.85E+01	1.46E-02
Serrate RNA effector molecule homolog	SRRT	2.57E+01	2.04E-03
Serine/arginine-rich splicing factor 1	SRSF1	2.74E+01	1.86E-04
Serine/arginine-rich splicing factor 2	SRSF2	2.69E+01	4.59E-02
Serine/arginine-rich splicing factor 3	SRSF3	2.87E+01	1.42E-03
Double-stranded RNA-binding protein Staufen homolog 1	STAU1	2.88E+01	1.18E-02
Serine/threonine-protein kinase 38	STK38	2.78E+01	2.59E-02
SUN domain-containing protein 2	SUN2	2.97E+01	6.35E-04
Heterogeneous nuclear ribonucleoprotein Q	SYNCRIP	2.82E+01	1.08E-02
Very-long-chain enoyl-CoA reductase	TECR	2.70E+01	4.59E-03

**Table 1** continued

Protein name	Gene ID	Log2 ratio	P-value
Testis-expressed sequence 10 protein	TEX10	2.64E+01	1.64E-08
THO complex subunit 2	THOC2	2.53E+01	1.37E-02
Tight junction protein ZO-2	TJP2	2.65E+01	6.69E-08
Transmembrane protein 33	TMEM33	2.74E+01	1.11E-02
Tropomodulin-3	TMOD3	2.63E+01	4.62E-08
TRMT1-like protein	TRMT1L	2.82E+01	9.34E-08
Tubulin beta-3 chain	TUBB3	2.57E+01	5.04E-04
Tubulin beta-4A chain	TUBB4A	2.61E+01	2.90E-02
Splicing factor U2AF 35 kDa subunit	U2AF1	2.90E+01	7.02E-08
Splicing factor U2AF 65 kDa subunit	U2AF2	2.98E+01	4.30E-08
U2 snRNP-associated SURP motif-containing protein	U2SURP	2.78E+01	1.78E-05
E3 ubiquitin-protein ligase UBR5	UBR5	2.78E+01	2.75E-02
U4/U6/U5 tri-snRNP-associated protein 2	USP39	2.88E+01	2.14E-02
Transitional endoplasmic reticulum ATPase	VCP	2.80E+01	7.61E-05
Vimentin	VIM	1.35E+00	2.08E-02
Methylome protein 50	WDR77	3.30E+01	2.27E-02
Exportin-T	XPOT	2.64E+01	7.27E-08
Nuclease-sensitive element-binding protein 1	YBX1	3.07E+01	3.00E-08
YTH domain-containing protein 1	YTHDC1	2.78E+01	8.82E-08
YTH domain-containing family protein 2	YTHDF2	1.60E+00	3.42E-02
Zinc finger CCH domain-containing protein 18	ZC3H18	2.79E+01	1.14E-02
Zinc finger CCH-type antiviral protein 1	ZC3HAV1	2.79E+01	1.27E-02
Zinc finger protein 622	ZNF622	2.75E+01	1.14E-02

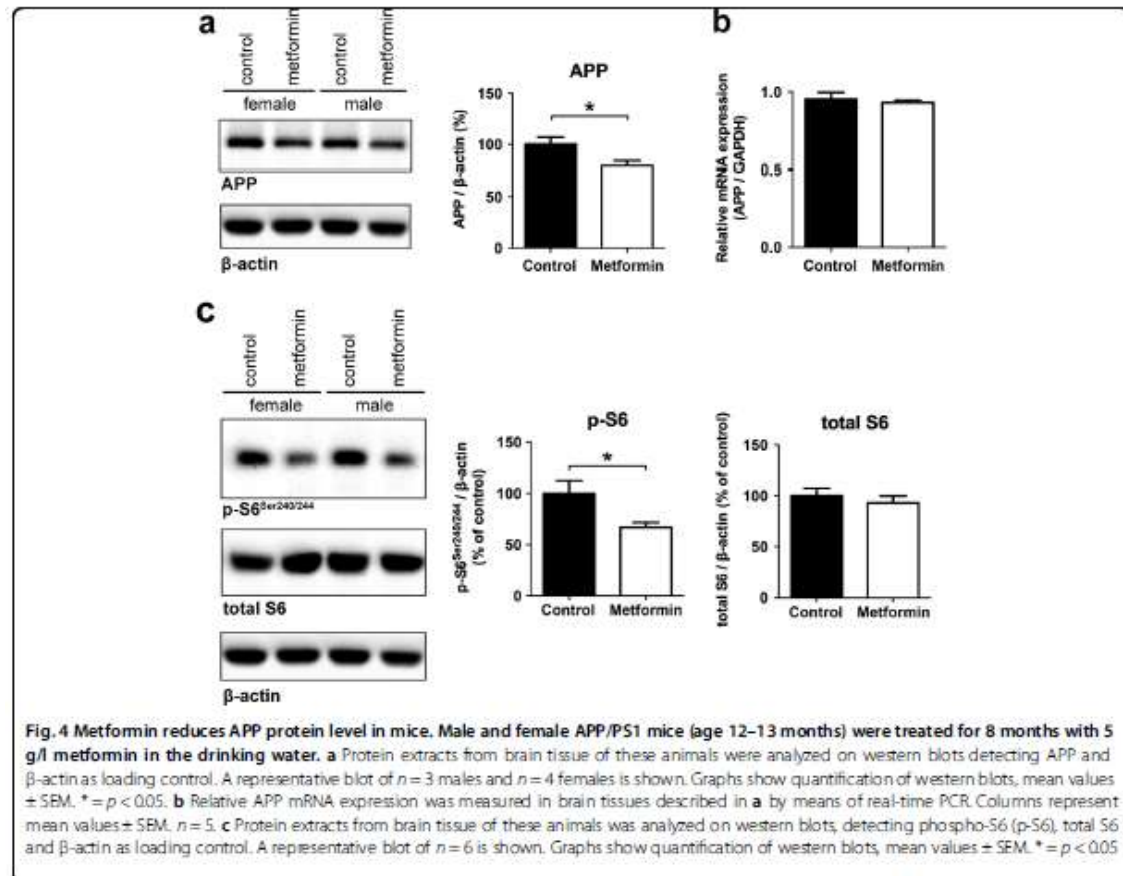
Log2 ratio and *p*-values were calculated using measured protein intensities, i.e. extracted ion current (XIC) of all isotopic clusters associated with the identified amino acid sequence. Log2 ratio was calculated from the intensity sum of samples/controls. *p*-values are the result of a two-sided *t*-test, samples vs. control. In cases where intensities had been measured in 2 (out of 3) replicates, the third intensity value was added through imputation. If no intensity could be measured in all 3 replicates, the intensities were set from 0 to 1 in order to still be able to calculate a ratio (same applies to cases where only 1 intensity could be measured).



In summary, all these data suggest that metformin inhibits the MID1-dependent translation of APP and thereby reduces Aβ plaque burden and improves cognitive impairments in an AD mouse model.

## Discussion

In this study, we show a novel regulatory mechanism controlling the protein synthesis of APP; this mechanism involves the MID1 protein, which induces the translation



of APP by regulating mTOR-eIF signaling. Disassembly of the MID1 protein complex by metformin reduces the protein production of APP. Furthermore, we show that chronic treatment of AD mice with metformin decreases the protein level of APP and its cleavage products, including A $\beta$ . This together with our previous observation that disassembly of the MID1 protein complex by metformin also decreases tau-phosphorylation<sup>7</sup>, makes MID1 a particularly interesting drug target for treating AD.

Among other effects, metformin induces PP2A activity by interfering with the assembly of the MID1-PP2A-complex<sup>7</sup>. Although MID1 has an inhibitory effect on PP2A<sup>8</sup>, it positively regulates mTOR<sup>9</sup>. Therefore, metformin activates PP2A, while at the same time it suppresses mTOR. Decreased mTOR signalling results in activation of autophagy and decreased translation of mRNAs regulated by its downstream effectors S6K and 4E-BP1<sup>21</sup>. The MID1 protein complex via PP2A and mTOR stimulates translation of mRNAs that are associated with this protein complex, some of which play a role in neurodegeneration<sup>11–13,16</sup>.

Here we identified APP mRNA as a novel binding partner of MID1, suggesting that the MID1 complex also induces its translation. Since the biguanide metformin interferes with the assembly of the MID1 protein complex, it thereby reduces translation of the APP mRNA, leading to decreased processing by the amyloidogenic pathway. This mode of action of metformin has also been shown for other mRNAs that are associated with the MID1-complex, including the androgen receptor (AR) and BACE1 mRNA<sup>14,15</sup>. Furthermore, we report a so far unknown additional connection between MID1 and the mTOR-dependent translation initiation pathway: MID1 binds to RPLP0, a protein of the large ribosomal subunit. Metformin treatment interferes with the MID1-complex assembly and thus inhibits MID1-dependent translation<sup>7,14,15</sup>. Overall, metformin seems to decrease translation of several MID1-PP2A-mTOR dependent mRNAs. However, since chronic administration of metformin is well tolerated in type 2 diabetes patients, this does not seem to be particularly deleterious. Additionally, both induction of autophagy and reduced protein translation

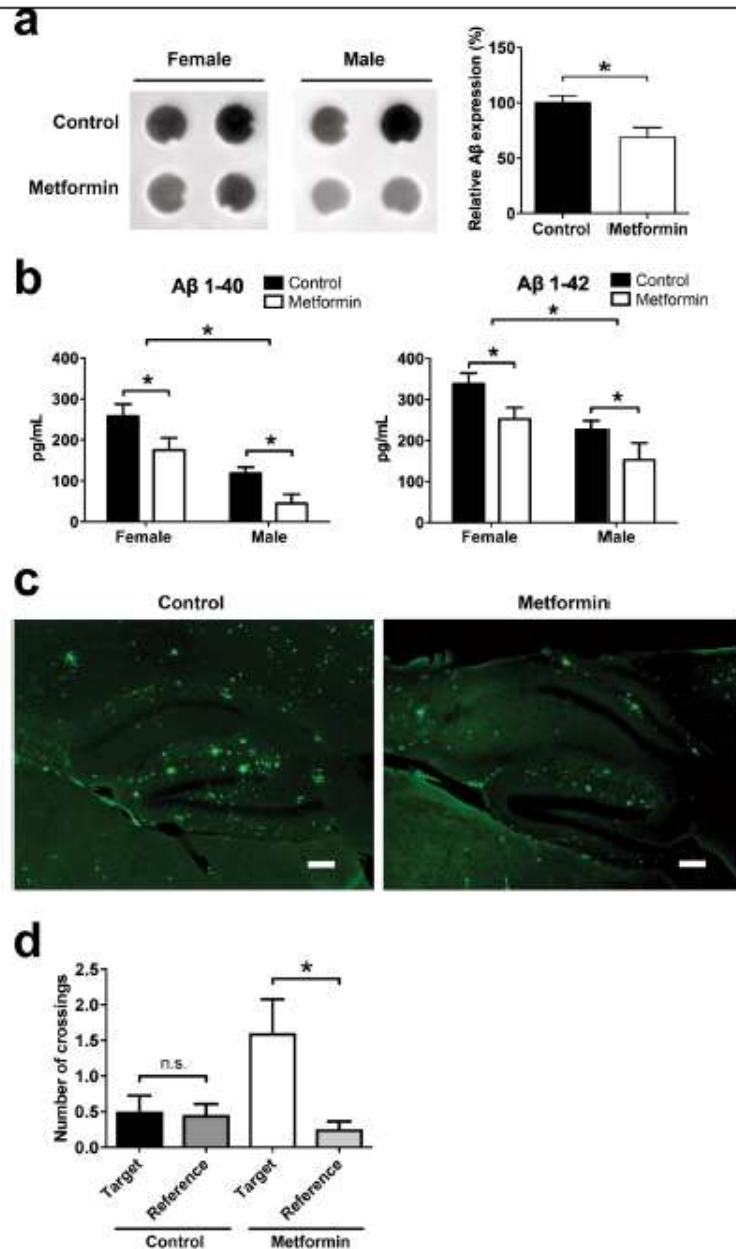
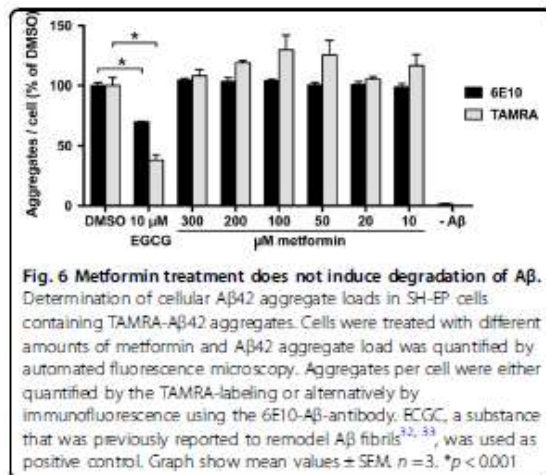


**Fig. 5 Metformin reduces Aβ plaque burden in mice.** Male and female APP/PS1 mice (age 12–13 months) were treated for 8 months with 5g/l metformin in the drinking water. **a** Protein extracts from brain tissue of these animals was analyzed on dot blots detecting Aβ. Representative blots of  $n = 4$  females and  $n = 3$  males are shown. Graphs show quantification of dot blots, mean values  $\pm$  SEM, the mean value of control animals was set to 100%.  $*p < 0.05$ . **b** ELISA measurements of Aβ in brain tissues described in **a**. Columns represent mean values (pg/ml)  $\pm$  SEM,  $n = 4$  females,  $n = 3$  males.  $*p < 0.05$ . **c** Sagittal brain sections of mice were stained with Thioflavin-S for Aβ aggregates. Scale bar = 200  $\mu$ m. **d** Spatial learning and memory in the Morris water maze. Mice were trained on a hidden version of the Morris water maze. After completion of training, we performed a probe trial to test how accurately the animals had learned the location of the escape platform (target). The graph shows the number of crossings of the target location vs. averaged crossings of corresponding positions in the adjacent, non-target quadrants (reference). Shown are means  $\pm$  SEM.  $n = 10$  mice per group.  $*p < 0.05$



are especially vital for the adult nervous system, since these processes control homeostasis of Aβ and phospho-tau<sup>19,20</sup>. Therefore, we believe that reduced protein translation of several mRNAs regulated by MID1/PP2A/mTOR would be beneficial.

The use of metformin as a putative drug for treating AD has been discussed controversially<sup>15,21–27</sup>. While in some studies metformin treatment increased APP<sup>27</sup> or Aβ levels<sup>24</sup>, other studies showed that metformin attenuated AD-like neuropathology for example by decreasing the level of the APP processing enzyme BACE1<sup>15</sup>, or by decreasing tau hyperphosphorylation<sup>7,25</sup>. This discrepancy can be explained by differences in the experimental set-up in the different studies. First, the effect of metformin seems to be dose- and time-dependent. For example, in cell culture models high doses of metformin (5–50 mM) or long incubation times result in an increased expression of APP and BACE1<sup>24,27</sup>, while lower doses (1–2.5 mM) decrease BACE1 protein levels as well as APP cleavage products and tau phosphorylation<sup>7,15,23</sup>. In wild-type mice treatment with 2 g/l metformin in the drinking water results in increased expression of BACE1 and APP as well as APP cleavage products<sup>24,27</sup>, while treatment with 5 g/l reduces BACE1 protein expression<sup>15</sup> as well as tau-phosphorylation<sup>7</sup>. Also the period of treatment seems to be important. Different to studies in which increased APP and BACE1 levels were detected<sup>24,27</sup>, our study lasted over a treatment period of 8 months. Therefore, differences between acute and chronic pharmacological treatments could account for the observed effects. Of note, in our experiments we detected a significant difference in Aβ levels between female and male mice, with female mice having an increased Aβ burden compared to male mice. This observation is in line with previous findings, showing that female mice exhibit much higher γ-secretase activity in

aged brain compared to male mice and therefore, Aβ plaque pathology in female mouse models of AD is increased compared to males<sup>28</sup>. Interestingly, another study in which metformin had been used in a chronic treatment demonstrated that learning and memory were improved by metformin treatment in female mice, while it had an opposite effect in male mice<sup>26</sup>. This shows that also the sex of the experimental animals used could account for different findings. Another important point is the age of the experimental animals in which the treatment was initiated. To our knowledge our study is the first study in which metformin treatment was initiated in aged mice displaying an already progressed state of the disease.

Taken together, our study shows that long-term treatment with metformin inhibits the MID1-dependent translation of APP and thus reduces Aβ plaque burden without any side effects for the animals. The administration of metformin for a prolonged period (8 months) started late in life and in an already progressed state of the disease. Therefore, our data represent the effects of metformin on biochemical and cognitive changes of the CNS in a progressed disease stage of AD. In addition, we could show in our previous work, that disassembly of the MID1 protein complex by metformin also decreases tau-phosphorylation<sup>7</sup>, making the MID1 complex a particularly interesting target for treating all AD neuropathologies.

## Materials and methods

### In vitro translation

To create an hAPP-Luciferase fusion construct, the human APP wild type splice variant 695 cDNA sequence was amplified by PCR from the pcDNA-hAPP695wt plasmid using primers APP-pGL3m-fwd and APP-pGL3m-rev (Table 2), thereby creating HindIII and NcoI restriction sites, which were used to insert the amplified sequence into the pGL3m plasmid<sup>11</sup> 5' of the firefly luciferase sequence. To enable in vitro transcription, a T7 site was inserted by PCR using primers T7-hAPP-ivts-fwd and pGL3-2258-ivts-rev (Table 2). The resulting amplicon was phenol-chloroform purified and subjected to in vitro transcription using the RiboMAX<sup>TM</sup> Large scale RNA production system-T7 (Promega, Mannheim, Germany) according to the manufacturer's instructions. In vitro transcribed RNA was phenol-chloroform purified and translated in vitro using the Flexi Rabbit Reticulocyte Lysate System (Promega) in presence or absence of inhibitors. Luciferase activity was quantified using the Firefly Luciferase Assay System (Promega) on a FLUOstar Omega 96-well plate reader (BMG Labtech, Ortenberg, Germany).

### Immunoprecipitation

Cells have been authenticated by PCR-single-locus-technology (service by Eurofins (Ebersberg, Germany)) in December 2016. HEK293T cells were transfected with

**Table 2** Primer sequences

mAPP-RT-fwd	CAC ATC GTG ATT CCT TAC CG
mAPP-RT-rev	GTC TCA CAA ACA TCC ATC CG
mGAPDH-RT-fwd	GCA CAG TCA AGG CCG AGA AT
mGAPDH-RT-rev	GCC TTC TCC ATG GTG GTG AA
APP-pGL3m-fwd	TGC AAA AAG CTT GGC ATT CCG GTA CTG TTG GTA AAG CCA
APP-pGL3m-rev	CGT CTT CCA TGG CGC CTG GAC CGT TCT GCA TCT GCT CAA AGA ACT TGT AGG T
T7-hAPP-ivts-fwd	CGA AAT TAA TAC GAC TCA CTA TAG GGG TAA AGC CAC CAT GCT GCC CGG TTT GGC ACT GC
pGL3-2258-ivts-rev	CCG CGC CCA CCG GAA GGA GCT GAC TGG

pCMV-MID1-Tag2A using PolyFect (Qiagen, Hilden, Germany) according to the manufacturer's instructions. Untransfected cells were used as control. Cell pellets were lysed in TKM buffer (20 mM Tris pH 7.4, 100 mM KCl, 5 mM MgCl<sub>2</sub>, 0.5% NP40, 1 mM DTT, protease inhibitors) using a Precellys cell homogenizer. For pre-clearing, 200 µl of IgG-agarose beads were added to the lysates and incubated rotating for 30 min at 4 °C. The beads were pelleted for 5 min at 21,000 × g. Precleared lysates were then added to 200 µl anti-FLAG M1 Agarose Affinity Gel (Sigma-Aldrich/Merck, Darmstadt, Germany). After overnight rotation at 4 °C, the beads were washed 6 times and resuspended in 50 µl 1x SDS Buffer and boiled for 10 min at 95 °C. The proteins were then either identified by mass spectrometry analysis or analyzed on a western blot. For ribosome disassembly, immunoprecipitation was performed in TKM buffer containing 40 mM EDTA. For RNase digest, the beads were washed three times after overnight incubation, anti-FLAG beads were split into two aliquots and resuspended in NEBuffer 3 (B7003S, New England Biolabs, Frankfurt, Germany). RNase If (M0243, New England Biolabs) was added to a final concentration of 500 U/ml to one immunoprecipitate and incubated for 45 min at 37 °C. Subsequently, beads were washed three times and treated as described above.

#### Mass spectrometry

The eluted proteins were concentrated into one band on an SDS-PAGE gel. The band was excised and the proteins contained were processed using an automated sample preparation setup<sup>29</sup>. The generated peptides were purified on StageTips<sup>30</sup>. Samples were measured on a Q-Exactive mass spectrometer (Thermo-Fisher, Waltham, MA, USA) coupled to a Proxeon nano-LC system (Thermo-Fisher) in data-dependent acquisition mode, selecting the top 10 peaks for HCD fragmentation. A 1h gradient (solvent A: 5% acetonitrile, 0.1% formic acid; solvent B: 80% acetonitrile, 0.1% formic acid) was applied for the samples using an in-house prepared nano-LC column (0.075 mM × 150 mM, 3 µm Reprosil C18, Dr.

Maisch GmbH, Ammerbuch-Entringen, Germany). A volume of 2 µl sample was injected and peptides were eluted with 3 h gradients of 5–75% solvent B at flow rates of 0.25 µl/min. MS acquisition was performed at a resolution of 70,000 in the scan range from 300 to 1700 *m/z*. The normalized collision energy was set to 26 eV. The mass window for precursor ion selection was set to 2.0 *m/z*. The recorded spectra were analyzed using the MaxQuant software package (Version 1.3.0.5)<sup>31</sup> by matching the data to the Uniprot human database (downloaded on 06.05.2012) with a false discovery rate (FDR) of 1%.

#### Peptide treatments

Murine primary cortical neurons were treated with 2.5 µM of a peptide that mimics the MID1-α4 binding site and thus outcompetes MID1 from binding to α4-PP2Ac. As control a mutant peptide was used. Peptides (GSK'364A and GSK'365A) containing a 29-residue sequence from α4 (AQAKVFGAGYPSLPTMTVSDWYEQHRKYG and AQAKVFGAGYPSLPTMTVSDWAEQHRKYG, respectively) with an N-terminal sequence derived from HIV-TAT protein (RKKRRQRRR) were supplied by Cambridge Research Biochemicals (Billingham, UK). They were synthesized using standard automated solid-phase peptide synthesis via the Fmoc/tBu strategy. Cleavage from the resin was performed using 95% trifluoroacetic acid. Crudes were purified by preparative high-performance liquid chromatography (HPLC), freeze dried and characterized by high-performance liquid chromatography (HPLC) and matrix-assisted laser desorption/ionization time-of-flight (MALDI-TOF) mass spectrometry.

#### In vivo treatments mice

Male and female APP/PS1 (B6C3-Tg(APP<sup>sw</sup>,PSEN1<sup>de9</sup>)85Dbo/Mmjax) mice (age 12–13 months) were treated for 8 months with 5 g/l metformin in the drinking water with daily change of water and addition of fresh metformin. Water intake and body weight of the animals were monitored. After 8 months of treatment, animals were sacrificed and brains were snap-frozen in liquid nitrogen and broken up using a

mortar. All procedures were in compliance with German Animal Protection Law and were approved by the competent authorities (Landesamt für Naturschutz und Verbraucherschutz Nordrhein-Westfalen; AZ 87-51.04.2011, A049/01).

#### Morris water maze

We assessed spatial learning and memory in the Morris water maze in APP/PS1 mice treated with metformin or vehicle control. The water pool (Med Associates) had a diameter of 1.2 m and was filled with opaque water (temperature: 24 °C). Mice received 6 daily training trials for 3 consecutive days on a hidden version of the Morris water maze (i.e., the maze contained an escape platform hidden underneath the water surface in a constant location of the pool). To evaluate the accuracy with which the animals had learned the position of the escape platform, we performed a probe trial (during which the platform was removed from the pool) once training was completed. Behavior of the animals was recorded using an automated tracking system (Ethovision XT, Noldus). We determined the number of crossings of the exact target location (i.e., where the platform was located during training) and compared it to the average crossings of analogous positions in the adjacent, non-target quadrants (reference).

#### Thioflavin-S staining

Sagittal brain sections were incubated in 1x TBS buffer containing 10% Triton X-100 and transferred onto glass slides. The slides were dried overnight at room temperature. Slides were washed 3 times for 3 min in distilled water, and incubated for 3 min in 0.1% Thioflavin-S staining solution (dissolved in 10% ethanol diluted in distilled water) in the dark. Sections were washed 3 times in distilled water and incubated for 20 min in 1% acetic acid in the dark. Slides were washed with tap water, cover-slipped with mounting medium (Thermo-Fisher), and stored in the dark at 4 °C.

#### Western blot

Brain samples were homogenized either in RIPA buffer (20 mM Tris-HCl (pH 7.5), 150 mM NaCl, 1 mM EDTA, 1 mM EGTA, 1% NP-40, 1% sodium deoxycholate, 2.5 mM sodium pyrophosphate, 1 mM  $\beta$ -glycerophosphate, 1 mM  $\text{Na}_3\text{VO}_4$ , 1  $\mu\text{g}/\text{ml}$  leupeptin) or in SDS PAGE buffer B (40 mM Tris-HCl pH 6.8, 4% Glycerol, 2% SDS, 0.01% bromophenolblue, 2 mM 2-mercaptoethanol), sonicated and boiled for 5 min at 95 °C. Proteins were analyzed on 10 or 12% SDS gels and blotted onto PVDF membranes (Roche, Mannheim, Germany). Blots were blocked in milk and incubated with the antibodies listed below.

Bands were densitometrically quantified using AIDA software v4.27 (Raytest, Straubenhardt, Germany).

#### Statistical analysis

Statistical analyses were performed using two-way ANOVA, as well as Student's t-test or Mann-Whitney test (two-tailed) for two-group comparisons, as appropriate.

#### Dot blot

Brain samples were homogenized in RIPA buffer. 50  $\mu\text{g}$  total protein per well were loaded and proteins were transferred to a PVDF membrane using a HYBRI-DOT manifold. The aggregates on the membrane were detected by incubation with anti-beta-amyloid 6E10 antibodies (BioLegend, San Diego, CA, USA).

#### ELISA

ELISA assays to measure A $\beta$  were performed using the A $\beta$ 40 / A $\beta$ 42 ELISA Kits (Life Technologies) according to the manufacturer's protocol.

#### Antibodies

The following antibodies were purchased from Cell Signaling (Leiden, Netherlands): S6 (#2317), pS6 (#4858), actin (#4967), eIF3A (#3411), eIF4G (#2498), RPL5 (#51345) and GAPDH (#2118). FLAG-HRP (A8592) antibody was purchased from Sigma; RPLP0 (ab192866), RPS3 (#128995), and APP (ab2071) from Abcam (Cambridge, UK), and anti-beta-amyloid 6E10 from BioLegend (803001).

#### Real-time PCR

Total RNA was isolated using the RNeasy Plus Mini Kit (Qiagen). cDNA was synthesized using the TaqMan reverse transcription reagents kit (Applied Biosystems, Waltham, MA, USA) and real-time PCR was carried out using the SYBRGreen PCR master mix (Applied Biosystems). Primers used are listed in Table 2.

#### RNA immunoprecipitation

Murine primary cortical neurons were transfected with FLAG-tagged MID1 using Lipofectamine 2000 (Invitrogen Waltham, MA, USA). 48 h after transfection, cells were treated with or without 2.5 mM metformin and incubated another 24 h. After UV-crosslinking (200 mJ/cm<sup>2</sup>) cells were lysed in TKM buffer (20 mM Tris pH 7.4, 100 mM KCl, 5 mM MgCl<sub>2</sub>, Complete protease inhibitor cocktail (Roche), RNase inhibitor, 0.2% NP40) and MID1 protein complexes were purified by immunoprecipitation using anti-FLAG M1 Agarose Affinity Gel (Sigma-Aldrich) or IgG-agarose (Sigma-Aldrich) as a negative control. Protein-bound mRNA was isolated after DNase and proteinase K digestion by phenol-chloroform purification and analyzed by RT-PCR. Primers used are listed in Table 2.

### Automated fluorescence microscopy and determination of cellular A $\beta$ 42 aggregate loads

For fluorescent labeling of A $\beta$  aggregates, 20  $\mu$ M A $\beta$ 42 peptide stock solutions diluted in low salt buffer (10 mM NaCl, 1.9 KH<sub>2</sub>PO<sub>4</sub>, 8.1 mM K<sub>2</sub>HPO<sub>4</sub>, pH 7.4) were mixed with 5% A $\beta$ 42 peptides which have been N-terminally labeled with the fluorophore 5-Carboxytetramethylrhodamine (TAMRA) in solid-state peptide synthesis by AnsSpec, Fremont, USA. Then, mixed A $\beta$  peptide solutions were aggregated at 37 °C for 18 h under 300 rpm constant agitation followed by sonication with a Sonic Dismembrator Model 120 from Fisher Scientific GmbH (Schwerte, Germany) at low intensity for 6 rounds of 10 s. SH-EP cells (DSMZ, Braunschweig, Germany) were cultured in DMEM (Gibco by Thermo-Fisher GmbH, Dreieich, Germany) containing 10% fetal bovine serum (FBS), 5% Glucose, 100 units/ml penicillin and streptomycin, respectively. Incubation was carried out at 37 °C with 5% (v/v) CO<sub>2</sub>. For A $\beta$ 42 aggregate internalization, cells were treated with 600 nM or 1  $\mu$ M TAMRA-A $\beta$ 42 for 18 h. To ensure removal of free and surface-bound aggregates, A $\beta$  containing medium was aspirated, cells were washed with phosphate-buffered saline (PBS), trypsinized and collected in fresh medium. Then, cells were seeded into 96-well cell culture plates and treated with different amounts of metformin for 6 h. Cells were fixed in 2% paraformaldehyde for 20 min at room temperature, followed by Nuclei staining with Hoechst (1:2500 Hoechst 33342, Sigma-Aldrich Chemie GmbH Munich, Germany) and then washed twice with PBS, before fluorescent microscopy was performed in a Cellomics ArrayScan High-Content System (Thermo-Fisher) using an objective with 20-fold magnification. After image acquisition, automated data analysis was performed using ArrayScan VTI (700 Series, Thermo-Fisher). For quantification, individual cells were detected via Hoechst fluorescent signals (XT53, filter and dichroic-emitter pair) and total TAMRA fluorescent areas per cell (XT32, filter and dichroic-emitter pair) were measured and calculated from technical triplicates. Alternatively, A $\beta$  was stained by immunofluorescence using the 6E10 antibody (BioLegend).

### Acknowledgements

This work was supported by the Else Kröner-Fresenius-Stiftung. We thank Iain Ulings at GlaxoSmithKline for supplying the peptides.

### Author details

<sup>1</sup>Deutsches Zentrum für Neurodegenerative Erkrankungen e.V., Bonn, Germany. <sup>2</sup>Max Delbrück Center for Molecular Medicine (MDC) Berlin-Buch, Berlin, Germany. <sup>3</sup>Luxembourg Institute of Health, Strassen, Luxembourg

### Competing interests

The authors declare that they have no competing interests.

**Publisher's note:** Springer Nature remains neutral with regard to jurisdictional claims in published maps and institutional affiliations.

Received: 15 September 2017 Accepted: 29 September 2017

Published online: 29 January 2018

### References

1. Alzheimer, A., Steitzmann, R. A., Schnitzlein, H. N. & Murtagh, F. R. An English translation of Alzheimer's 1907 paper, "Über eine eigenartige Erkrankung der Hirnrinde". *Clin. Anat.* **8**, 429–431 (1995).
2. Walsh, J. S., Welch, H. G. & Larson, E. B. Survival of outpatients with Alzheimer-type dementia. *Ann. Intern. Med.* **113**, 429–434 (1990).
3. Burns, A., Jacoby, R. & Levy, R. Psychiatric phenomena in Alzheimer's disease. I: Disorders of thought content. *Br. J. Psychiatr.* **157**, 72–76 (1990).
4. Alonso, A. D., Grundke-Iqbal, I., Barra, H. S. & Iqbal, K. Abnormal phosphorylation of tau and the mechanism of Alzheimer neurofibrillary degeneration: sequestration of microtubule-associated proteins 1 and 2 and the disassembly of microtubules by the abnormal tau. *Proc. Natl. Acad. Sci. U. S. A.* **94**, 298–303 (1997).
5. Gong, C. X., Liu, F., Grundke-Iqbal, I. & Iqbal, K. Post-translational modifications of tau protein in Alzheimer's disease. *J. Neural. Transm.* **112**, 813–838 (2005).
6. Tian, Q. & Wang, J. Role of serine/threonine protein phosphatase in Alzheimer's disease. *Neurosignal.* **11**, 262–269 (2002).
7. Kikstein, E. et al. Biguanide metformin acts on tau phosphorylation via mTOR/protein phosphatase 2A (PP2A) signaling. *Proc. Natl. Acad. Sci. U. S. A.* **107**, 21830–21835 (2010).
8. Trockenbacher, A. et al. MID1, mutated in Opitz syndrome, encodes an ubiquitin ligase that targets phosphatase 2A for degradation. *Nat. Genet.* **29**, 287–294 (2001).
9. Liu, F., Knutzen, C. A., Krauss, S., Schweiger, S. & Chiang, G. G. Control of mTORC1 signaling by the Opitz syndrome protein MID1. *Proc. Natl. Acad. Sci. U. S. A.* **108**, 8680–8685 (2011).
10. Gingras, A.-C., Raught, B. & Sorensen, N. Regulation of translation initiation by FRAP/mTOR. *Genes. Dev.* **15**, 807–826 (2001).
11. Aenda-Orgilles, B. et al. Protein phosphatase 2A (PP2A)-specific ubiquitin ligase MID1 is a sequence-dependent regulator of translation efficiency controlling 3-phosphoinositide-dependent protein kinase-1 (PDK1). *J. Biol. Chem.* **286**, 39945–39957 (2011).
12. Krauss, S. et al. Translation of HTT mRNA with expanded CAG repeats is regulated by the MID1-PP2A protein complex. *Nat. Commun.* **4**, 1511 (2013).
13. Aenda-Orgilles, B. et al. The Opitz syndrome gene product MID1 assembles a microtubule-associated ribonucleoprotein complex. *Hum. Genet.* **123**, 163–176 (2008).
14. Demir, U., Koehler, A., Schneider, R., Schweiger, S. & Klocker, H. Metformin anti-tumor effect via disruption of the MID1 translational regulator complex and AR downregulation in prostate cancer cells. *BMC. Cancer.* **14**, 52 (2014).
15. Herrich, M. M. et al. The anti-diabetic drug metformin reduces BACE1 protein level by interfering with the MID1 complex. *PLoS. ONE.* **9**, e102400 (2014).
16. Kohler, A. et al. A hormone-dependent feedback-loop controls androgen receptor levels by limiting MID1, a novel translation enhancer and promoter of oncogenic signaling. *Mol. Cancer.* **13**, 146 (2014).
17. Nolan, R. D. & Amstein, H. R. The dissociation of rabbit reticulocyte ribosomes with EDTA and the location of messenger ribonucleic acid. *Eur. J. Biochem.* **9**, 445–450 (1968).
18. Wulfschieger, S., Loewth, R. & Hall, M. N. TOR signaling in growth and metabolism. *Cell.* **124**, 471–484 (2006).
19. O'Neill, C., Kiely, A. P., Coakley, M. F., Manning, S. & Long-Smith, C. M. Insulin and IGF-1 signalling longevity, protein homeostasis and Alzheimer's disease. *Biochem. Soc. Trans.* **40**, 721–727 (2012).
20. Caccamo, A., Majumder, S., Richardson, A., Strong, R. & Oddo, S. Molecular interplay between mammalian target of rapamycin (mTOR), amyloid-beta and Tau effects on cognitive impairments. *J. Biol. Chem.* **285**, 13107–13120 (2010).
21. Infeld, P., Bodmer, M., Jick, S. S. & Meier, C. R. Metformin, other antidiabetic drugs, and risk of Alzheimer's disease: a population-based case-control study. *J. Am. Geriatr. Soc.* **60**, 916–921 (2012).
22. Moore, E. M. et al. Increased risk of cognitive impairment in patients with diabetes is associated with metformin. *Diabetes. Care.* **36**, 2981–2987 (2013).
23. Gupta, A., Bisht, B. & Dey, C. S. Peripheral insulin-sensitizer drug metformin ameliorates neuronal insulin resistance and Alzheimer's-like changes. *Neuropharmacology.* **60**, 910–920 (2011).

24. Chen, Y. et al. Antidiabetic drug metformin (Glucophage®) increases biogenesis of Alzheimer's amyloid peptides via up-regulating BACE1 transcription. *Proc. Natl. Acad. Sci. U. S. A.* **106**, 3907–3912 (2009).
25. Li, J., Deng, J., Sheng, W. & Zuo, Z. Metformin attenuates Alzheimer's disease-like neuropathology in obese, leptin-resistant mice. *Pharmacol. Biochem. Behav.* **101**, 564–574 (2012).
26. DiTacchio, K. A., Heinemann, S. F. & Dzielawski, G. Metformin treatment alters memory function in a mouse model of Alzheimer's disease. *J. Alzheimers. Dis.* **44**, 43–48 (2015).
27. Pione, P. et al. Metformin increases APP expression and processing via oxidative stress, mitochondrial dysfunction and NF- $\kappa$ B activation: Use of insulin to attenuate metformin's effect. *Biochim. Biophys. Acta* **1853**, 1046–1059 (2015).
28. Pácanica, L., Zhu, L. & Li, Y. M. Gender- and age-dependent gamma-secretase activity in mouse brain and its implication in sporadic Alzheimer disease. *PLoS. ONE* **4**, e5088 (2009).
29. Kanashova, T. et al. Differential proteomic analysis of mouse macrophages exposed to adsorbate-loaded heavy fuel oil derived combustion particles using an automated sample-preparation workflow. *Anal. Bioanal. Chem.* **407**, 5965–5976 (2015).
30. Rappsilber, J., Mann, M. & Ishihama, Y. Protocol for micro-purification, enrichment, pre-fractionation and storage of peptides for proteomics using Stage-Tips. *Nat. Protoc.* **2**, 1896–1906 (2007).
31. Cox, J. & Mann, M. MaxQuant enables high peptide identification rates, individualized p.p.b.-range mass accuracies and proteome-wide protein quantification. *Nat. Biotechnol.* **26**, 1367–1372 (2008).
32. Beschle, J. et al. EGCG remodels mature alpha-synuclein and amyloid-beta fibrils and reduces cellular toxicity. *Proc. Natl. Acad. Sci. U. S. A.* **107**, 7710–7715 (2010).
33. Ehrnhoefer, D. E. et al. EGCG redirects amyloidogenic polypeptides into unstructured, off-pathway oligomers. *Nat. Struct. Mol. Biol.* **15**, 558–566 (2008).

## 7. Acknowledgments

I would like to thank Professor Rüegg for giving me the opportunity of working in this project, and for the challenge that contribute to my personal and scientific growth.

I want to thank Professor Doetsch, Professor Bettler and Professor Scheiffele for advices and guidance during my project.

I want to thank specially my family who keep me strong, they never let me down and gave me all the support to fulfill my goals. My dear sister, Gis: I am so grateful of having you as my sister, I thank my parents for the most beautiful treasure: YOU! Thank you for all the advices, support, words! I could not have done it without you! Thank you for always look after me and share my happiness and accomplishments. I am so lucky to have you as my sister, I am so proud of you! Mike: Thank your for all! You supported me since the beginning of this journey and gave me all the support I needed to complete my dreams. Fam Ross Flores: You are best family I could ever dream to have! I appreciate all that you do for me. My little ones: Addi and Tori, my girls, you are the reason I do not give up. Your enthusiasms and smile transmit me happiness and make me strong to continue. Can't wait to play with you both! Mom and Dad: thank you! Although you cannot be with me physically, you have showed me in infinite ways that I am not alone. Mom: thanks for giving all so that I can accomplish my dream. I hope that you know that I did it. Dad: I will always follow you example, Thank you for showing me the right way.

Liz: Thank you for your guidance, support and advices during all this process. There are not words that can express how grateful I am with you!

Jamie: Thank you for all your support during this time. Thank you for the advices, for listening and hugging me when I needed it most. Thank you for the special moments together, for make me laugh until my stomach hurts. Thank your for the team work, I could not have done it without you!

My friends: I was lucky to meet you all! I appreciate your understanding, support, trips, and all the special moments together. Distance gave me the opportunity to build a new family. Those far away no matter the distance, we were always close in our hearts. Thanks!

## 8. Curriculum Vitae

### **Diana Flores Dominguez**

#### **Curriculum Vitae**

**Peter Merian-strasse 2 · Basel 4052 · +41 (0) 79 942 7256**

[diana.flores@unibas.ch](mailto:diana.flores@unibas.ch) / [dianefd@gmail.com](mailto:dianefd@gmail.com)

#### **INTRODUCTION**

I am an inquisitive and perseverant research scientist, who is committed to work and enthusiastic about new challenges. Throughout my career, I have participated in the planning and evaluation of experiments and results. I have developed strong organizational skills as well as the ability to manage multiple activities and set priorities.

My experience includes toxicology, pharmacology and physiology in research projects related to Alzheimer disease, brain plasticity, oxidative stress, brain metastasis, lung cancer and aging. My career has been international, having studied and researched in Mexico, Germany and Switzerland. I can manage challenging research schedules while working in complex and highly demanding environments. I enjoy collaborating as part of a team but I am also proficient when working individually.

#### **CORE COMPETENCIES AND AREAS OF EXPERTISE**

- Interpersonal and communications skills
- Laboratory technical skills
- Applied Research
- Neurological disorders and Neurodegenerative disease
- Critical thinking and problem solving
- Database management
- Reporting and Documentation
- Project management
- Time management
- Good Clinical Practice (GCP)
- International Conference on Harmonization Guidelines (ICH)
- Basics on drug safety

#### **EDUCATION**

**Postgraduate advanced studies Clinical Research I** | Clinical Trial Unit, University of Basel, Switzerland (2018-2019)

**PhD Neurobiology** | University of Basel, Switzerland (expected 02.2019)

**MSc. Neuroscience** | Friedrich-Wilhelms-University of Bonn, Germany (12.2012)

**B.Sc. Hons Biology** | National Autonomous University of Mexico (UNAM), Mexico BS, Biology (06.2009)

#### **PROFESSIONAL EXPERIENCE AND INTERNSHIPS**

**PhD Research Associate** | Biozentrum Basel, Switzerland 11.2014- (present)

- Planning, organizing, coordinating and executing projects with competing priorities related to neuroplasticity mechanism and aging by using mouse models
- Designed and performed experiments

- Applied strong research and analytical skills to conduct analysis based on the results of the study
- Develop and write protocols, reports and manuscripts for further publication
- Presentation of results in conferences and meetings
- Established collaborations and worked effectively on collaborated projects both independently and in teams

**Research Assistant** | National Institute of Cancer, Mexico

National Institute of Respiratory Diseases, Mexico

07.2013/08.2014

- Designed and performed experiments for biomarkers in lung cancer and brain metastasis using blood and tissue samples from patients
- Design, develop and write investigator protocol and preparing final reports
- Prepared and presented reports
- Established collaborations with other institutes, worked effectively on collaborated projects both independently and in teams
- Set up of laboratory and equipment
- Teaching medical students

## **INTERNSHIPS**

**German Center for Neurodegenerative Diseases (DZNE), Germany**

Department Molecular and Cellular Cognition

04.2012/12.2012

**Institute of Reconstructive Neurobiology, Germany**

Neural Stem Cells and Neurodevelopment

01-03/2012

Cellular Neurobiology of Disease

10-12/2011

## **CERTIFICATES**

**Good Clinical Practice (GPC-E6 (R2) 2016).** Clinical Trial Unit, University Hospital Basel University, TREE online learning (02.2018)

**Project Management in Medicines Development.** Clinical Trial Unit, University Hospital Basel (09.2018)

**Certificate in Animal Management System Pyrat.** University of Basel, Switzerland (07.2017)

**Introduction to Clinical Trials (including ICH-GCP).** CTC Clinical Trial Consulting AG (05.2017)

**FELASA B. License LTK2934** University of Zürich (04.2015)

## **OTHER SKILLS**

**Languages** Spanish (Native) English (Advanced) German (Intermediate B1)

- I am proficient in Microsoft Office Suite software, Adobe Illustrator and PhotoShop.

## **PUBLICATIONS**

1. Flores-Dominguez, D., Reinhard JR., Rüegg M.A., (2018). Calcium binding of Copine-6 has a profound effect in the structural plasticity (under preparation).
2. Matthes, F., Hettich, M. M., Schilling, J., **Flores-Dominguez, D.**, Blank, N., Wiglenda, T., & Dagane, A. (2018). Inhibition of the MID1 protein complex: a novel approach targeting APP protein synthesis. *Cell death discovery*, 4(1), 4.
3. Neff, F., **Flores-Dominguez, D.**, Ryan, D. P., Horsch, M., Schröder, S., Adler, T., ... & Hans, W. (2013). Rapamycin extends murine lifespan but has limited effects on aging. *The Journal of clinical investigation*, 123(8), 3272-3291.
4. Quiroz-Baez, R., **Flores-Dominguez, D.**, & Arias, C. (2013). Synaptic aging is associated with mitochondrial dysfunction, reduced antioxidant contents and increased vulnerability to amyloid- $\beta$  toxicity. *Current Alzheimer Research*, 10(3), 324-331.